SEISMIC BEHAVIOR OF CRACKED CONCRETE GRAVITY DAMS

Xueye Zhu

A Thesis

in

The Department of

Building, Civil and Environmental Engineering

Presented in Partial Fulfillment of the Requirements

for the Degree of Doctor of Philosophy at

Concordia University

Montreal, Quebec, Canada

April 2004

Your file Votre référence
ISBN: 0-612-96955-X
Our file Notre référence
ISBN: 0-612-96955-X

ABSTRACT

Seismic Behavior of Cracked Concrete Gravity Dams

Xueye Zhu, Ph. D.

Concordia University, 2004

Two models are proposed to analyze the seismic behavior of cracked concrete gravity dams in order to assess the safety against sliding and overturning. A proposed rigid model first designed for cracked concrete dams considers the geometry of the cracked dam and includes all possible modes of motion with 3 degrees-of-freedom. The other model proposed is a flexible finite element model, which represents a penalty approach, based on the incremental displacement constraint equations between the nodes on both sides of the crack.

All governing equations and corresponding conditions for every mode of motion are derived for the rigid model. Verifications show that this simple rigid model is effective in the prediction of the seismic response of cracked dams. Its applications to the cracked Koyna Dam and a typical dam cracked at the base demonstrate its advantages of simplicity, accuracy and ability to reveal the important features of seismic behavior of cracked concrete dams.

The flexible model is verified with available solutions, showing its very good applicability in estimation of the dynamic response of cracked concrete dams, owing to its adequate treatment of contact conditions at the crack. Its applications to Koyna Dam

and a typical dam prove its adequacy to the cases of cracks at both the base and at a height.

Computations with both proposed models show that the cracked Koyna Dam and the cracked typical dam are safe under the earthquakes considered provided the effective coefficient of friction is sufficient large. However, both models suggest that the rocking mode must be considered since it affects the sliding displacement even if the rocking itself is very small. The partial dam above the crack might experience drifting if severe impact occurs. Therefore even a large coefficient of friction cannot prevent sliding. The residual sliding displacement along the crack for a specific cracked dam depends on factors such as coefficient of friction, water level, peak acceleration of earthquake and its details.

The consistency of two proposed models is noted when increasing the stiffness in the flexible model. This suggests that the rigid model is applicable to the case when the upper part of the cracked dam is very stiff, while the flexible model is capable of revealing more details of the seismic behavior of cracked dams.

ACKNOWLEDGEMENTS

The author acknowledges with gratitude the guidance, support and encouragement provided persistently by his thesis supervisor, Professor O. A. Pekau, during the entire course of this research. His profound knowledge in related studies and excellent sense of engineering judgment, together with his highly responsible attitude toward scientific research, as well as his critical reviews have proved invaluable to the quality of this work.

The Natural Sciences and Engineering Research Council of Canada under Grant No. A8258 provided the financial support for this work. The supportive staff and excellent computing facilities offered at the Building, Civil and Environmental Engineering Department at Concordia University have been very helpful in conducting the huge amount of computation in this research.

The deepest gratitude goes to the author's wife Minglei for her unconditional support and encouragement through her patience and understanding throughout this study. The lovely daughter Jenny deserves the author's greatest appreciation for her cleverness and sensibility that encouraged the author to overcome all difficulties to finish this work.

The most sincere thanks are given to the author's highest respected principle "Truth-Compassion-Tolerance" that has guided him to search the profound meaning of the world and life with his heart through this research.

TABLE OF CONTENT

LIST OF FIGURES

LIST OF TABLES

LIST OF NOTATIONS

μ	the coefficient of friction
μ_k	the kinetic coefficient of friction
μ_s	the static coefficient of friction
ν	the Poisson's ratio of the material
θ	the rotation of a rigid block
$\dot{\theta}_1$	the angular pre-impact velocity at the center of the mass
$\dot{\theta}_2$	the angular post impact velocity at the center of the mass
ρ	the mass density
t	the tangential direction, shearing stress
e	the coefficient of restitution
m_y	the equivalent mass of the rigid block in horizontal direction
m_z	the mass of the dam
n	the normal direction
t	time variable
u	the displacement in τ
v	the displacements in n
y	the horizontal displacement at the center of the mass of the rigid block with respect to the support
$\dot{y}_1$	the horizontal pre-impact velocity at the center of the mass
$\dot{y}_2$	the horizontal post impact velocity at the center of the mass

z	the vertical displacement at the center of the mass of the rigid block with respect to the support
$\dot{z}_1$	the vertical pre-impact velocity at the center of the mass
$\dot{z}_2$	the vertical post impact velocity at the center of the mass
B	the width of the base of rigid block
B_b	the width at the bottom of a rigid block
B_l	the horizontal distance from the center of the mass to the left corner
B_m	the width at the change of the section of a rigid block
B_r	the horizontal distance from the center of the mass to the right corner
B_t	the width at the top of a rigid block
C	the global damping matrix of the system
E	the elastic modulus of the material
F	the friction force
F_l	the contact forces tangent to the surface at the left corner
F_r	the contact forces tangent to the surface at the right corner
F_y	total friction force provided by the support
H	the height of the center of the mass
H_b	the height of the lower portion of a rigid block
H_t	the height of the top portion of a rigid block
H_w	the height of water
K_t	the tangential contact stiffness
K_c	the contact stiffness matrix of the system

K_e	the assembled elastic stiffness matrix of the system
K_n	the normal contact stiffness
M	the global mass matrix of the system
M_P	the moment with respect to the center of mass O by all the static forces
N	the normal force
N_l	the contact forces normal to the surface at the left corner
N_r	the contact forces normal to the surface at the right corner
P_y	the horizontal hydrostatic pressure
P_z	the uplift force
R	the external load vector of the system
$\ddot{Y}_g$	the horizontal acceleration of the support surface
U	the vector of nodal displacements of the system

CHAPTER I

INTRODUCTION TO THIS THESIS

Concrete dams are very special and important structures in civil engineering. Their safety concerns not only economy but also lives. Therefore designers and analysts have been working for assuring their safety, especially in cases of severe earthquake excitations.

The safety of concrete dams relies mainly on its stability against sliding and overturning under hydraulic pressure and ground motion. The safety of concrete dams is traditionally checked with static stability criterion, by computing factors of safety against sliding and overturning using a friction model of the interface zone and equivalent static loads that represent the dynamic effects of an earthquake on the dam. It has been observed, however, that the static stability criterion is not appropriate for evaluating the base sliding displacement of dam due to oscillatory and transient ground motions (Chopra and Zhang, 1991). Nor in the case when overturning is concerned due to highly oscillatory motions with varying peak acceleration values of ground motion during earthquakes (Saini and Krishna, 1974).

Cracks existing in concrete dams reduce their safety against sliding and overturning. These cracks may be at the lift joints in concrete dams during their construction. In current design practice, these joints are considered as locations where crack opening and closing, as well as sliding, are likely to occur. Aging effects in old concrete dams are becoming more and more visible at lift joint locations (Fronteddu *et al.*, 1998). Although very few concrete gravity dams have actually failed because of the weakness at lift joints (Daay and Adeghe, 1991), it is a common fact that there exist

cracks under normal practical conditions. These cracks formed during construction or normal usage may become crucial because of leakage and aging, and may decrease the stability of the dam, especially under severe earthquake excitation.

Severe earthquakes may also cause cracks in concrete dams. Many dams experienced cracking although they did not fail during earthquakes. Some dams were damaged so severely that the crack might penetrate the monolith at certain level of the dam, as in the case of Koyna Dam in India during the 1967 earthquake (Saini and Krishna, 1974). This damage not only causes severe leakage, but also decreases the stability of the dam during aftershocks. Thus in dam safety analysis, for both existing dams, with or without cracks, and ones under design, it is essential to evaluate the stability under severe ground motions.

Much attention of previous work in this regard was given to base sliding response of dams. It was suggested that sliding is the major concern and other motions of the cracked dams can be neglected (Tinawi *et al.*, 2000; Fronteddu *et al.*, 1998; Chopra and Zhang, 1991; Chávez and Fenves, 1995). This reduced the complexity of the problem and many useful results were obtained. A few studies (Fronteddu, 1998; Danny and Adeghe, 1993; El-Aidi and Hall, 1989) dealt with cracked concrete dams with more complicated models to consider closing and opening of the crack. Although the results obtained are limited, it is clear that the seismic behavior is very complex and sensitive to many factors, such as fundamental assumptions for modes of motion, stiffness of the structure, coefficient of friction, aspect ratio of the dam, water uplift pattern and depth of the water.

Stability of a damaged concrete dam, especially in the case that the crack penetrates the dam, is concerned mainly because people are worried about the dynamic

stability during strong earthquakes when the reservoir water level is relatively high. Although the effective coefficient of friction at the crack may be as high as or larger than 1.0 (Fronteddu, Léger, and Tinawi, 1998), it is hard to say that sliding would be prevented (Danay and Adeghe, 1993; Fronteddu, 1997), as the geometric shape, the uplift and static and dynamic effects of the hydraulic pressure make the dynamic response of the cracked concrete dam so complicated that engineers need more tools to predict its seismic behavior, before they take or do not take measures to deal with the damaged concrete dam.

For a general cracked concrete dam, the expected movements during earthquakes could include sliding, rocking and impact. If the impact is strong enough, the material near the impact points might be crushed. There exists also a possibility that the portion above the crack drifts because of hydraulic pressure, uplift and vertical momentum. Therefore the true seismic behavior of a cracked concrete dam is very difficult to predict.

However, if strict assumptions are introduced, the major seismic behavior might be suppressed. To reveal as fully as possible the seismic behavior of cracked concrete dams with reasonable efforts, this study developed two models, 3-*DOF* rigid and *IDCE* finite element models.

This study focuses on the seismic behavior of concrete dams with existing crack formed before to reveal the characteristics of sliding, rocking and other combined motions under earthquakes, so as to assess the safety of cracked concrete dams against sliding and overturning.

In this thesis, the objectives of this study are described in chapter 2. The literature is reviewed in chapter 3, in which both rigid models and finite element models are

discussed. Based on the reviewed models, two models, one of which is 3-*DOF* rigid model and another is *IDCE* finite element model, are proposed, which are explained in detail in chapter 4, 5 and 6. After that, the seismic behavior of three cracked concrete dams are studied in chapter 7, in which the effects of parameters, such as the coefficient of friction, water level and type of earthquake, are studied. Based on the studies in chapters 5, 6 and 7, the seismic behavior of cracked concrete dams is concluded in chapter 8.

CHAPTER II

OBJECTIVES OF THIS STUDY

The seismic behavior of a cracked concrete dam is not clear, even if much research on it has been carried out. From previous work, it is noted that this problem is so complicated that many assumptions, not only on the properties of material but also on the modes of motion of the cracked dam, were introduced to study this problem. But all these assumptions, especially on the modes of motion of the cracked dam, were introduced by, in some sense, conceptual judgment without proof because we do not yet have accurate solutions or experiments as references.

Logically speaking, before we become aware of the seismic behavior of cracked dams, any assumption on modes of its motion may be a restriction to the motion, therefore perhaps making the behavior impossible to be revealed.

For a damaged concrete dam with a crack through its section, the motion of the portion above the crack is quite similar to that of a block resting on a frictional surface. Therefore the seismic behavior of cracked concrete dam is, from the point of view of structural analysis, a non-linear dynamic problem, which mainly focuses on the overall motion of the frictionally supported body above the crack that locates at the base of the dam or at the height where the cross section changes abruptly.

Hence, this study aims to develop methods for the non-linear dynamic problem, from which to reveal the seismic behavior of a cracked concrete dam in order to estimate its safety against sliding and overturning under aftershocks.

2.1 Develop models

Considering the physical situation of the cracked concrete dam, this study proposes two models: rigid model and finite element model.

The rigid model treats the portion above the crack as a rigid body. The crack is also regarded as a rigid and frictional surface of unlimited length. This model just focuses on the global motion of the upper portion of the cracked dam, omitting the local deformation. This will help estimate the movement of the upper portion for a given excitation.

This model is strictly speaking not applicable to the case of a crack at a height, when the upper portion of the cracked dam rests on a limited width surface, which violates the basic assumption in the rigid model. The upper portion of the cracked dam might rock with respect to a middle point other than its corners after large sliding, which is not considered in the rigid model.

Therefore a finite element model is developed as well. This model treats the dam as elastic with plane variable-node iso-parametric elements, focusing on the contact conditions. With this finite element model, it is expected to predict more accurately the seismic behavior of a cracked concrete dam, as the elastic deformation and change of contact conditions at the interface zone between the two portions are taken into consideration.

2.2 Study the seismic behavior of a cracked concrete dam to examine its stability

Applying the proposed models, this research studies the seismic behavior of cracked concrete dam by taking a triangular dam with assumed crack at the base, Koyna

Dam with a crack at the crest and a typical dam cracked at both the base and at a height as examples. Based on the seismic behavior revealed from the studies, the safety against sliding and overturning of cracked concrete dams are estimated under seismic conditions.

CHAPTER III

LITERATURE REVIEW

There are some studies on the seismic behavior of cracked concrete dams. They can be classified, according to the models established to describe the concrete dam, into two categories: rigid and flexible (finite element). In the rigid models, the portion above the crack of the concrete dam was considered as a non-deformable block with 1 or 3 degrees-of-freedom with rigid support (Chopra and Zhang, 1991) or flexible foundation (Saini and Krishna, 1974; Danny and Adeghe, 1993; Tinawi *et al.*, 1999; Tomas *et al.*, 1999). For the flexible models, the concrete dam, foundation rock and /or reservoir water were idealized by finite elements (Danay and Adeghe, 1993; Chavez and Fenves, 1995; Fronteddu *et al.*, 1998; Tinawi *et al.*, 1999; Tomas *et al.*, 1999; Tinawi *et al.*, 2000).

Regarding the friction at the crack surface, studies show that Mohr-Coulomb law cannot accurately represent the characteristics of the friction features of the concrete surface due to the interlock of the aggregates and the damage on the surface during the seismic process. Walraven (1981) proposed a two-phase model to describe the shear transmitting behavior, in which the strength of mortar and its plastic properties are critical. Tassios and Vintzeleou (1987) proposed formalistic models based on the experimental results for several surface roughnesses to study the concrete-to-concrete friction. Studies show that the concrete strength and load history affect shear friction capacity of a concrete crack (Walraven *et al.*, 1987; Mohamed and Richard, 1999). Experiments on concrete joints show that the regularity of the asperities on the surface affects the shear strength and corresponding ductility (Kpdikara and Johnston, 1994). Walraven (1993) proposed a model to explain and predict the behavior of concrete cracks

under cyclic loading by use of matrix strength and the coefficient of friction between the matrix and the aggregate particles. Jefferson (1998) suggested a plastic-damage model to simulate the joints in mass concrete structures under earthquake loading. However, the factors affecting the shear friction models are so complicated and hard to measure that most of the researchers adopted Mohr-Coulomb law for concrete cracks (Aslam *et al.*, 1980; Chopra and Zhnag, 1991; Danay and Adeghe, 1993; Chávez and Feves, 1995; Fronteddu, 1997; Tinawi *et al.*, 2000).

3.1 Rigid models and some results

3.1.1 Rocking-only rigid mode

Saini and Krishna (1974) studied the seismic safety against overturning for the cracked Koyna Dam. This dam experienced a severe earthquake (Richter magnitude 6.5) that occurred on December 11, 1967 with the epicenter very close to it. The peak ground accelerations are 0.372g and 0.480g (the gravity acceleration) in transverse and longitudinal directions, respectively. This earthquake caused severe damage to Koyna Dam in that the higher monoliths of the non-flow section suffered severe distress endangering their stability during future earthquake shocks. Figure 3.1 shows the cross-section of the highest non-flow monoliths of the dam with an assumed horizontal crack at the level where downstream slope changes abruptly.

Due to the fact that the actual crack may have penetrated the cross-section, its stability was problematic. Saini and Krishna (1974) adopted a rigid model to study its overturning stability. In their study, the top profile was considered as rigid. It was assumed that the crack surface is also rigid and it has sufficient friction to prevent the top

profile from sliding. Therefore the only degree of freedom is rotation. The excitation to this rigid block at the crack was the response to the earthquake of the lower portion by modeling it as an elastic beam with varied cross-section. For the beam the first three modes of vibration with a damping of 10 per cent were used. Figure 3.2 is the top profile and forces applied on it. Figure 3.3 shows the rigid model adopted by Saini and Krishna. The only degree of freedom is the rotation θ.

Their study showed that the top profile of cracked Koyna Dam will not overturn under severe aftershock with the peak acceleration at the crack level as high as 1.3g caused by longitudinal component of Koyna earthquake, due to the high oscillation of varying ground peak acceleration during the earthquake.

Rectangular rigid blocks were investigated by Yim *et al* (1980) to deal with the rocking response, assuming rocking is the only mode of motion. It was shown that the response of the block is very sensitive to small changes in its size and slenderness ratio *H/B* and to the details of ground motion. However, systematic trends of response were observed when the problem is studied from a probabilistic point of view with the ground motion modeled as a random process.

This study showed that the block will change its rocking direction after impact for small values of slenderness *H/B*. But for relative large values of slenderness, the coefficient of restitution *e*, which suggests the energy dissipation during impact, has very little effect on the rocking response.

3.1.2 Sliding-only rigid model

Chopra and Zhang (1991) studied earthquake-induced base sliding of concrete gravity dams by considering the dams as rigid. In this model, as shown in Figure 3.4, only sliding was included, because rocking was considered either not easy to occur or having not notable effect in evaluating the sliding response. The interface between the dam base and the foundation rock followed Mohr-Coulomb law. Some results from this study can be concluded as follows:

- The dam tends to slide only in the downstream direction because much smaller ground acceleration is required to initiate downstream sliding compared with upstream sliding.
- The permanent sliding displacement would be expected to increase as the coefficient of friction decreases.
- If the slope of the downstream face becomes steeper, the water depth increases, or the uplift force increases, sliding displacement will increase.
- The permanent sliding displacement depends on the amplitudes, time variation and duration of the ground acceleration. However, the sliding of concrete gravity dams is limited during most earthquakes.
- The sliding displacement usually increases because of vertical ground motion.

Danay and Adeghe (1993) used a "sliding block model" as shown in Figure 3.5 to study seismic-induced slip at the base of concrete gravity dams. The dam was considered rigid with two lumped masses, horizontal (including the virtual mass of reservoir water) and vertical. The rigid dam was connected to a gap-friction element, which can transmit only shear and compressive forces, which follow Coulomb friction law. The tangential

stiffness, which is required when the shear force is below the friction limit, is equal to the equivalent horizontal stiffness of the sliding block model, simulating both concrete and rock deformation.

By using this model, Danay and Adeghe studied dozens of concrete dams, and then proposed an empirical formula for predicting the seismic-induced slip of concrete gravity dams at the rock interface. The results from their sliding block model were compared with finite element analysis. Table 3.1 shows the comparison of two models for a 20.9 m high bulkhead.

This table shows that sliding from both models decreases as the coefficient of friction increases. The sliding depends on not only the coefficient of friction, the ratio of critical acceleration of the model to the peak acceleration of ground motion, but also the type of ground motion. This means that details of ground motion also play a very important role in sliding of cracked concrete dams.

This table also shows that results from two models are much different in most cases. However, they are consistent in the order of magnitude. Therefore rigid mode can serve as a reference before doing complicated analysis.

Tinawi *et al.* (1999) also used sliding-only rigid model to simulate numerically the sliding response and to compare with the results from finite element method and experiments.

In the shake table tests of Tinawi *et al.* (2000), measures were taken to avoid rocking during the process of experiments. The rigid model gave very close prediction of sliding to the experimental results. However, numerical simulations indicated that the calculated results were very sensitive and only with properly selected coefficient of

friction could they be consistent with the experiments. Figure 3.7 illustrates the numerical solutions and experimental results of the same specimen with different excitation inputs for the shake table.

Tomas *et al.* (1999) compared their shake table experimental results with responses by rigid models of single degree of freedom. The comparison showed that the rigid model could predict well the behavior for low frequencies. However, it was shown that rigid model could not simulate satisfactorily the response of the physical model caused by the excitation of high frequencies.

3.1.3 3-*DOF* rectangular rigid model

Many researchers studied rectangular rigid models with 3 degrees of freedom as shown in Figure 3.6, including sliding, rocking and other modes of motion. In this model, all degrees of freedom, which are transverse displacement, vertical displacement and rotation, can be represented at the centre of the mass.

Ishiyama (1982) considered all possible modes of motion and studied the overturning problem of rectangular rigid block on a rigid floor subject to earthquake excitations. The obtained criteria for overturning the block take into account the horizontal acceleration and the velocity of the floor. Shenton Ⅲand Jones (1991) also studied a rectangular rigid block including all modes of motion and systematically discussed all the governing equations especially those for impact. Applying the theoretical formula, they obtained an approximate closed-form solution for a single-mode, steady-state slide-rocking response resulting from harmonic ground acceleration. Shenton Ⅲ(1995) studied criteria for initiating motions of slide, rock, and slide-rock for

the rectangular block, pointing out that slide-rock can also be initiated from rest. Pompei and Sumbatyan (1996) mentioned that disregarding of the sliding could involve mistakes in the study of the body rotation.

3.2 Finite element models and some results

It is more reasonable to consider the flexibility of both upper portion and lower potion of the cracked concrete dam in the study of its seismic behavior. Although other numerical methods, such as boundary element method (Lorenzana and Garrido, 1998; Leahy and Becker, 1999), distinct element method (Zhang *et al.*, 1997) and discontinuous deformation analysis (MacLaughlin *et al.*, 2001), can be employed to deal with this dynamic contact problem, the finite element method has been widely adopted in the research due to its many advantages.

In the studies of seismic behavior of cracked concrete dams by using finite element method, the major attention has been paid to the treatment of the crack surface, meaning how to set up a model to describe the features of the interface in sliding, opening and closing (impact).

Among the models for the crack interface, sliding-only, gap-element and smeared element were studied and implemented in the finite element method. And some meaningful results were obtained from previous studies.

3.2.1 Sliding-only friction model

As shown in Figure 3.8, Chávez and Fenves (1995) took a numerical approach based on the hybrid frequency-time domain procedure to evaluate the earthquake

response of concrete gravity dams. The nonlinear sliding behavior at the interface with foundation rock was included. Sliding of the dam at the foundation rock interface is the only source of non-linearity in the system. The concrete dam was idealized with finite elements. The dam base was modeled as a rigid supported by flexible foundation rock, as the base deformation was considered having little effect on the dynamic response. The compressible water impounded in the reservoir was idealized as two-dimensional domain extending to infinite in the upstream direction.

The interface between the dam and the foundation rock is assumed to be a straight surface governed by the Mohr-Coulomb law. Zero cohesion was used for the fact that little cohesive resistance can be expected during earthquake-induced sliding of the dam. The value of coefficient of the friction was assumed relatively high, between 0.8 and 1.2, to consider the roughness of the surface after the formation of the crack at the sliding interface. Partial uplift was not considered in the solution procedure. The system was subject to horizontal and vertical components of free-field earthquake ground motion at the base of the dam.

Because the rocking was considered insignificant compared with sliding, only sliding probability is included in the system. As a case study, Pine Plat Dam was analyzed numerically to show the influence of parameters such as type of ground motion, coefficient of friction, foundation rock flexibility and amplitude of ground acceleration.

The very important assumption implied in this sliding-only finite element model is that the contact interface at the base plane between the dam and the foundation rock remains straight. Only in this way, could the dam slide smoothly without impact on the foundation rock.

3.2.2 Gap-friction element model

The gap element, as shown in Figure 3.9, was frequently used in both rigid models and finite element models to simulate cracks in concrete dams due to its simplicity.

Léger and Katsouli (1989) studied the stability of concrete gravity dams using finite element formulation for the dam, rock and foundation. In their study, the gap-element was used to model the interface at the base. Computation showed that non-linear behavior of the dam-foundation rock interface reduced the seismic response of the dam.

For developing the empirical formula to estimate the sliding displacement of concrete gravity dams, Danay and Adeghe (1993) set up a finite element model, in which the rock foundation was represented by horizontal, vertical and rotational springs which are connected to the mid-base point of a rigid line located underneath the base, and this rigid line connects the concrete dam by three gap-friction elements located at mid-base, heel and toe of the dam, as shown in Figure 3.10.

To study static and dynamic behavior of concrete lift joint interfaces, Fronteddu (1997) and Fronteddu *et al.* (1998) reported an experimental study for different type of joints. They proposed a friction formula for the lift joints, which was used for a gap-element model (Figure 3.11). Finite element analysis showed that their friction formula and gap-element model can be used for sliding analysis at the base or multiple joints at different levels in concrete dams.

3.2.3 Smeared element model

El-Aidi and Hall (1989), Bhattacharjee and Léger (1993, 1994) studied the non-linear earthquake response of the concrete gravity dams using a finite element procedure. The non-linear behavior at the crack was treated by means of the smearing technique, as shown in Figure 3.12. It considered tensile cracking with subsequent opening, closing and sliding.

In the smearing technique, the nonlinear behavior of the crack is considered in the constitutive law of the material of the element, i.e. changing the constitutive matrix of the element according to the strain-stress status. Iteration is required, if sliding, opening or closing along the smeared cracks occurs, by changing the shear stiffness to conform to the friction law.

Pine Flat Dam was analyzed numerically to study the effect of water cavitation and cracking on the earthquake response of the dam-water-foundation system. A two-dimensional idealization was adopted for the dam and water in order to simplify the analysis and reduce the computational effort. The foundation of the dam was modeled as a rigid rectangular massless plate attached to a three-dimensional visco-elastic- half-space. It was shown that for some cases the crack might experience 3.4 ft sliding away from the water when the dam is subject to 1.5 times of El Centro earthquake with full reservoir.

3.2.4 Node-to-surface contact model

Bathe and Chaudhary (1985) proposed a model to describe the contact conditions and implemented it in the general-purpose program *ADINA* (1999), a powerful

commercial finite element analysis software widely used in engineering practice and research.

Their model, as shown in Figure 3.13, is to define a pair of surfaces to potentially come in contact with each other in the process of calculation. One surface of the pair is called as a target surface. The other one is termed as a contactor surface defined by contactor nodes. At every time step the contactor nodes will be checked in order to avoid penetration into the target surface, which in general guarantees that no penetration occurs on both surfaces. However, the sharp angle, if any, on the target surface as shown in Figure 3.13 is likely to penetrate the contactor surface. Of course, this penetration can be reduced by adding more contactor nodes adjacent to the sharp angle. The model can be briefly stated as follows:

- If the normal contact force between a contactor node and the target surface tends to be tensile, this node will be treated as opened in the next time step and corresponding normal and tangential contact forces will become zero.
- If the tangential force exceeds the friction limit given by the Mohr-Coulomb friction law, this node will be treated as sliding in next time step, and the tangential (friction) force will be obtained by iteration to conform to the friction law.
- If an opened contactor node comes into contact with the target surface, its contact condition will be determined by iteration.
- However, once a contact node penetrates the target surface, the normal contact force needs to be increased to position this node onto the target surface so as to prevent contactor node from overlapping the target surface.

Mathematically, this model is a Lagrange algorithm to deal with the contact conditions by introducing the contact forces as additional unknowns in the system. So it can be called "Force Method" to deal with contact problems.

This model has many advantages. The most important one, compared with other models, is its ability to properly deal with large sliding due to its feature of "node-to-surface" contact description.

Also, it is convenient to obtain the contact forces directly from the system equations due to its treatment of contact forces as independent unknowns. Of course, this increases the number of unknowns in the system and makes the program code more complicated.

Another disadvantage of this model is that the penetration of target nodes through the contactor surface is not detected. Although this penetration can be lessened in many cases if the mesh on the contactor surface is fine enough, it is almost impossible to avoid this in a cracked concrete dam. For example, if the bottom surface of the upper portion of a cracked dam is defined as the contactor surface, one of the upper corners of the lower portion of the cracked dam, which is a target node that is free to penetrate the contactor surface, must penetrate the contactor surface when relative rocking occurs after sliding. In this case, the algorithm will not detect the true pivot, and the upper portion will rock with respect to a fake pivot, which is the nearest contactor node on the inner side of that corner.

Treating the interface of the crack at the base with the similar idea as *ADINA*, Mir and Taylor (1996) modeled a typical low height gravity dam monolith with the finite element method. The monolith was tested on a shaking table without uplift pressure and

hydrodynamic force. The analytical results of the sliding response of the monolith were compared with slip tests, which showed good consistency only for low frequency of excitation.

3.2.5 Node-to-node contact model

SAP2000 (1999) is also well-known finite element analysis software widely used for structural analysis and design. It provides the special element *NLLink* (Non Linear Link element) to treat the discontinuity in structures, such as gap, hook, friction, separation and contact. This element is very suitable to describe the frictional contact feature of the crack in concrete dams if displacement is small.

When applied to cracked concrete dams with finite element method, *NLLink*s can link node pairs on both surfaces of the crack. The *NLLink* can only resist compression and the magnitude of the tangential force is determined by iteration to conform to the friction law when it reaches the friction limit.

Mathematically, this is a penalty method in which relatively large values are assigned to the *NLLink* stiffness to make sure the relative displacements between the linked nodes along the desired direction are negligible.

The advantage of this method is that no extra unknowns need to be added to the system. This makes it easier to program in the computer code than the Lagrange method. However, how to choose a proper "large stiffness" for the *NLLink* relies on the analyzer's experience, sometimes requiring trials.

Actually, this *NLLink* is principally the same as the gap-element from the point of view of numerical analysis.

Compared with node-to-surface contact model in *ADINA* in which large sliding can be properly included, this node-to-node/gap-element method can only be applied to the situation that relative displacements of linked nodes do not affect the response. Therefore, it is reasonable to use this model to deal with small amount of sliding in cracked concrete dams. Remarkable errors can be expected if quite large sliding and rocking occur for cracked concrete dams especially when cracked at a height.

3.2.6 Some results from finite element models

Chávez and Fenves (1995) employed the sliding-only friction model to analyze earthquake response of concrete dams including base sliding. They studied effects on the sliding of parameters such as type of ground motion, amplitude of ground acceleration, coefficient of friction and foundation rock flexibility. Figure 3.14 shows only the sliding displacement of Pine Flat Dam (122m high) with rigid foundation rock, $\mu = 1$, for three ground motions (Taft S69E, El Centro S00E and Pacoima S16E) with the same peak ground acceleration of 0.4g.

Their research shows:

- Base sliding displacement accumulates in the downstream direction because the combination of hydrostatic forces and dynamic forces exceed the shear strength of the interface zone.
- The maximum sliding displacement is influenced by the duration and characteristics of the free-field ground motion. A ground motion with a large number of acceleration peaks induced more sliding than a ground motion with a

single large pulse. A strong acceleration produces considerable larger sliding than moderate ground motion.

- Dam-foundation rock interaction generally reduces the earthquake responses of cracked concrete dams. The assumption of rigid foundation rock can significantly overestimate the base sliding displacement compared with more realistic estimations obtained from including dam-foundation rock interface, particularly for tall dams.
- The sliding displacement is sensitive to the value of coefficient of friction. Taller dams are more affected by the coefficient of friction than shorter dams. But it is less important for dams on flexible foundation rock.
- Water compressibility is also an important factor in determining the base sliding of dams particularly with stiff foundation rock.

El-Aidi and Hall (1989) used smeared elements to simulate the assumed initial crack in Pine Flat Dam in three cases as shown in Figure 3.15. The dash lines represent the assumed cracks.

Simultaneous horizontal and vertical components of the 1940 El Centro earthquake ground motion scaled in amplitude by 1.5 provided the excitation. Calculation showed that all of the sliding takes place in the downstream direction, and the permanent slips are about 1.9 ft, 0.9 ft and 3.4 ft for horizontal crack, inclined crack up to upstream face and inclined crack up to downstream face, respectively. This indicates that the direction of crack considerably affects the sliding displacement.

The calculation also shows that the top portion pivots on a single element (for courser mesh) or several elements (for finer mesh) at each end of the crack. This

dependence on mesh fineness certainly affects the predicted stresses at the pivots, hence the rocking and sliding motion.

3.3 Discussion about models

3.3.1 Discussion about rigid models

A rigid model has only one or a few degrees of freedom. It is easier to implement the analysis, especially for models of one degree of freedom. For the case that the concrete dam has small slenderness for which rocking will not occur, the rigid model of one degree of freedom will give a good estimation for sliding. When rocking is likely to happen, as is unavoidable in the case of a crack at a height, a 3-*DOF* rigid model taking into consideration of sliding, rocking, impact and drifting is necessary to simulate the movement of the cracked dam.

Impact will significantly affect the seismic behavior of the cracked dam, hence affecting its residual sliding. The local deformation (elastic or plastic) within the impact area could be significant. Therefore the rigid model can hardly predict the seismic response of cracked concrete dams if the impact is severe.

It is obvious that the rigid model, even with 3-*DOF*, is mainly suitable for very coarse estimation of the seismic response for cracked concrete dams when impact is not likely to happen or the impact is slight and would not affect considerably the residual sliding. However, rigid models are very useful to give quick estimation for the seismic behavior of cracked concrete dams and could serve as a reference for more complicate calculation. If quite remarkable rocking is predicted with 3-*DOF* rigid model, a more accurate model is suggested.

However, previous research on cracked dams by the rigid models is quite insufficient. It is focused on either the base sliding or the rocking alone. There is no study with a rigid model to reveal the whole seismic behavior of cracked concrete dams.

3.3.2 Discussion about finite element models

Finite element models can adequately represent the flexibility of concrete dams, so it is always anticipated to be more accurate than rigid models to predict the seismic behavior of cracked concrete dams. In this kind of model, the key point is to correctly describe the contact conditions at the crack, and this will determine the accuracy and efficiency of the calculation.

Finite element models have many advantages, such as capability of dealing with flexibility of the dam and foundation and of handling multiple cracks. But application of this kind of model to a practical problem needs much more data preparation effort and much higher computation cost than rigid models.

Finite element analyses of cracked concrete dams yielded many results to help understand cracked concrete dams under seismic conditions. Different models were used to analyze the dynamic response of concrete dams cracked at the base or at a height. Much attention was paid to base sliding response, whereas the rocking mode was either intentionally omitted or less addressed. As for the case of the crack at a height, the present models are either applicable to the situation of small sliding or with necessity of very fine element mesh near the ends of the crack to avoid penetration. Nevertheless more effort is still needed to reveal thoroughly the seismic behavior of cracked concrete dams.

Table 3.1 Comparison of finite element block with sliding block (Danay & Adeghe, 1993)

Ground motion	Ratio of critical acceleration of the model to the peak acceleration of the motion R=a/A	Sliding (mm)		
		Coefficient of friction μ	Finite element model	Sliding block model
N6D45	0.3625	0.70	1.12	2.03
	0.6024	0.85	0.94	0.99
M6.5R40	0.8181	1.00	0.46	0.84
	0.6000	0.70	21.30	31.76
El-Centro	0.5057	0.85	25.50	11.50
	0.6868	1.00	6.90	7.60

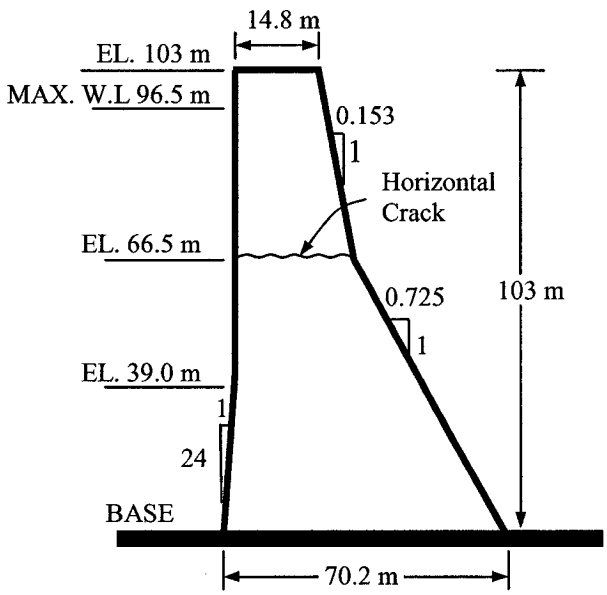

Figure 3.1 The monolith of Koyna Dam with assumed horizontal crack at the crest (Saini and Krishna, 1974)

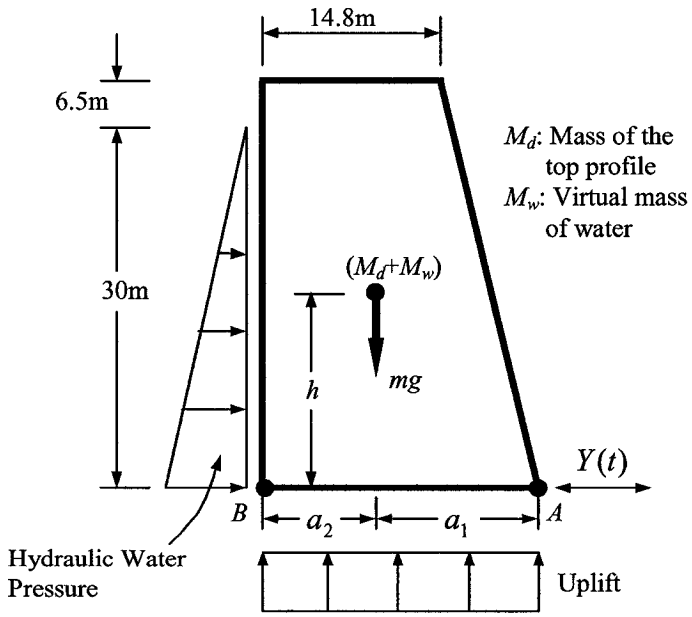

Figure 3.2 Top profile of the dam with various forces under full reservoir water (Saini and Krishna, 1974)

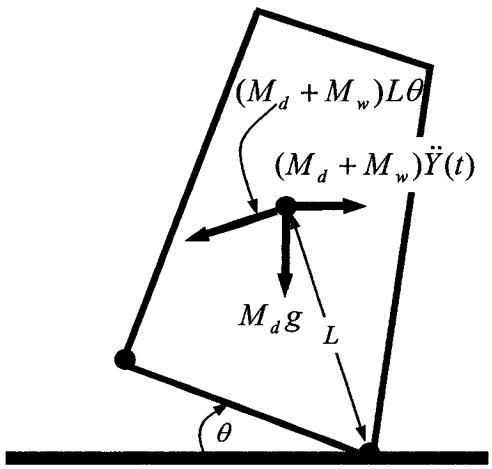

Figure 3.3 Rocking-only rigid model for overturning analysis of the top profile (Saini and Krishna, 1974)

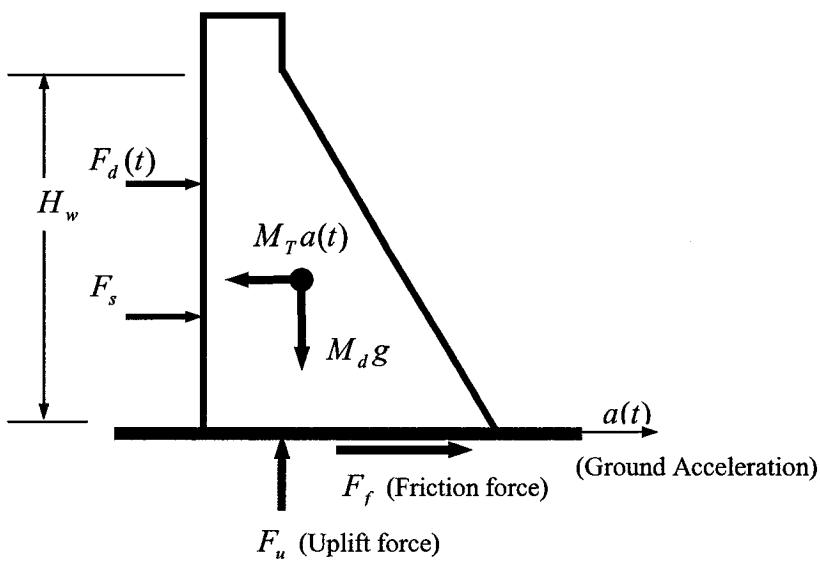

Figure 3.4 Sliding-only rigid model (Chopra and Zhang, 1991)

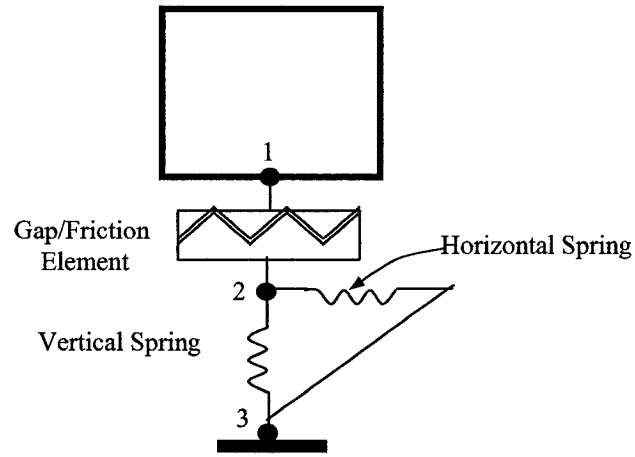

Figure 3.5 Sliding block model (Danay and Adeghe, 1993)

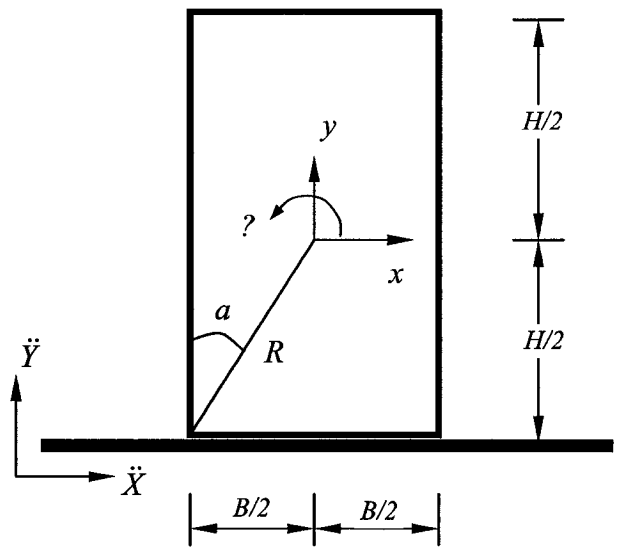

Figure 3.6 3-*DOF* rigid rectangular model (Ishiyama, 1982)

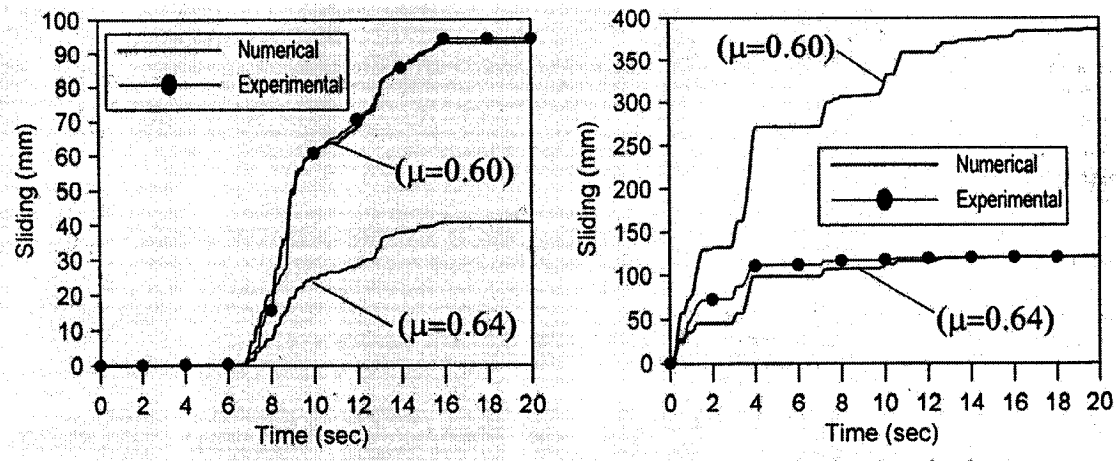

Figure 3.7 Comparison of rigid model with shake table test (Tinawi *et al.*, 2000)

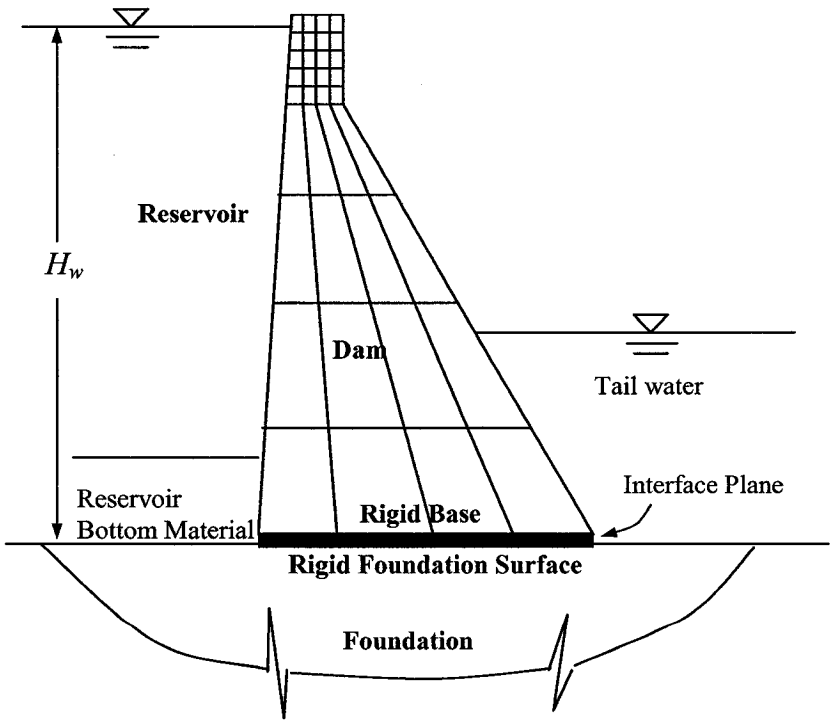

Figure 3.8 Sliding-only finite element model (Chávez and Fenves, 1995)

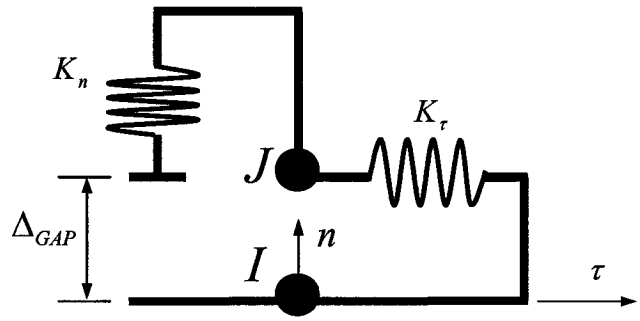

a) Model illustration

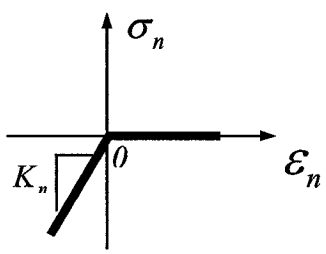

b) Normal constitutive law

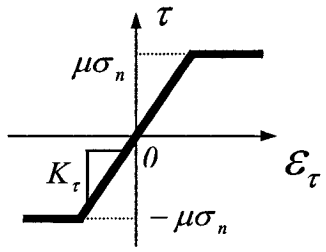

c) Tangential constitutive law

Figure 3.9 Gap/friction element

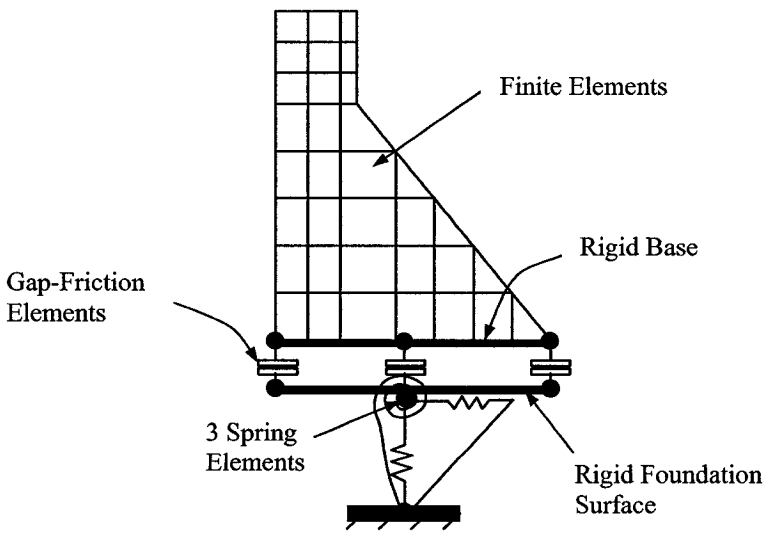

Figure 3.10 Gap-element model including effects of foundation (Danay and Adeghe, 1993)

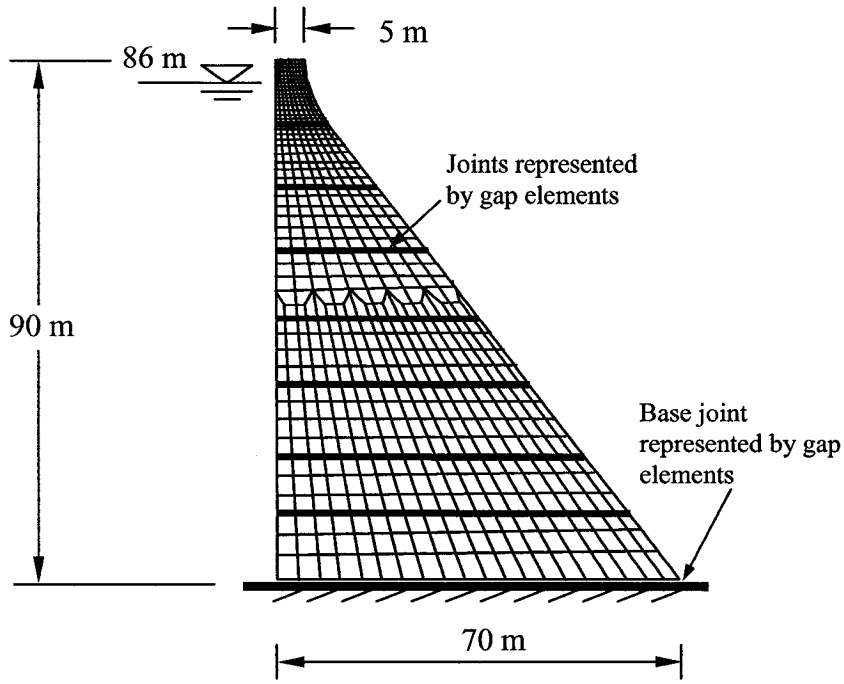

Figure 3.11 Gap-element model for multiple joints (Fronteddu, 1997)

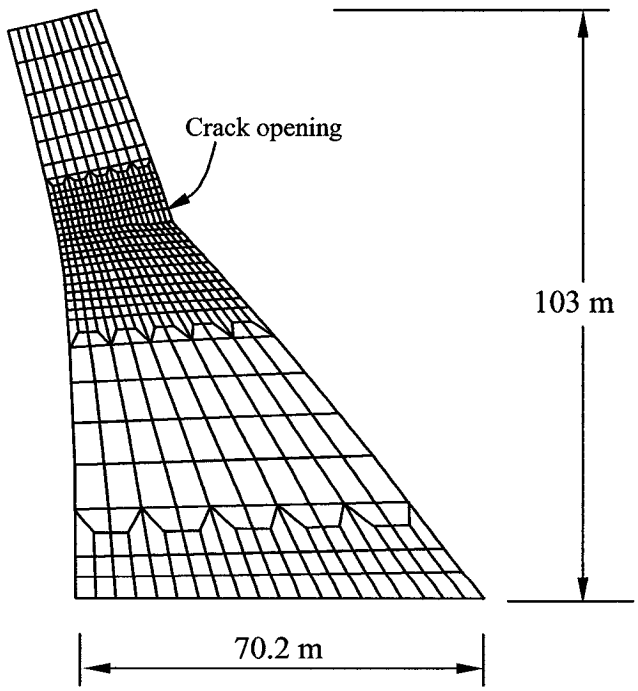

Figure 3.12 Deformed configurations of Koyna Dam (Bhattacharjee and Léger, 1993)

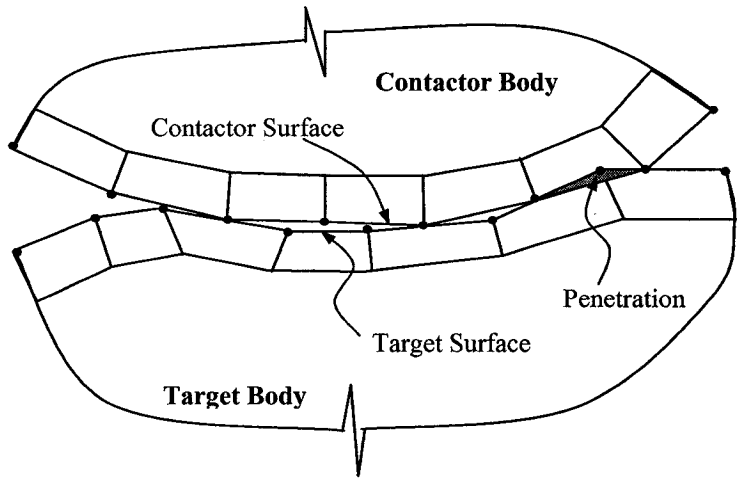

Figure 3.13 Contact model in *ADINA* (Bathe and Chaudhary, 1985)

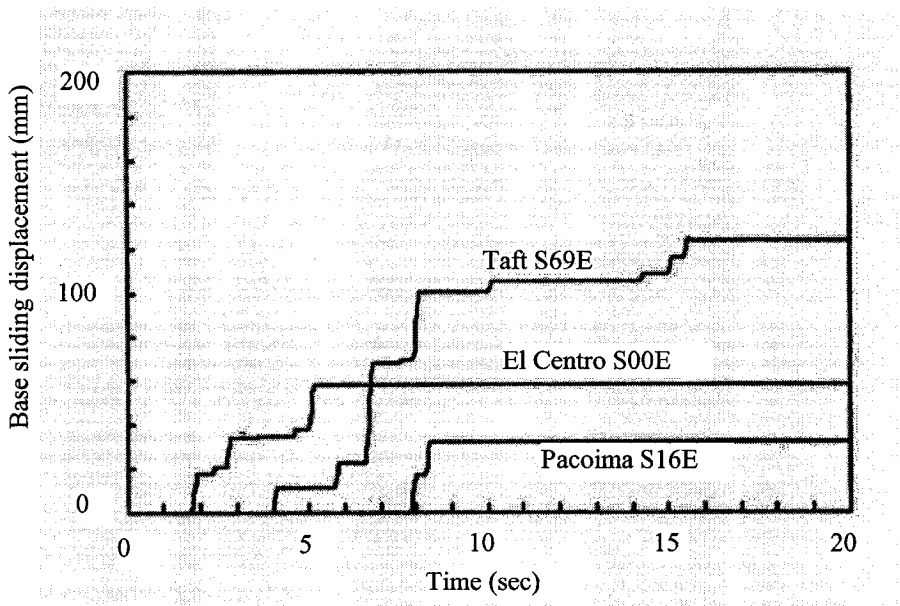

Figure 3.14 Sliding displacement of Pine Flat Dam with rigid foundation rock (Chávez and Fenves, 1995)

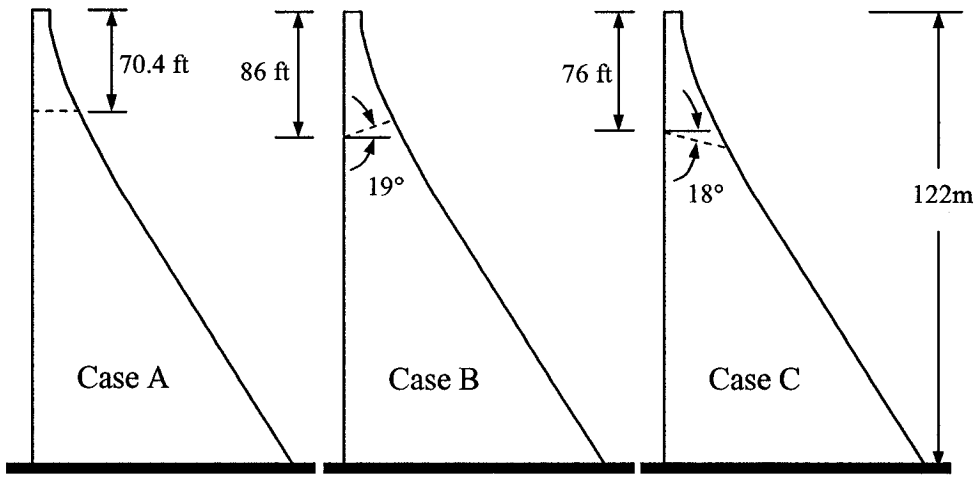

Figure 3.15 Pine Flat Dam with assumed initial crack (El-Aidi and Hall, 1989)

CHAPTER IV

3-*DOF* RIGID MODEL FOR DAMS: THEORY

4.1 Introduction

For the damaged concrete dam with a crack through its section, the movement of the upper portion above the crack can be taken as a block resting on a flexible block with finite width and fixed at the base. If the excitation at the base is not strong enough, the upper portion will move integrally with the lower portion, behaving like an undamaged dam. However, there exists in general a possibility that the upper portion slides along the crack or loses contact partially while rocking or completely while drifting when the excitation at the base is strong enough. Once the upper portion moves with respect to the lower portion at the crack, i.e. the contact condition between the two parts changes because of the overall movement of the upper portion, the upper portion behaves very much like a rigid block, as the deformation of the upper portion is relatively negligible. The movement of the lower portion fixed to the foundation also can be neglected if compared with the overall movement of the upper portion. Therefore the behavior of the upper portion of a cracked concrete dam can be modeled as a rigid block resting on a frictional surface.

For the dam cracked at the base, it is quite suitable to take the crack as infinitely wide. Contrarily, if the crack is at a height and considerable sliding is expected, it is not reasonable to assume the surface infinitely wide, and the contact condition is obviously different from that of the case when the crack locates at the base of the dam, once relative movement tangent to the crack occurs.

Therefore, it is reasonable, on the one hand, to model the upper portion above the crack as a rigid block resting on an infinitely wide surface to study its overall dynamic behavior; it is not suitable, on the other hand, to apply this model when the crack locates at a height of the dam when the upper portion slides significantly.

The surface of the crack is obviously flexible no matter where the crack is. The crack is moving in both horizontal and vertical directions and rotating if it is at a height of the dam. So the upper portion, taken as a rigid block, rests on a moving flexible frictional surface. However, it can be expected that the deformation of the moving surface is negligible compared with the overall movement when the excitation from the foundation is strong.

Having considered the dynamic features of the upper portion of cracked concrete dam and its geometry as well as the advantages of the 3-*DOF* rigid model for rectangular block (Shenton III and Jones 1991), a modified 3-*DOF* rigid model for generalized concrete dams is proposed. All theoretical formulas will be presented in this chapter. Its verifications and applications will be discussed in chapter 5.

4.2 Description of proposed 3-*DOF* rigid model

4.2.1 Geometry of the model

Unlike the rectangular block studied by many researchers (Yim, Chopra and Penzien, 1980; Ishiyama, 1982; Shenton III, 1996; Pomlei, Scalia and Sumbatyan, 1998), concrete dams have complex geometry and loading. These make the geometry unsymmetrical and unequal masses in horizontal and vertical directions when the virtual mass of water is included (Chopra and Zhang, 1991). Therefore, the expressions and

criteria for different modes of motion should be modified accordingly. Figure 4.1 shows the generalized geometry and loading of the 3-*DOF* rigid model proposed for the seismic analysis of a concrete dam cracked at the base. With H_t=0 and $\ddot{Y}_g$ replaced by the response of the acceleration at the crack surface of the lower portion, Figure 4.1 represents the upper portion of the cracked dam, as shown in Figure 3.1 for cracked Koyna Dam.

4.2.2 Parameters in the model

In this model, the portion above the crack is a rigid block. It rests on a rigid surface fixed to the foundation. As shown in Figure 4.1, the geometry of this model is described by the following parameters: the width at the top B_t, the width at the change of the section B_m, the width at the bottom B_b, the height of the top portion H_t, the height of the lower portion H_b and the water depth H_w.

Considering these parameters and the mass m_z of the dam, as well as mass m_y in horizontal direction comprised of m_z and the virtual mass to approximately represent the dynamic effect of the incompressibility of water (Westergaard 1931), the center of the mass, denoted by H and B_l or B_r, and the polar moment of inertia J_o with respect to the center of the mass can be determined.

N_l and F_l are the contact forces normal to and tangential to the surface, respectively, at left lower corner. N_r and F_r are those at right lower corner. $\ddot{Y}_g$ is the acceleration of the support surface. P_y, P_z and M_P represent, respectively, the hydrostatic pressure, uplift force and moment with respect to the center of mass O by all

the static forces. The rigid body has three degrees-of-freedom assigned at the center of mass, namely horizontal displacement *y*, vertical displacement *z* and rotation *?* as shown in Figure 4.1.

4.2.3 Basic assumptions in the model

Beside the rigid assumption for the dam and the crack surface, this model has a few extra assumptions for calculation simplicity:

Contact forces concentrate at one or both lower corners of the block. With this assumption, the distributed contact between the block and the crack is simplified as point contact. This assumption will not raise any problem if the whole base is in contact with the cracked surface or the rotation corner is within the width of the crack. However, once considerable sliding occurs and part of the base loses contact, which is very likely to happen, one cannot expect this assumption to correctly represent the contact forces. This assumption implies the crack surface as infinitely wide.

The rocking of the block is small. This linearizes the equation of rocking and will not introduce noticeable errors for small rocking. In fact, present studies show that rotation of the cracked dam is quite limited in both cases of crack at the base and at a height.

Only horizontal ground excitation is included in the analysis in this study. This assumption helps simplify the solution. In reality, the vertical component of the earthquake must affect the seismic response of cracked dams, which would be involved in later study of this model.

4.2.4 Modes of motion in the model

Disregarding the sliding can involve mistakes in the study of rotation for rectangular blocks (Pomlei, Scalia and Sumbatyan, 1998). The block might drift after severe impact if both lower corners acquire upward velocities (Shenton III and Jones, 1991). In the case of a cracked concrete dam, with the effects of horizontal hydraulic pressure and uplift pressure, it is natural to reckon that the cracked dam is more likely to slide, rock and drift. Therefore the proposed 3-*DOF* model should include all possible modes of motion, namely sliding, rocking, slide-rocking, impact and drifting, to fully reveal the seismic behavior of cracked concrete dams.

4.2.5 Difference from rectangular rigid model

This model differs from the isolated rectangular block model in that: a) the mass in the horizontal direction m_y, including the mass of the dam m_z and the virtual mass of the water (Westergaard, 1931), is different from the mass m_z in vertical direction which is only the mass of the dam; and b) the distances from the mass center to the left corner (B_l) and to the right corner (B_r) are different because of the asymmetric shape. These make the solutions very complicated for all modes as well as corresponding criteria.

4.3 Sliding mode

4.3.1 Governing equations

When the rigid block is in pure sliding without rotation and vertical displacement (see Figure 4.2), the motion of sliding along the horizontal direction on the surface is governed by following equation (Kane and Levinson, 1985):

$$m_y(\ddot{Y}_g + \ddot{y}) - P_y + F_y = 0 \tag{4.3.1}$$

where

$$F_y = F_l + F_r = \mu_k S_{\dot{y}_b} N \tag{4.3.2}$$

Equation (4.3.2) represents the friction law, in which μ_k is the kinetic coefficient of friction between the block and the support surface. $S_{\dot{y}_b}$ is the sign function of relative sliding velocity $\dot{y}_b$ of the dam at the base with respect to the surface. $\ddot{y}$ is the relative horizontal acceleration of the block. The total normal contact force N in (4.3.2) is the net weight N_0 of the block:

$$N_0 = m_z g - P_z \tag{4.3.3}$$

From (4.3.1), (4.3.2) and (4.3.3), the governing equation for the sliding mode becomes

$$\ddot{y} = \ddot{y}_0 - \ddot{Y}_g \tag{4.3.4}$$

where

$$\ddot{y}_0 = \frac{P_y}{m_y} - \mu_k S_{\dot{y}_b} \frac{N_0}{m_y} \tag{4.3.5}$$

4.3.2 Conditions to maintain pure sliding mode

The angular velocity must be zero otherwise the block will rock. This leads the requirement for moment as

$$F_y H + N_l B_l - N_r B_r - M_P = 0 \tag{4.3.6}$$

Considering Equations (4.3.2) and (4.3.3), the normal contact forces at both corners can be expressed as follows:

$$N_l = [M_P - (\mu_k S_{\dot{y}_b} H - B_r) N_0] / B \tag{4.3.7}$$

$$N_r = [-M_P + (\mu_k S_{\dot{y}_b} H + B_l) N_0] / B \tag{4.3.8}$$

Therefore, the conditions to maintain the pure sliding motion can be obtained from (4.3.7) and (4.3.8) by considering that both normal contact forces N_l and N_r are positive:

$$\frac{M_P / N_0 - B_l}{H} \le \mu_k \le \frac{M_P / N_0 + B_r}{H} \qquad \text{when } \dot{y}_b > 0 \tag{4.3.9}$$

$$-\frac{M_P / N_0 + B_l}{H} \le \mu_k \le \frac{-M_P / N_0 + B_r}{H} \qquad \text{when } \dot{y}_b < 0 \tag{4.3.10}$$

4.3.3 Conditions to initiate pure sliding mode from rest

For a given coefficient of friction, the block starts to slide, if rocking mode will not be initiated first, when the ground acceleration is large enough to overcome the maximum friction force:

$$F_y = -\mu_s S_{\ddot{Y}_g} N_0 \tag{4.3.11}$$

where μ_s is the static coefficient of friction.

Therefore the minimum ground acceleration to initiate pure sliding can be obtained from (4.3.1) and $|F_y| \ge \mu_s N$ (by assuming $\ddot{y} \ge 0$ or $\ddot{y} \le 0$):

$$\begin{cases} \ddot{Y}_g \ge \dfrac{P_y}{m_y} + \mu_s \dfrac{N_0}{m_y} & (\ddot{y} < 0, \quad \dot{y} = 0) \\ \qquad\qquad or \\ \ddot{Y}_g \le \dfrac{P_y}{m_y} - \mu_s \dfrac{N_0}{m_y} & (\ddot{y} > 0, \quad \dot{y} = 0) \end{cases} \tag{4.3.12}$$

From (4.3.12) it is clear that less ground acceleration is needed to initiate sliding in downstream direction than upstream direction because of the hydraulic pressure.

The condition expressed in (4.3.12) is not sufficient to initiate the pure sliding mode, because the block may rock if the coefficient of friction is too big. To avoid rocking, both normal forces N_l and N_r must be positive. Therefore the additional requirement to maintain this mode, besides the (4.3.12), can be obtained as

$$g_0 - g_1 \frac{B_r}{H} \le \ddot{Y}_g \le g_0 + g_1 \frac{B_l}{H} \tag{4.3.13}$$

where

$$g_0 = \frac{P_y H - M_P}{m_y H} \quad , \quad g_1 = \frac{N_0}{m_y}$$

From (4.3.12) and (4.3.13), the requirement to avoid rocking in terms of the coefficient of friction becomes

$$\begin{cases} \mu_s \le \dfrac{B_l}{H} - \mu_0 & (\ddot{y} < 0) \\ \qquad or & \\ \mu_s \le \dfrac{B_r}{H} + \mu_0 & (\ddot{y} > 0) \end{cases} \tag{4.3.14}$$

in which

$$\mu_0 = \frac{M_P}{N_0 H} \tag{4.3.15}$$

If (4.3.14) is violated, meaning that the coefficient of friction is too big, the block will rock instead of slide from rest, when the ground acceleration is strong enough.

4.4 Rocking mode

4.4.1 Governing equation

When rocking without sliding, the horizontal and vertical displacements at the center of the mass depend on the rotation θ (see Figure 4.3). However, there are three equilibrium equations in the horizontal direction, the vertical direction and rotation as follows:

$$m_y(\ddot{Y}_g + \ddot{y}) - P_y + F_y = 0 \tag{4.3.1}$$

$$m_z(\ddot{z} + g) - P_z - N = 0 \tag{4.4.1}$$

$$J_o\ddot{\theta} - M_P + F_y H + S_\theta N B_i = 0 \tag{4.4.2}$$

in which

$$\left|F_y\right| \le \mu_s N \tag{4.4.3}$$

$$\ddot{y} = -H\ddot{\theta} \tag{4.4.4}$$

$$\ddot{z} = S_\theta \ddot{\theta} B_i \tag{4.4.5}$$

where S_θ and $S_{\dot{\theta}}$ are the sign functions of the rotation and angular velocity, respectively. B_i in (4.4.2) and (4.4.5) is the horizontal distance from the center of mass to the corner around which the dam rotates. The corner around which the dam rotates can be determined by the rocking angle ?:

$$B_i = B_l, \quad \text{when } \theta > 0 \tag{4.4.6}$$

or

$$B_i = B_r, \quad \text{when } \theta < 0 \tag{4.4.7}$$

Substituting (4.3.1), (4.4.1) and (4.4.5) into (4.4.2), the governing equation for pure rocking becomes

$$\ddot{\theta} = \ddot{\theta}_0 + \frac{m_y H}{J_0'} \ddot{Y}_g \tag{4.4.8}$$

where

$$\ddot{\theta}_0 = \frac{M_P - P_y H - S_\theta N_0 B_i}{J_0'} \tag{4.4.9}$$

$$J_0' = J_0 + m_y H^2 + m_z B_i^2 \tag{4.4.10}$$

4.4.2 Condition to maintain rocking mode

To ensure that pure sliding will not occur, the coefficient of friction should be large enough. This yields, from (4.3.1), (4.4.1) and (4.4.3), the requirement for the coefficient of friction as

$$\mu_s \geq \frac{S_\theta [m_y (\ddot{Y}_g - \ddot{\theta} H) - P_y]}{S_\theta \ddot{\theta} B_i m_z + N_0} \tag{4.4.11}$$

If (4.4.11) is violated in the process of rocking, the block will enter the status of slide-rocking mode.

To avoid drifting, the normal contact force should be positive. From the governing equations (4.3.1), (4.4.1) and (4.4.2) as well as the relations (4.4.4) and (4.4.5), this requirement can be expressed as follows:

$$\begin{cases} \ddot{Y}_g \geq \dfrac{P_y - M_P / H}{m_y} - \dfrac{N_0}{m_y m_z B_l H / J_0'} & (\theta > 0) \\ \ddot{Y}_g \leq \dfrac{P_y - M_P / H}{m_y} + \dfrac{N_0}{m_y m_z B_l H / J_0'} & (\theta < 0) \end{cases} \tag{4.4.12}$$

4.4.3 Conditions to initiate rocking mode from rest

Noting in equilibrium equation (4.4.2) that when the block initiates to rock from rest

$$\begin{cases} S_\theta B_i = B_l, & \ddot{\theta} > 0 \\ S_\theta B_i = -B_r, & \ddot{\theta} < 0 \end{cases}$$

the requirement for ground acceleration to initiate the rocking mode from rest can be derived from (4.4.8) as

$$\begin{cases} \ddot{Y}_g \geq \dfrac{-M_P + P_y H + N_0 B_l}{m_y H} \\ \qquad or \\ \ddot{Y}_g \leq \dfrac{-M_P + P_y H - N_0 B_r}{m_y H} \end{cases} \tag{4.4.13}$$

Of course, the static coefficient of friction should be big enough to prevent the block from sliding. Referring to the discussion on sliding mode, it is clear that the requirement on the static coefficient of friction is

$$\begin{cases} \mu_s \geq \dfrac{B_l}{H} - \mu_0 & (\ddot{y} < 0) \\ \qquad or \\ \mu_s \geq \dfrac{B_l}{H} + \mu_0 & (\ddot{y} > 0) \end{cases} \tag{4.4.14}$$

4.5 Slide-rocking mode

4.5.1 Governing equations

It is possible that sliding is initiated while the block is rocking or that rock is initiated while it is sliding (see Figure 4.4). It was also shown (Shenton III, 1996) that the slide-rocking mode can also be initiated from rest. In this mode, the horizontal displacement becomes independent, yet the vertical displacement remains dependent on the rocking degree. So the governing equations for the slide-rocking mode can be derived from equilibrium equations (4.3.1), (4.4.1) and (4.4.2) by considering the relation between z and y as in (4.4.5) and the friction law in (4.3.2):

$$\ddot{\theta} = \frac{M_P}{\bar{J}_0} - \frac{N_0}{\bar{J}_0 / [S_\theta B_i (1 + \mu_k S_\theta S_{\dot{y}_b} H / B_i)]} \tag{4.5.1}$$

$$\ddot{y} = -\ddot{Y}_g + [P_y - \mu_k \frac{N_0}{\bar{J}_0 / (S_{\dot{y}_b} J_0)} - \mu_k \frac{M_P}{\bar{J}_0 / (S_\theta S_{\dot{y}_b} m_z B_i)}] / m_y \tag{4.5.2}$$

where

$$\bar{J}_0 = J_0 + m_z B_i^2 (1 + \mu_k S_\theta S_{\dot{y}_b} H / B_i) \tag{4.5.3}$$

4.5.2 Conditions to maintain slide-rocking mode

When the block is in the slide-rocking mode, the contact corner should have horizontal velocity, and the normal contact force must be positive to avoid drifting. Therefore conditions to maintain this mode are

$$\dot{y} + H\dot{\theta} \neq 0 \tag{4.5.4}$$

and

$$S_\theta \frac{M_P}{N_0} \geq -\frac{J_0}{m_z B_i} \tag{4.5.5}$$

4.5.3 Conditions to initiate slide-rocking mode

The slide-rocking mode can be initiated from the sliding mode or the rocking mode. If (4.3.9) or (4.3.10) is violated when the block changes the sliding direction, it will start to slide-rock. If the ground excitation reaches such an extent that (4.4.11) is violated for the rocking mode, it will also start to slide-rock.

To initiate the slide-rocking mode from rest, both (4.3.12) and (4.4.13) should be fulfilled. These two conditions put requests on the shape of the block, water depth, uplift, coefficient of friction and magnitude of exciting acceleration. That is to say the block will start to slide-rock from rest when all the parameters are such that both (4.3.12) and (4.4.13) are satisfied.

4.6 Drifting mode

4.6.1 Governing equations

Theoretically, it is possible that the dam loses contact with the foundation surface (see Figure 4.5) if impact happens during severe earthquakes. In this case the three degrees-of-freedom are completely independent and the governing equations become relatively simple

$$m_y(\ddot{Y}_g + \ddot{y}) - P_y = 0 \tag{4.6.1}$$

$$m_z(\ddot{z} + g) - P_z = 0 \tag{4.6.2}$$

$$J_o\ddot{\theta} - M_P = 0 \tag{4.6.3}$$

4.6.2 Condition to maintain drifting mode

To maintain this mode, both corners should be above the surface. So the condition to maintain drifting mode is

$$z - S_\theta B_i \theta \geq 0 \tag{4.6.4}$$

Once (4.6.4) is violated the block will have impacted the surface.

4.6.3 Conditions to initiate drifting mode

Because only horizontal excitation is considered in the 3-*DOF* rigid model, the drifting mode cannot be initiated from rest nor pure sliding mode. However, as discussed in the rocking and the slide-rocking modes, there are requirements to avoid loss of contact. This means that once the conditions expressed in (4.4.12) for rocking mode or (4.5.5) in the slide-rocking mode, the drifting mode will be initiated.

Of course, it will be shown in the next section that impact from the rocking mode and the slid-rocking mode may also initiate the drifting mode if vertical post-impact velocities at both corners are positive.

4.7 Impact

4.7.1 Governing equations

Impact is always expected if the rocking or slide-rocking mode occurs. Because the block is assumed rigid, impact will take no time when one or both corners of the block come into contact with the surface from above. At that instant, the rigid block changes its translation velocities and angular velocity at its position. The change can be

determined by use of momentum principle (Ishiyama, 1982; Shenton III and Jones, 1991).

Denoting the impact corner of the dam base with i, the pre-impact velocities and post-impact velocities with subscripts 1 and 2, respectively, the momentum principle can be expressed in three directions as (Shenton III and Jones, 1991)

$$\int F_y dt = m_y(\dot{y}_1 - \dot{y}_2) \tag{4.7.1}$$

$$\int N dt = m_z(\dot{z}_2 - \dot{z}_1) \tag{4.7.2}$$

$$-H\int F_y dt - B_l \int N_l dt + B_r \int N_r dt = J_o(\dot{\theta}_2 - \dot{\theta}_1) \tag{4.7.3}$$

At the instant of impact, at least one of the lower corners touches the surface with a downward vertical velocity. Therefore conditions for this mode to happen are

$$z - S_\theta B_i \theta = 0 \quad \text{and} \quad \dot{z} - S_\theta B_i \dot{\theta} < 0 \tag{4.7.4}$$

Substituting (4.7.1) and (4.7.2) and noting that

$$N = N_l + N_r$$

the momentum equation (4.7.3) for impact becomes

$$-Hm_y\dot{y}_2 + S_{\dot{\theta}_1} B_I m_z \dot{z}_2 + J_0\dot{\theta}_2 = -Hm_y\dot{y}_1 + S_{\dot{\theta}_1} B_I m_z \dot{z}_1 + J_o\dot{\theta}_1 + S_{\dot{\theta}_1} B \int N_c dt \tag{4.7.5}$$

in which N_c is the normal contact force at the rotating corner, B_I is the horizontal distance from the center of mass to the impact corner.

Momentum equation (4.7.5) has four unknowns, $\dot{y}_2$, $\dot{z}_2$, $\dot{\theta}_2$ and $\int N_c dt$. Obviously three more equations are needed to determine the post-impact terms $\dot{y}_2$, $\dot{z}_2$ and $\dot{\theta}_2$, which depend on the mode prior to impact.

4.7.2 Impact from slide-rocking mode

Approximate momentum equation

If the block is in the slide-rocking mode, both corners will contact the surface during impact and both N_l and N_r as well as N_c exist. Nevertheless, it is reasonable to assume that the vertical impulse at the rotating corner, where the vertical pre-impact velocity is zero, is much smaller than that at the impact corner (Shenton III and Jones, 1990). In this case, therefore, $\int N_c dt$ on the right side of (4.7.4) can be neglected. So the momentum equation for the impact from slide-rocking mode becomes

$$-Hm_y\dot{y}_2 + S_{\dot{\theta}_1} B_I m_z \dot{z}_2 + J_0\dot{\theta}_2 = -Hm_y\dot{y}_1 + S_{\dot{\theta}_1} B_I m_z \dot{z}_1 + J_o\dot{\theta}_1 \qquad (4.7.6)$$

Now two more equations are required, which can be acquired from the concept of restitution and the consideration of friction during impact.

Restitution equation

For the collision between two rigid balls *a* and *b*, the relative separating velocity after impact can be expressed (Kane and Levinson, 1985) in terms of the coefficient of restitution as

$$V_2^b - V_2^a = -e(V_1^b - V_1^a)$$

in which V_2^a and V_2^b are, respectively, the post-impact velocities of *a* and *b* normal to the contact surface between them, and V_1^a and V_1^b are those of pre-impact velocities. The constant *e* is the coefficient of restitution. When *e*=0, the collision is said to be inelastic; *e*=1 characterizes an idealized event termed as a perfectly elastic collision. Due to energy dissipation, the coefficient of restitution is between 0 and 1:

$$0 \le e \le 1 \tag{4.7.7}$$

Adopting this concept in the proposed rigid mode for the cracked concrete dam and noting that the normal post-impact velocity of the surface is zero, the vertical post-impact velocity at the impact corner $\dot{z}_{i2}$ for the case of impact from slide-rocking mode can be expressed in terms of e and the vertical pre-impact velocity $\dot{z}_{i1}$ at the same corner as follows:

$$\dot{z}_{i2} = -e\dot{z}_{i1} \tag{4.7.8}$$

where the pre-impact and post-impact velocities $\dot{z}_{i1}$ and $\dot{z}_{i2}$ can be expressed in terms of corresponding velocities at the center of mass:

$$\dot{z}_{i1} = -S_{\dot{\theta}_1} B\dot{\theta}_1 \tag{4.7.9}$$

Similar to (4.7.9), the pre-impact vertical velocity at the mass center is

$$\dot{z}_1 = -S_{\dot{\theta}_1} B_I\dot{\theta}_1 \tag{4.7.10}$$

The post impact vertical velocity at the impact corner can be expressed also in terms of the vertical velocity and angular velocity at the mass center:

$$\dot{z}_{i2} = \dot{z}_2 - S_{\dot{\theta}_1} B_I\dot{\theta}_2 \tag{4.7.11}$$

Substituting (4.7.9) and (4.7.11) into (4.7.8), an additional equation relating the vertical pre-impact velocity and post-impact velocity is obtained:

$$\dot{z}_2 = eS_{\dot{\theta}_1} B\dot{\theta}_1 + S_{\dot{\theta}_1} B_I\dot{\theta}_2 \tag{4.7.12}$$

Substitute (4.7.10) and (4.7.12) into (4.7.6), the governing equation for impact from slide-rocking mode now becomes:

$$-Hm_y\dot{y}_2 + (J_0 + B_I^2 m_z)\dot{\theta}_2 = -Hm_y\dot{y}_1 + [J_0 + B_I^2 m_z - (1+e)BB_I m_z]\dot{\theta}_1 \tag{4.7.13}$$

Now this momentum equation has two unknown post-impact velocities $\dot{y}_2$ and $\dot{\theta}_2$. Therefore one more additional equation is required.

Obviously the horizontal velocity $\dot{y}_2$ is related to the horizontal impulse $\int F_y dt$, in which F_y is determined by the friction law. So the last additional equation can be obtained from the friction condition as follows to determine the post-impact velocities.

With sufficient friction

If the coefficient of friction is big enough to prevent sliding during impact, the horizontal post-impact velocity at the base $\dot{y}_{i2}$ will be zero:

$$\dot{y}_{i2} = 0 \tag{4.7.14}$$

In this case the post-impact mode is rocking. Therefore the additional equation is similar to (4.4.4):

$$\dot{y}_2 = -H\dot{\theta}_2 \tag{4.7.15}$$

Substituting (4.7.15) into (4.7.13) yields the post-impact angular velocity

$$\dot{\theta}_2 = -\alpha_{\dot{y}_1}\dot{y}_1 + \alpha_{\dot{\theta}_1}\dot{\theta}_1 \tag{4.7.16}$$

where

$$\alpha_{\dot{y}_1} = \frac{Hm_y}{J_0 + B_I^2 m_z + H^2 m_y} \tag{4.7.17}$$

$$\alpha_{\dot{\theta}_1} = \frac{J_0 + B_I^2 m_z - (1+e)BB_I m_z}{J_0 + B_I^2 m_z + H^2 m_y} \tag{4.7.18}$$

From (4.7.16) it is noted that if the friction coefficient is big enough the post-impact angular velocity is linearly related to the pre-impact velocities $\dot{y}_1$ and $\dot{\theta}_1$ in the

slide-rocking mode. By examining (4.7.17) and (4.7.18), we noted that both the geometry of the block and the coefficient of restitution affect the post-impact angular velocity.

Substituting (4.7.16) into (4.7.12) and (4.7.15), the other two post-impact velocities are

$$\dot{z}_2 = \beta_{\dot{y}_1}\dot{y}_1 + \beta_{\dot{\theta}_1}\dot{\theta}_1 \tag{4.7.19}$$

$$\dot{y}_2 = H(\alpha_{\dot{y}_1}\dot{y}_1 - \alpha_{\dot{\theta}_1}\dot{\theta}_1) \tag{4.7.20}$$

In (4.7.19), the coefficients

$$\beta_{\dot{y}_1} = -\alpha_{\dot{y}_1} S_{\dot{\theta}_1} B_I \tag{4.7.21}$$

$$\beta_{\dot{\theta}_1} = S_{\dot{\theta}_1}(eB + \alpha_{\dot{\theta}_1} B_I) \tag{4.7.22}$$

- *Requirement for coefficient of friction*

Knowing that the above solutions to post-impact velocities in (4.7.17), (4.7.19) and (4.7.20) are obtained by assuming the friction is sufficient, i.e., that the following inequality must be valid during impact:

$$\left|\int F_y dt\right| \le \mu_s \left|\int N dt\right| \tag{4.7.23}$$

From (4.3.1), (4.3.2), (4.7.19) and (4.7.20), (4.7.23) becomes

$$\mu_s \ge \frac{m_y}{m_z}\left|\frac{(1-\alpha_{\dot{y}_1}H)\dot{y}_1 + \alpha_{\dot{\theta}_1}H\dot{\theta}_1}{\beta_{\dot{y}_1}\dot{y}_1 + (\beta_{\dot{\theta}_1} + S_{\dot{\theta}_1}B_i)\dot{\theta}_1}\right| \tag{4.7.24}$$

- *Consideration of impulse at the pivot corner*

The above solution to impact from the slide-rocking mode is made with the assumption that the impulse at the pivot corner is negligible. This is correct if the vertical

post-impact velocity $\dot{z}_{r2}$ at the pivot corner is positive. However, $\dot{z}_{r2}$ could be negative from (4.7.11) and (4.7.19), meaning that the pivot corner would have a downward velocity after impact. This conflict arises because of the neglect of impulse at this corner. To avoid this situation, one should ensure that $\dot{z}_{r2} \geq 0$, which results from (4.7.16) and (4.7.19):

$$S_{\dot{\theta}_1}[-\alpha_{\dot{y}_1}\dot{y}_1 + (\alpha_{\dot{\theta}_1} + e)\dot{\theta}_1] \geq 0 \tag{4.7.25}$$

If (4.7.25) is violated, the impulse $\int N_c dt$ in (4.7.5) cannot be neglected. In this case, we assume this impulse has a magnitude such that the vertical post-impact velocity at the pivot corner is zero, i.e., $\dot{z}_{r2} = 0$. This gives

$$\dot{z}_2 + S_{\dot{\theta}_1} B_i \dot{\theta}_2 = 0 \tag{4.7.26}$$

From (4.7.12), (4.7.15) and (4.7.26), we get the impact solution for the case that the impulse at the pivot corner cannot be neglected:

$$\begin{cases} \dot{y}_2 = eH\dot{\theta}_1 \\ \dot{z}_2 = S_{\dot{\theta}_1} eB_i\dot{\theta}_1 \\ \dot{\theta}_2 = -e\dot{\theta}_1 \end{cases} \tag{4.7.27}$$

The friction condition (4.7.24) now becomes:

$$\mu_s \geq \frac{m_y H}{m_z(eB_i + B)}\left| e - \frac{\dot{y}_1}{H\dot{\theta}_1} \right| \tag{4.7.28}$$

If (4.7.24) or (4.7.28) is not satisfied, the rigid block must slide during impact.

Without sufficient friction

If the block slides when the block impacts from the slide-rocking mode, the friction law determines the friction force. Therefore the two impulses in horizontal and vertical directions will have the following relation:

$$\int F_y dt = \mu_k S_{\dot{y}_{2b}} \int N dt \tag{4.7.29}$$

where $S_{\dot{y}_{2b}}$ is the sign of $\dot{y}_{2b}$, the post-impact sliding velocity at the base.

Substituting (4.7.1) and (4.7.2) into (4.7.29), the friction equation for impact will become

$$m_y \dot{y}_2 + \mu_k S_{\dot{y}_{2b}} m_z \dot{z}_2 = m_y \dot{y}_1 + \mu_k S_{\dot{y}_{2b}} m_z \dot{z}_1 \tag{4.7.30}$$

If the vertical impulse at the pivot corner is negligible, the momentum equation for impact will remain (4.7.6). Combined with the additional equations (4.7.8) and (4.7.30), solution to impact is as follows:

$$\begin{cases} \dot{y}_2 = \dot{y}_1 - (1+e)\rho\dot{\theta}_1 \\ \dot{z}_2 = [\phi + (1+e)\gamma]\dot{\theta}_1 \\ \dot{\theta}_2 = [1-(1+e)\lambda]\dot{\theta}_1 \end{cases} \tag{4.7.31}$$

where

$$\begin{cases} \lambda = \dfrac{B/B_I}{1 + J_0 / [(\mu_k S_{\dot{y}_{2b}} S_{\dot{\theta}_1} H B_I + B_I^2) m_z]} \\ \rho = \mu_k S_{\dot{y}_{2b}} S_{\dot{\theta}_1} (B - \lambda B_I) m_z / m_y \\ \phi = -S_{\dot{\theta}_1} B_i \\ \gamma = S_{\dot{\theta}_1} (B - \lambda B_I) \end{cases} \tag{4.7.32}$$

- *Requirement for coefficient of friction*

Solution (4.7.31) is valid provided the vertical post-impact velocity at the pivot corner is not negative, i.e.,

$$\dot{z}_{r2} = \dot{z}_2 + S_{\dot{\theta}_1} B_i \dot{\theta}_2 \geq 0 \tag{4.7.33}$$

This yields:

$$\mu_k \leq S_{\dot{y}_{2b}} S_{\dot{\theta}_1} \left(\frac{J_0}{HB_I} - \frac{B_i}{H} m_z\right) \tag{4.7.34}$$

(4.7.34) indicates that the solution in (4.7.31) is valid when the kinetic coefficient of friction is below a limit defined by the geometry of the block as well as its pre- and post- velocities.

- *Consideration of impulse at the pivot corner*

Similar to the case with sufficient friction, if (4.7.34) is violated, meaning that the vertical impulse at the pivot corner should be included, we again assumed that this impulse has such a magnitude that the vertical post-impact velocity at the pivot corner is zero. The corresponding solution to impact is:

$$\begin{cases} \dot{y}_2 = \dot{y}_1 - [(1+e) - B_I / B]\rho' \dot{\theta}_1 \\ \dot{z}_2 = eS_{\dot{\theta}_1} B_i \dot{\theta}_1 \\ \dot{\theta}_2 = -e\dot{\theta}_1 \end{cases} \tag{4.7.35}$$

where

$$\rho' = \mu_k S_{\dot{y}_{2b}} S_{\dot{\theta}_1} B m_z / m_y \tag{4.7.36}$$

4.7.3 Impact from rocking mode

The impact from pure rocking mode can be taken as a simpler case of that from slide-rocking mode. The only difference is that not only the vertical pre-impact velocity $\dot{z}_1$ but also the horizontal pre-impact velocity $\dot{y}_1$ depend on the angular velocity $\dot{\theta}_1$. Therefore the solution to impact from the rocking mode can be obtained from previous section 4.7.2 simply by introducing the relationship

$$\dot{y}_1 = -H\dot{\theta}_1 \tag{4.7.37}$$

4.7.4 Impact from drifting mode

If the block impacts the surface from the drifting mode, there will be two cases: one-corner impact and two-corner impact. For one-corner impact, the vertical impulse exists only at this corner, and two more equations are needed in addition to the three momentum equations (4.7.1.), (4.7.2) and (4.7.3). For two-corner impact, both corners have impulses. Therefore three additional equations should be provided.

One-corner impact

In this case, momentum equations (4.7.1) and (4.7.2) remain. Knowing that only one corner has impulse, we can modify the angular momentum (4.7.3) as

$$J_o\dot{\theta}_2 + H\int F_y dt + S_o B_i \int N dt = J_o\dot{\theta}_1 \tag{4.7.38}$$

The restitution equation remains as (4.7.8). Another additional equation comes from the consideration of friction as in the case of impact from slide-rocking mode.

- *With sufficient friction*

If there is no sliding during impact, the horizontal post-impact velocity will be zero. Therefore the governing equations for one-corner impact from the drifting mode with sufficient friction can be deduced by substituting (4.7.1) and (4.7.2) into (4.7.38) and considering (4.7.8) and (4.7.14):

$$\begin{cases} -m_y H\dot{y}_2 + S_\theta B_i m_z \dot{z}_2 + J_0\dot{\theta}_2 = -m_y H\dot{y}_1 + S_\theta B_i m_z \dot{z}_1 + J_0\dot{\theta}_1 \\ \dot{z}_2 - S_\theta B_i\dot{\theta}_2 = -e(\dot{z}_1 - S_\theta B_i\dot{\theta}_1) \\ \dot{y}_2 + H\dot{\theta}_2 = 0 \end{cases} \tag{4.7.39}$$

The corresponding solution to (4.7.39) is

$$\begin{cases} \dot{y}_2 = -\omega_{\dot{y}_1}\dot{y}_1 - \omega_{\dot{z}_1}\dfrac{H}{B_i}\dot{z}_1 - \omega_{\dot{\theta}_1}H\dot{\theta}_1 \\ \dot{z}_2 = S_\theta\omega_{\dot{y}_1}\dfrac{B_i}{H}\dot{y}_1 + (S_\theta\omega_{\dot{z}_1} - e)\dot{z}_1 + S_\theta B_i(\omega_{\dot{\theta}_1} + e)\dot{\theta}_1 \\ \dot{\theta}_2 = \omega_{\dot{y}_1}\dfrac{\dot{y}_1}{H} + \omega_{\dot{z}_1}\dfrac{\dot{z}_1}{B_i} + \omega_{\dot{\theta}_1}\dot{\theta}_1 \end{cases} \tag{4.7.40}$$

in which

$$\begin{cases} \omega_{\dot{y}_1} = m_y H^2 / J_0' \\ \omega_{\dot{z}_1} = S_\theta B_i^2 m_z / J_0' \\ \omega_{\dot{\theta}_1} = (J_0 - eB_i^2 m_z)/J_0' \end{cases} \tag{4.7.41}$$

where

$$J_0' = J_0 + m_y H^2 + m_z B_i^2 \tag{4.7.42}$$

To make sure the solution (4.7.40) is valid, the friction condition (4.7.23) must be satisfied. Otherwise, the block slides during impact of the surface with one corner.

- *Without sufficient friction*

In this case, the first two governing equations in (4.7.39) remain. The third governing equation will be replaced by (4.7.30) which considers the friction law. The corresponding solution is

$$\begin{cases} \dot{y}_2 = \dot{y}_1 + \mu_k S_{\dot{y}_{2b}} \dfrac{m_z}{m_y} \dfrac{(1+e)\delta}{1+\delta} (\dot{z}_1 - S_\theta B_i \dot{\theta}_1) \\ \dot{z}_2 = \dfrac{1-e\delta}{1+\delta} \dot{z}_1 + S_\theta B_i \dfrac{(1+e)\delta}{1+\delta} \dot{\theta}_1 \\ \dot{\theta}_2 = S_\theta \dfrac{1+e}{(1+\delta)B_i} \dot{z}_1 + \dfrac{\delta - e}{1+\delta} \dot{\theta}_1 \end{cases} \tag{4.7.43}$$

where

$$\delta = \frac{J_0}{(\mu_k S_{\dot{y}_{2b}} S_\theta H + B_i) B_i m_z} \tag{4.7.44}$$

Obviously, solution (4.7.43) is valid when (4.7.23) is violated.

Two-corner impact

If $\theta = 0$ when the block impacts the surface from the drifting mode, both lower corners will have impulses in both directions. Considering the restitution equations at both corners as well as the friction condition, we have three equations to determine post-impact velocities.

- *With sufficient friction*

Applying (4.7.8) to both corners and noting (4.7.14), we have the governing equations

$$\begin{cases} \dot{z}_2 - B_l\dot{\theta}_2 = -e(\dot{z}_1 - B_l\dot{\theta}_1) \\ \dot{z}_2 + B_r\dot{\theta}_2 = -e(\dot{z}_1 + B_r\dot{\theta}_1) \\ \dot{y}_2 + H\dot{\theta}_2 = 0 \end{cases} \tag{4.7.45}$$

The corresponding solution for which is

$$\begin{cases} \dot{y}_2 = eH\dot{\theta}_1 \\ \dot{z}_2 = -e\dot{z}_1 \\ \dot{\theta}_2 = -e\dot{\theta}_1 \end{cases} \tag{4.7.46}$$

This solution is valid provided that (4.7.23) is satisfied. Otherwise, the block will slide during impact, which is the case without sufficient friction.

- *Without sufficient friction*

If (4.7.23) is violated, it means that friction is insufficient to prevent the block from sliding during impact. In this case, the first two equations in (4.7.45) remain, and the third equation will be replaced by (4.7.30) which relates the friction and normal forces according to the friction law. The corresponding solution to the post-impact velocities is

$$\begin{cases} \dot{y}_2 = \dot{y}_1 + \mu_k S_{\dot{y}_{2b}} \dfrac{m_z}{m_y}(1+e)\dot{z}_1 \\ \dot{z}_2 = -e\dot{z}_1 \\ \dot{\theta}_2 = -e\dot{\theta}_1 \end{cases} \tag{4.7.47}$$

4.8 Remarks

Owing to the basic assumptions in section 4.2.3, the proposed 3-*DOF* model can be analytically solved for sliding, rocking, slide-rocking and drifting modes. Regarding impact, the solution relies on the two additional assumptions: one is the restitution equation, which is adopted from the collision between two rigid balls; another is either assuming that the vertical impulse at the pivot corner is negligible, or this impulse is such that the post-impact vertical velocity at this corner is zero.

This means we do not have enough equations to describe the post-impact status of a rigid block, owing to the fundamental assumption of being rigid. Therefore the solution for impact is an estimation based on the additional assumptions. This implies that more proper approaches, which involve the deformation of the block, may handle the impact issue better for a cracked concrete dam.

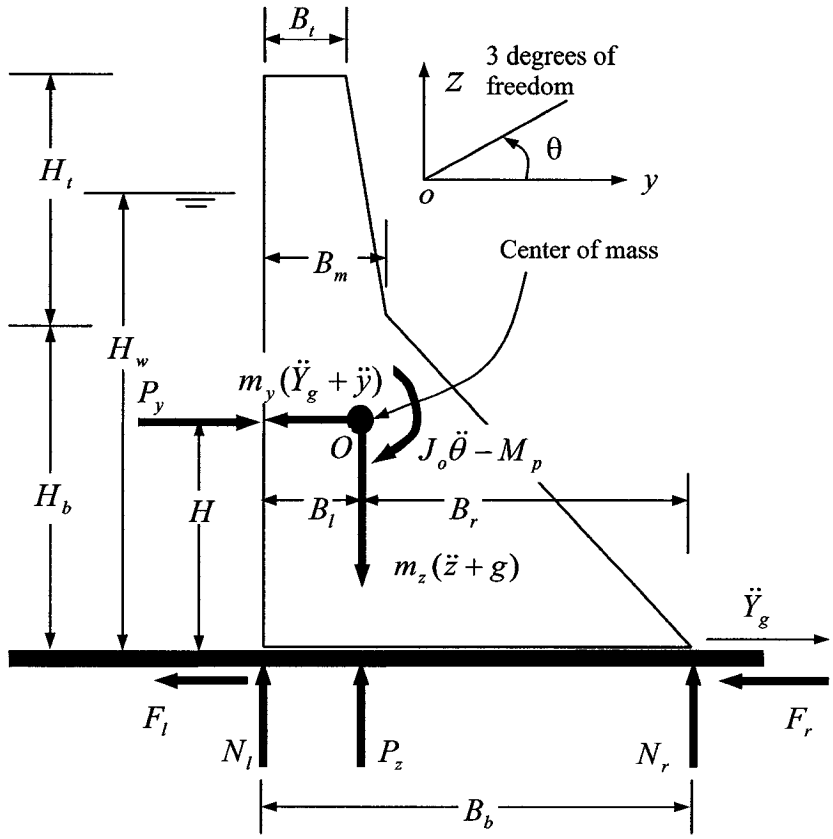

Figure 4.1 3-*DOF* rigid model

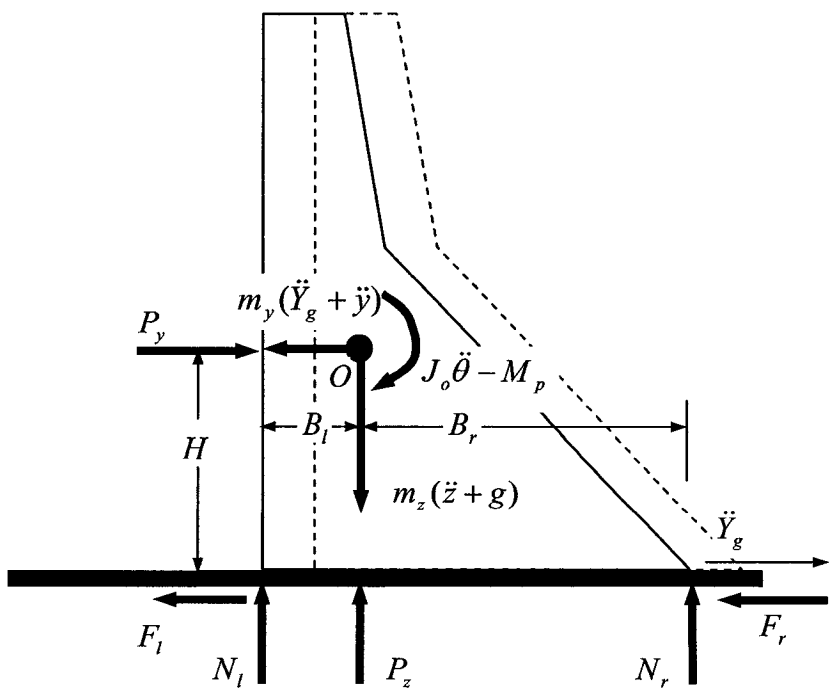

Figure 4.2 3-*DOF* rigid model: pure sliding

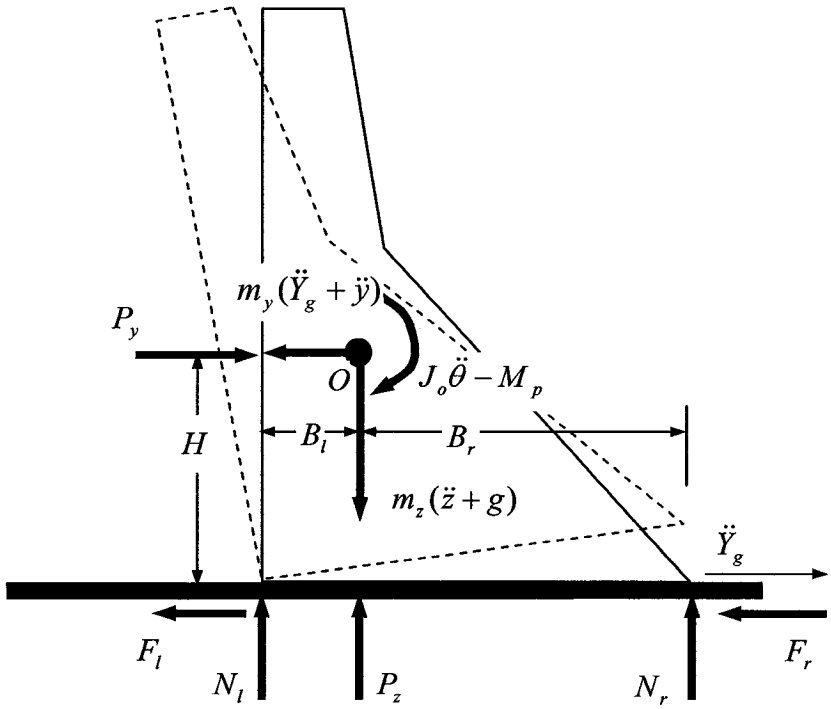

Figure 4.3 3-*DOF* rigid model-pure rocking

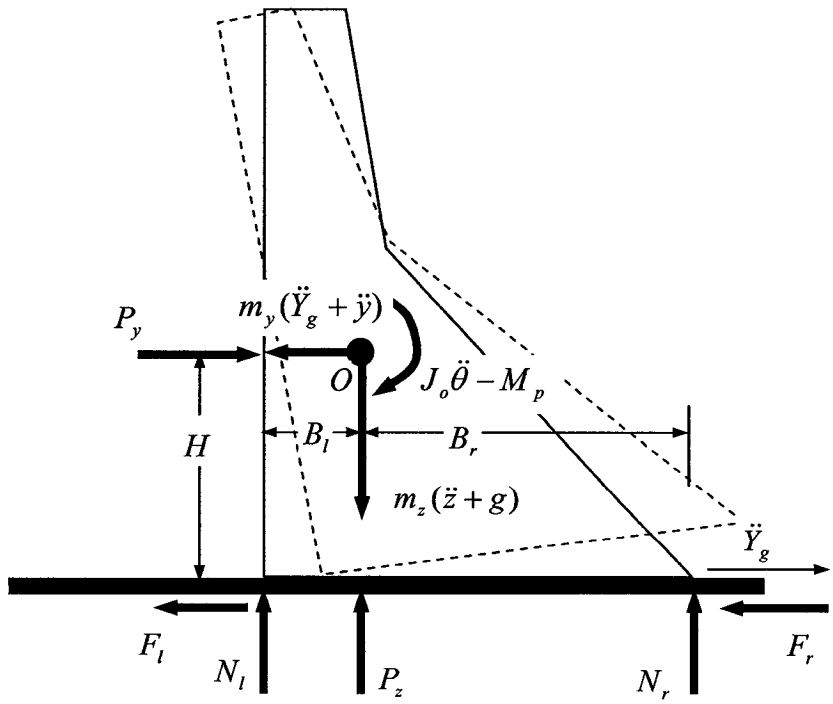

Figure 4.4 3-*DOF* rigid model: slide rocking

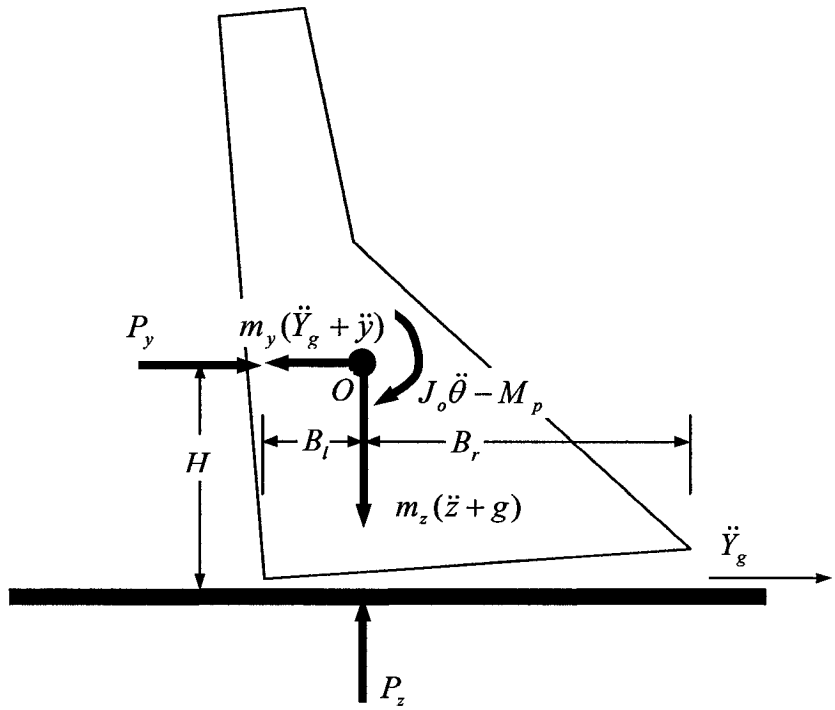

Figure 4.5 3-*DOF* rigid model: drifting

CHAPTER V

3-*DOF* RIGID MODEL: VERIFICATIONS AND APPLICATIONS

5.1 Introduction

The 3-*DOF* rigid model described in the last chapter is developed based on the rectangular rigid model (Shenton III and Jones, 1991). Due to the generality of the geometry shape of the dam as well as the change between modes such as rest, sliding, rocking, slide-rocking, drifting and impact, the solution procedure becomes very complex. To implement this model, a program *SAD-R* (Seismic Analysis of cracked concrete Dam with Rigid model) was developed. This chapter will verify through some examples the validity of this rigid model, and then apply it to analyze the seismic behavior of cracked concrete dams.

5.2 Verification of sliding mode with a rectangular block

To verify the pure sliding mode, a 1×1 meter square block shown in Figure 5.1 was studied. This block rests on a rigid surface with coefficient of friction of 0.2. Therefore the requirement of ground acceleration to initiate sliding from (4.3.12) is

$$\ddot{Y}_g \geq 0.2g$$

From (4.3.14), the requirement for coefficient of friction to avoid rocking becomes

$$\mu_s \leq 1$$

Therefore this block will slide without rocking. Two cases of sliding were tested. One is the sudden impulse movement of the surface shown in Figure 5.2, which causes sliding in

one direction. The other one is the periodic excitation of a sine wave from the surface illustrated in Figure 5.3, which causes the block to slide back and forth on the surface.

5.2.1 Subjected to a sudden impulse

Because the constant acceleration in Figure 5.2 is $0.8g$, the block will start to slide at the beginning of the impulse. Then the block will keep sliding until it stops without rocking. Actually, the theoretical solution to this problem can be deduced from following equation:

$$\ddot{y} + \ddot{Y}_g + 0.2 S_{\dot{y}_b} g = 0 \tag{5.1}$$

According to the initial conditions:

$$\begin{cases} \dot{y}(0) = 0 \\ y(0) = 0 \end{cases}$$

the solution can be obtained as below:

$$\begin{cases} y = -0.3gt^2, & 0 \le t < 0.1s \\ y = 0.1gt^2 - 0.08gt + 0.004g, & 0.1s \le t < 0.4s \\ y = 0, & t \ge 0.4s \end{cases}$$

Figure 5.4 illustrates the sliding of this block due to the sudden impulse. The result by the 3-*DOF* is exactly the same as the above theoretical solution.

5.2.2 Subjected to a sinusoidal excitation

Differing from the case of impulse in only one direction as in Figure 5.2, Figure 5.3 shows a sinusoidal excitation:

$$\ddot{Y}_g = 0.5g\sin(\frac{\pi}{0.2}t)$$

Substitute this ground acceleration into (5.1), the solution for sliding and its velocity can be derived as

$$\begin{cases} \dot{y} = 0.1g[\frac{1}{\pi}(\cos\frac{\pi}{0.2}t - \cos\frac{\pi}{0.2}t_p) - 2S_{\dot{y}_b}(t-t_p)] \\ y = \frac{g}{50\pi^2}(\sin\frac{\pi}{0.2}t - \sin\frac{\pi}{0.2}t_p) - \frac{g}{10}(t-t_p)[\frac{1}{\pi}\cos\frac{\pi}{0.2}t_p + S_{\dot{y}_b}(t-t_p)] + y_p \end{cases} \quad (5.2)$$

in which y_p and t_p, are respectively, the sliding and corresponding time when sliding velocity is zero. t is the time following t_p which can be determined as

$$t_p = \begin{cases} 0.026198s \\ 0.261845s \\ 0.454995s \\ 0.657297s \\ 0.856571s \\ 1.056805s \\ 1.256730s \\ 1.456755s \end{cases}$$

The sliding from the proposed 3-*DOF* model also is exactly the same as expressed in (5.2) plotted in Figure 5.5.

5.3 Verification of rocking mode with rectangular blocks

5.3.1 Rectangular block with large slenderness (*H/B*)

A rectangular block with slenderness of 3.0 and coefficient of friction of 1.0, as shown in Figure 5.6 is studied. This block is subject to the same impulse shown in Figure 5.2. From the conditions in (4.4.13) and (4.4.14), both ground acceleration and static coefficient of friction fulfill the requirements to initiate rocking without sliding. Substituting all the parameters into (4.4.11) we know this block will maintain the mode of rocking in the process.

To verify the rocking mode, the block was also studied with *ADINA* (1999). For *ADINA*, the modulus $E = 20\,\text{GPa}$, $\nu = 0$, $\rho = 2650\,\text{kg/m}^3$, and the damping effect was neglected. It was noted that time step of 0.0001 seconds gave almost the same results as 0.00005 seconds, but quite different from 0.0002 seconds. Therefore 0.00005 seconds was chosen for the time step.

The rocking results of the block by the proposed 3-*DOF* rigid model and by *ADINA* are plotted in Figure 5.7. Figure 5.8 illustrates the mode of motion during the process. It is shown from Figure 5.7 that the 3-*DOF* rigid model with coefficient of restitution of 0.5 can describe the rocking of the block with satisfactory accuracy compared with complex finite element analysis. The effectiveness of the coefficient of restitution will become considerable after several impacts happen. Figure 5.8 also indicates that the block will drift for a period of time after each impact. It is worthy to mention that the corresponding *ADINA* analysis is not only time consuming for calculation and data preparation but also needs many trial and error attempts, as it is very

hard to get the result to converge. On the contrary, the proposed 3-*DOF* rigid model just spends a few seconds to carry out the computation.

From Figure 5.7, it is clear that the block with large aspect ratio keeps its direction of rocking after impact, which means that the rotation corner alters but the angular velocity remains. This coincides with the laboratory test of Aslam *et al.* (1980). The rocking response also shows that the coefficient of restitution affects the response but not by much. The difference for e=0.5 and e=0.9 is not differentiable until several impacts have occurred. This fact was also reported by Yim *et al.* (1980), i.e., the effect of coefficient of restitution for a block with large aspect ratio can be neglected.

5.3.2 Rectangular block with small slenderness (*H/B*)

For a block with small slenderness as shown in Figure 5.9, it is likely to change its direction of rocking after impact. Contrary to the case of large slenderness, the block maintains its corner of rotation and rocks in the opposite direction after impact. To initiate the block in Figure 5.9 to rock before sliding, an impulse similar to that in Figure 5.2 with the change of acceleration to 2.0g is applied. In the case of small slenderness, the coefficient of restitution will be crucial to determine the post-impact velocities.

In the case of slender block the coefficient $\alpha_{\dot{\theta}_1}$ in (4.7.18) is positive, and the angular velocity will maintain its direction. However, in the case of small slenderness, the impact will change the direction of angular velocity of the block.

Figure 5.10 illustrates the rocking of the block in Figure 5.9 from *SAD-R* (with e=0.5) as well as from *ADINA* (damping is neglected). Calculations show that the coefficient of restitution determines the post impact behavior of the block. Only with

properly selected coefficient of restitution can the rigid model adequately estimate the rocking-impact behavior of the block. And the block will change its rocking direction, regardless the value of coefficient of restitution, as assumed in the overturning study of Saini and Krishna (1974).

Figure 5.11 indicates that the block also experiences drifting motion after impact as in the case of large slenderness. The *ADINA* calculation also shows this phenomenon of drifting, which is indicated as straight segments in the curve. The drifting period becomes shorter and shorter, and then the block resumes at the end its status of rest.

5.4 Application to a triangular dam

As an application of the 3-*DOF* rigid model, an idealized triangular concrete dam (Chopra and Zhang, 1991) with full reservoir of water is studied. Figure 5.12 shows the dam, which is assumed to be cracked at the base. The height of the dam h is 100 meters. The width at the base B is 80 meters. The density of the water ρ_w is 1000 kg/m^3. The density of the dam ρ_d is 2430 kg/m^3. The coefficient of friction at crack is 1.0. The uplift pattern is cut-off triangular. The sliding of the dam excited by Taft S69E ground motion scaled to 0.5g of peak acceleration is illustrated in Figure 5.13, which is the same as the results by Chopra and Zhang (1991).

Calculation shows that this cracked dam will not rock under the given conditions. Therefore the coefficient of restitution has no effect on the response and only the sliding mode is initiated. This may be the reason that many researchers suggested to neglect rocking mode in estimation of the sliding in a dam cracked at the base.

However, strong ground motion may cause the cracked dam to rock if the aggregate interlock at the crack provides even higher effective coefficient of friction. Figure 5.14 and 5.15 illustrate sliding and rocking responses, respectively, of the same dam with $\mu_s = \mu_k = 1.4$ and $e = 0.75$ due to the same Taft S69E earthquake scaled to $0.8g$ of peak value of ground motion.

Figure 5.14 shows that the cracked dam will rock but the magnitude is quite small. The peak rotation is just 2.15×10^{-5} radians, and the corresponding gap at the upstream face is just 1.72 mm. However, this rocking affects the so-called sliding, which is actually the accumulated horizontal displacement in the modes of sliding, slide-rocking and drifting. The overall sliding and its components in the different modes are shown in Figure 5.15.

From Figure 5.15 we can see that rocking and slide-rocking modes may happen for a cracked dam in some circumstances. Ignoring the rocking and slide-rocking modes may under estimate the overall sliding of cracked dam. In Figure 5.15, the components of slide-rocking mode and drifting mode comprise 24.8% and 44.8%, respectively, of the overall horizontal displacement.

Because of the effect of aggregate interlock at the crack, it is hard to believe that the cracked dam will drift when the opening of the crack is as small as a few millimeters. However, the interlock effectiveness at the crack must be lessened, as the drifting intention of the block above the crack will cause horizontal impact, hence damaging the interlock at the crack. Therefore the effectiveness of the coefficient of friction will be lessened as a consequence and more sliding will be induced.

5.5 Application to cracked Koyna Dam

5.5.1 Introduction to Koyna Dam and its overturning study

The Koyna Dam in India, as shown in Figure 3.1, cracked in its highest non-overflow monolith at the level where there was an abrupt change in the downstream slope. During the severe earthquake on December 11, 1967 its epicenter was very close to the dam site. The stability of the top profile of this monolith of the dam above the crack was of concern, because it may rock during aftershocks as a free body without any restraint except aggregate effect at the crack surface. With the hydraulic pressure and uplift pressure, there exists a possibility that the upper part rocks, impacts and even drifts if the rock is substantial.

Saini and Krishna's study (1974) showed that the upper part is safe against overturning. This means that the upper part will rock but within limited angle and will not overturn. These results were obtained based on following assumptions:

Rigid assumption. The top profile of the monolith was treated as a rigid body and the mass was assumed to be concentrated at its center of gravity and treated as a point mass. The crack surface was also assumed to be rigid.

No sliding. The friction at the crack level between the upper and lower parts of the monolith is sufficient that no sliding of the top profile would take place. The coefficient of friction at the cracked concrete surface was expected to be larger than 1.0 because of the aggregate interaction.

Just rocking. The only possible mode of motion was rocking. The possibility of drifting due to impact was ignored. The virtual mass of water was assumed to be acting at

the center of gravity of the rigid body, that is, at a point which is at a higher elevation than the actual point of action to obtain rocking on the conservative side.

Impact assumption. For impact, the following assumption was used:

$$\dot{\theta}\,(\text{after impact}) = -e\dot{\theta}\,(\text{before impact}) \qquad (5.3)$$

This assumption is identical to the last equation in (4.7.27). This means it was assumed that the pivot corner has such an impulse that its vertical post-velocity is always zero. Therefore the upper portion will keep its corner of rotation once it starts to rock. The crack will open and close at either upstream face or downstream face till rocking stops. The corner of rotation may change only when the rocking stops and another rocking is initiated with respect to other corner (as indicated in Figure 5.18).

Uniformed uplift pressure. The uplift pressure was 100 per cent water pressure throughout the crack. Although this assumption is not practical, it was believed to yield a conservative rocking.

Considering only horizontal vibration at the crack level. The crack level will vibrate horizontally, vertically and rotationally under the excitation of transverse component of the earthquake. However, only the horizontal component of motion at the crack level was considered.

Records of both components of the earthquake are shown in Figures 5.16 and 5.17 were used to study the stability of the top profile of the highest monolith. The vibrations transmitted at the crack level, which excited the top part, was obtained by considering the lower part as a non-uniform cantilever beam fixed at the base and with a concentrated mass attached at the crack to represent the effect of the top part. The damping ratio is 10 percent of the critical damping.

The rocking response by Saini and Krishna is shown in Figure 5.18. The study indicated that cracked monolith of Koyna Dam will not overturn under severe earthquake ground motion and that Koyna Dam would be stable under similar aftershocks.

5.5.2 Approach to analyze the stability of Koyna Dam in present study

In the present study, a similar approach is adopted. The differences are in that:

Vibration at the crack level is obtained by finite element method. The vibration at the crack level due to the ground motion is obtained by finite element method with *ADINA*, which uniformly attaches along the crack the mass of the upper portion of the cracked dam and distributes along the upstream face the virtual mass of the water. Besides the transverse component of Koyna earthquake shown in Figure 5.16, the longitudinal component of the earthquake shown in Figure 5.17 was also imposed independently in the transverse direction in order to consider possible stronger ground motion.

Horizontal responses of acceleration at the crack level due to both the components applied in the transverse direction are respectively illustrated in Figure 5.19 and 5.20

Three values of coefficient of friction are tested. Three values 0.8, 1.0 and 1.2 for coefficient of friction at the crack are adopted to study the effectiveness of this parameter on the response. 0.8 is used as the lower limit of the coefficient of friction at the crack to check the upper limit of sliding. 1.2 is used as the upper limit of the coefficient of friction to check the lower limit of sliding.

Two patterns of uplift pressure are adopted. Uniform uplift pressure is adopted to compare with Saini and Krishna's results. Considering the geometry of the upper part

of the cracked monolith, it is noted that the resultant of a uniform uplift pressure will provide a counter clockwise moment with respect to the center of the mass. This moment will decrease the rocking in the downstream direction. Therefore, a triangular uplift pressure, which is considered more practical, will result in a clockwise moment increasing the downstream rocking. So the triangular uplift pressure is also employed for the purpose of comparison.

5.5.3 Analysis of the responses of the upper part of the cracked monolith

Seismic behavior of the upper part of the cracked monolith is studied with the proposed 3-*DOF* rigid model and summarized in Table 5.1 for two components of earthquake, two patterns of uplift pressure and three coefficients of friction. From these responses, we can analyze the behavior of the cracked dam and judge its stability for both overturning and sliding.

The upper part is safe in overturning for all considered cases. Calculations show that the upper part stops rocking after the excitation transmitted from the crack vanishes for all considered cases. From Table 5.1, the largest downstream rocking is 0.0142 radians and occurs in the case of longitudinal earthquake component, uniform uplift pressure and coefficient of friction 1.0. The largest upstream rocking 0.00586 radians happens in the same case. The corresponding openings of the crack are 289.5 *mm* and 119.3 *mm* at upstream and downstream faces, respectively. As shown in Figure 5.21 for this case, these two peak rotations occur just once. The rocking declines very quickly as the excitation at the crack level stops due to damping and impact.

The upper part is likely to rock more in downstream direction than in upstream direction. Because of the hydraulic pressure, the upper part is likely to rock more in the downstream direction. For instance as shown in Figure 5.22, the peak rocking in the downstream direction for the longitudinal component with triangle uplift pressure is 0.00264, 0.00294 and 0.00291 for coefficient of friction 0.8, 1.0 and 2.0, respectively. And the corresponding peak rocking in upstream direction is 0.00134, 0.00119 and 0.00119 radians, respectively. The same phenomenon is noted for other cases except in the case of transverse component of earthquake with unrealistic uniform uplift pressure.

The upper part changes its corner to rock after impact. Comparing the present results shown in Figure 5. 21 and 5.22 with Figure 5.18, it is found that the proposed 3-*DOF* rigid model predicts completely different pattern of rocking from Saini and Krishna (1974) for the upper part of the cracked monolith.

All calculations show that the upper part rocks in a pattern that it changes its corner of rocking after impact. The crack opens and closes at upstream face and downstream face alternatively. This is due to the property of the 3-*DOF* rigid model that is able to determine the post impact velocities for translations and rotation according to the geometric shape of the dam and its pre-impact status, which is different from the assumed relationship between the post and pre- impact velocities as expressed in (5.3).

Longitudinal component induces larger rocking. From Table 5.1, it is noted that the longitudinal component induces larger rocking than transverse component for all coefficients of friction. For instance, in the case of triangular uplift pressure and coefficient of friction of 1.2, the downstream (clockwise) peak rocking for the transverse component is 7.7×10^{-4} radians. The same term for the longitudinal component is

29.1×10^{-4} radians. The corresponding upstream (counter clockwise) peak rocking are 5.7×10^{-4} radians and 11.9×10^{-4} radians, respectively, for transverse and longitudinal components.

Larger coefficient of friction generally induces larger rocking. According to Table 5.1 and Figure 5.21, larger coefficient of friction induces larger rocking. The peak rocking for coefficient of friction of 0.8 is less than that for 1.0 and 1.2 in both directions except the upstream direction rocking in the case of triangular uplift pressure and longitudinal component of earthquake. But for larger coefficients of friction, 1.0 and 1.2, it is not consistent. In downstream direction the peak rocking for coefficient of friction 1.0 is larger than that for coefficient of friction 1.2 except in the case of triangular uplift pressure and transverse component of earthquake. These indicate that rocking of the upper part is not always consistent with the coefficient of friction because of the non-linearity of the dynamic contact features.

Uniform uplift pressure doesn't necessarily yield larger rocking. For coefficient of friction 1.0 and 1.2, if the longitudinal record is applied, the uniform uplift pressure really yields larger rocking in both directions than the triangular uplift pressure. However, it is just the opposite for coefficient of friction 0.8. For the case that transverse component is considered, uniform uplift pressure gives less rocking for coefficient of friction 0.8 and 1.2.

The inconsistency arises from the non-linearity of the problem and the fact that the uniform uplift pressure results in a counter clockwise moment but the triangular uplift pressure results in a clockwise moment. Whether or not the chosen uplift pattern will yield conservative rocking depends on in which direction that the upper part rocks.

Large coefficient of friction cannot prevent the upper part from "sliding". Figure 5.23 shows the horizontal displacement for coefficient of friction 1.2. From Figure 5.23 as well as the summary in Table 5.1 for residual sliding, it is noted that the upper part will slide to downstream for all cases due to hydraulic pressure. The residual sliding of the upper part can be 342.4 *mm* even if the coefficient of friction is as large as 1.2 in the case of longitudinal component of earthquake and uniform uplift pressure. In the more realistic case of triangle uplift pressure, the corresponding residual sliding is still 164.5 *mm*. This means the upper part of the cracked monolith can move downstream under strong excitation.

This phenomenon is due to the fact that although the aggregate interlock can prevent the upper part from sliding, as indicated in Table 5.1 that there is no pure sliding for coefficient of friction 1.2. Other modes of motion, like rocking, will reduce the normal contact force so that the upper part may slide while it rocks back to impact the surface. The more severe case is when both corners acquire upward velocities after impact and the upper part enters into the mode of drifting under hydraulic pressure.

Longitudinal component induces larger residual sliding than transverse component. Figure 5.23 shows clearly that longitudinal component induces much larger residual sliding than the transverse component. This is consistent for all coefficient of friction. For instance, in the case of coefficient of friction 1.0 with triangular uplift pressure, the residual sliding are 195.7 *mm* and 39.1 *mm*, respectively, for longitudinal and transverse components.

Larger coefficient of friction generally induces less residual sliding. Except in the case of transverse component with triangular uplift pressure, it is quite obvious that

larger coefficient of friction induces less residual sliding. In the case of longitudinal component of earthquake with triangular uplift pressure, for example, Figure 5.24 and Table 5.1 indicate that the residual sliding for coefficient of friction 0.8, 1.0 and 1.2 are 669.5 *mm*, 195.7 *mm* and 164.5 *mm*, respectively.

However, due to the non-linearity of the problem, impact may cause inconsistency for residual sliding. For instance, in the case of transverse component with triangular uplift pressure, the coefficient of friction 1.0 gives 39.1 *mm* residual sliding, which is less than the corresponding value 41.5 *mm* for coefficient of friction 1.2.

Sliding component decreases and drifting component increases as coefficient of friction increases. It is common sense to expect that the sliding displacement decrease as the coefficient of friction increase. If the aggregate interlock is very effective, the effective coefficient of friction can be larger than 1.0. Therefore it is quite natural to suggest that the sliding mode could be neglected for the case that aggregate interlock at the crack surface is high, as assumed in Saini and Krishna's study (1974).

However, in the situations such as the cracked Koyna Dam when rocking is unavoidable, residual sliding, which comprises horizontal displacements in sliding mode, slide-rocking mode and drifting mode, will be occur even if an impractical high coefficient of friction is adopted. The reasons are that rocking can lessen the normal contact force to cause the upper part to slide and that impact may cause it to drift. Figure 5.25 illustrates the components of horizontal displacement from different modes for the case that transverse component of the earthquake is used with triangle uplift pressure and coefficient of friction 0.8.

From Table 5.1, it is noted that the pure sliding mode never happens for coefficient of friction 1.0 and 1.2. The component of slide-rocking mode decreases as the coefficient of friction increases but does not vanish even if the coefficient of friction is as high as 1.2. This means that rocking reduces the normal contact force and this causes the upper part to slide while rocking.

The component of the drifting mode in the residual sliding increases consistently as the coefficient of friction increases. For longitudinal component with triangular uplift, the drifting mode contributes to the residual sliding 41.7%, 80.3% and 92.0% for coefficient of friction 0.8, 1.0 and 1.0, respectively.

5.5.4 Conclusions about the stability of cracked Koyna Dam

According to the above discussion and taking the triangular uplift pressure as realistic, we can conclude as follows:

The upper part of the cracked monolith will remain stable if the same earthquake as the Koyna earthquake of 1967 occurs again. The longitudinal earthquake component with larger peak acceleration than the transverse component will induce larger but limited rocking, which causes about 60 *mm* and 24 *mm* openings at upstream and downstream faces, respectively.

The aggregate effect at the crack surface cannot prevent the upper part from moving in the downstream direction. The upper part may slide while rocking or drifting after severe impact. The downstream residual sliding will be less than 200 *mm* if the aggregate effect provides an effective coefficient of friction no less than 1.0.

Table 5.1 Summary of the response of the upper part of the monolith of cracked Koyna Dam by 3-*DOF* rigid model (e=0.5)

Earthquake component		Transverse						Longitudinal					
Uplift pattern		Uniform			Triangular			Uniform			Triangular		
Coefficient of friction		0.8	1.0	1.2	0.8	1.0	1.2	0.8	1.0	1.2	0.8	1.0	1.2
Peak rocking (10^{-4} rad)	Downstream	1.7	23.1	4.3	6.3	7.6	7.7	16.5	142	137	26.4	29.4	29.1
	Upstream	2.4	13.2	6.1	3.9	6.0	5.7	7.2	58.6	60.4	13.4	11.9	11.9
Open (mm)	Upstream face	3.4	47.1	8.8	12.9	15.4	15.6	33.6	289.5	280.1	53.7	55.9	60.4
	Downstream face	4.9	26.9	12.5	7.9	12.2	11.6	14.8	119.3	123.0	27.3	24.4	24.4
Residual sliding (mm)		211.1	131.6	92.3	233.1	39.1	41.5	1687.9	701.7	342.4	669.5	195.7	164.5
Components of displacement (mm) and %	Sliding mode	71.0 33.6%	0.0 0.0%	0.0 0.0%	6.2 2.7%	0.0 0.0%	0.0 0.0%	441.4 26.2%	0.0 0.0%	0.0 0.0%	36.4 5.4%	0.0 0.0%	0.0 0.0%
	Slide-rocking mode	81.1 38.4%	43.1 32.8%	0.7 0.8%	153.6 65.9%	1.4 3.6%	1.2 2.9%	918.4 54.4%	241.4 34.4%	35.0 10.2%	353.9 52.9%	38.6 19.7%	13.2 8.0%
	Drifting mode	58.9 27.9%	88.5 67.2%	91.6 99.2%	73.3 31.4%	37.7 96.4%	40.3 97.1%	328.0 19.4%	460.3 65.6%	307.4 89.8%	279.2 41.7%	157.1 80.3%	151.3 92.0%

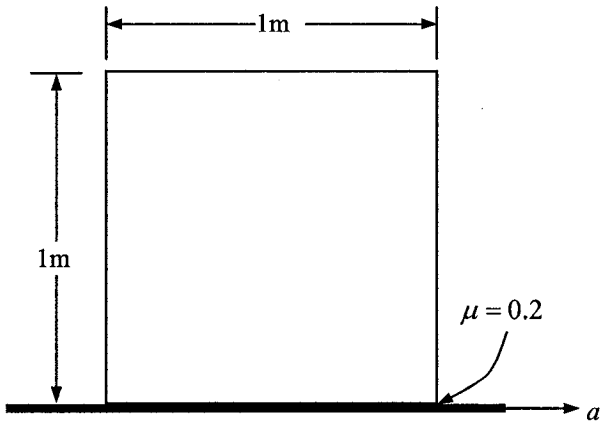

Figure 5.1 Square block

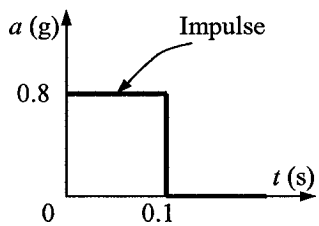

Figure 5.2 Sudden impulse

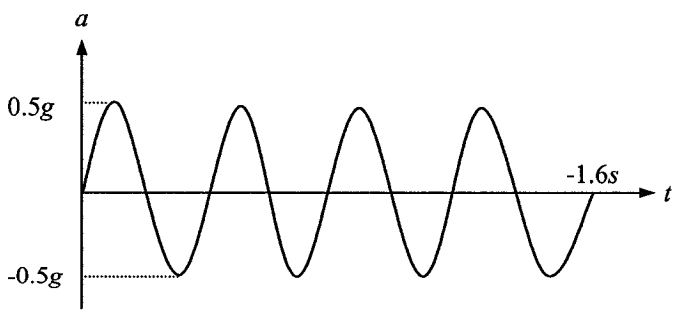

Figure 5.3 Periodic excitation of sinusoidal wave

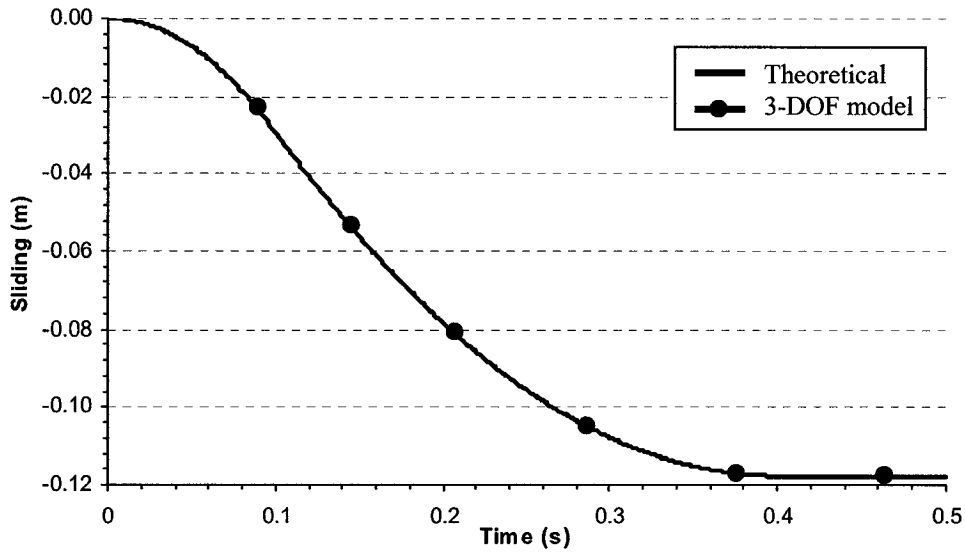

Figure 5.4 Sliding of the square block due to 0.8*g* sudden impulse

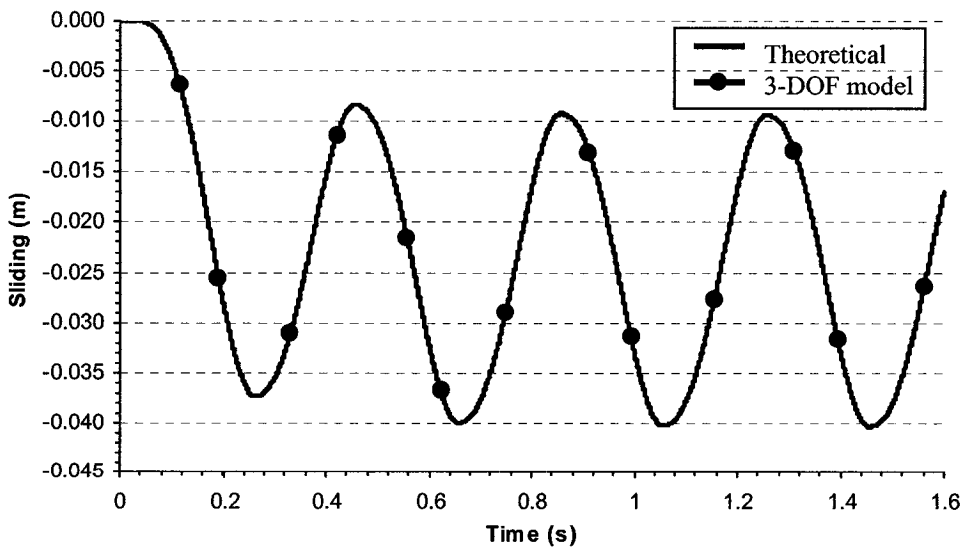

Figure 5.5 Sliding of the square block due to periodic excitation of sinusoidal wave

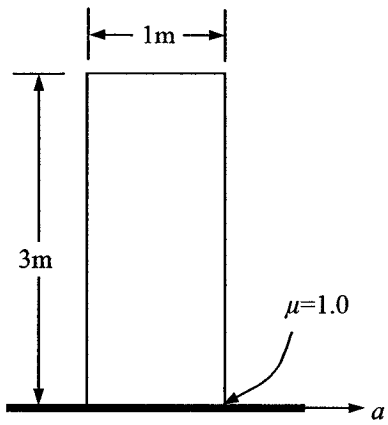

Figure 5.6 High-block

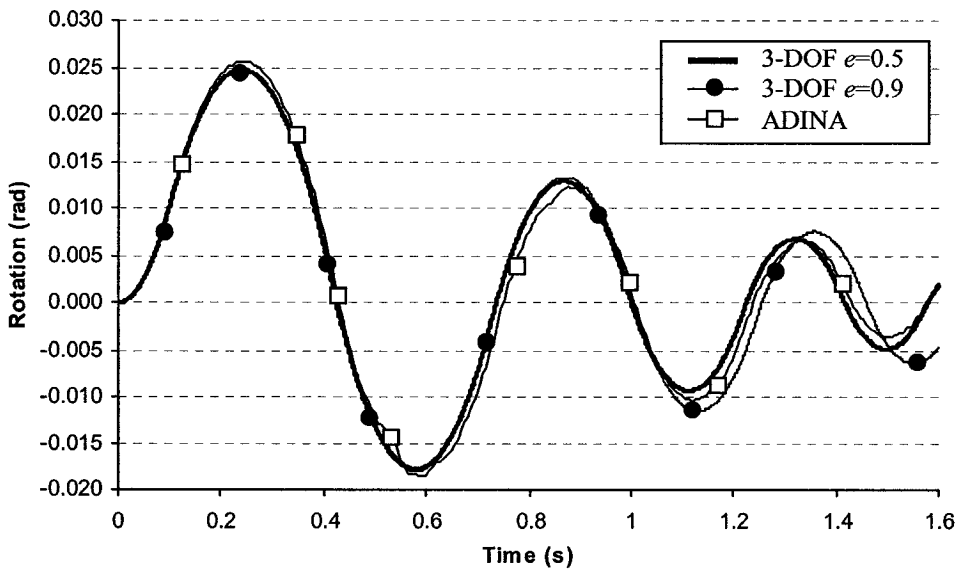

Figure 5.7 Rocking of high-block due to sudden impulse

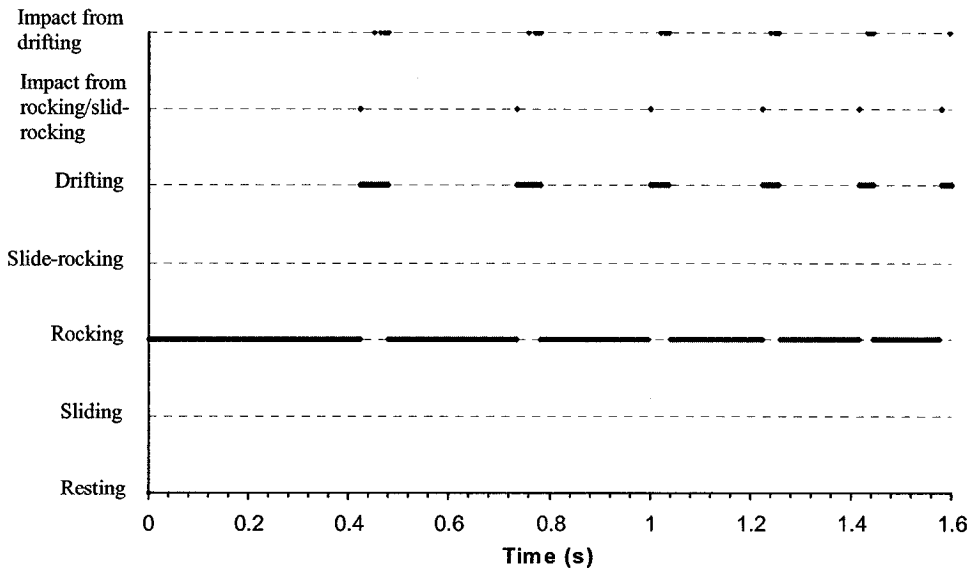

Figure 5.8 Mode of motion of high-block due to sudden impulse (e=0.5)

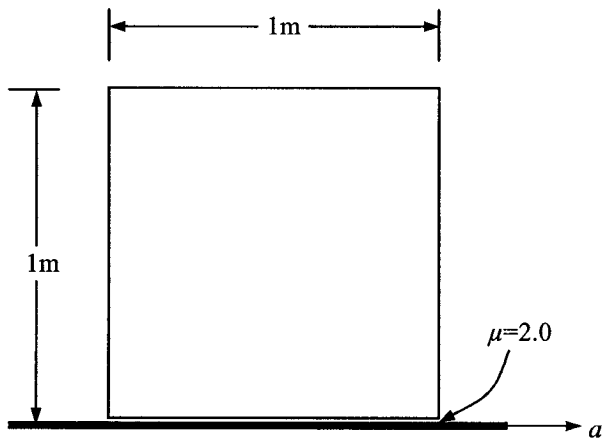

Figure 5.9 Low-block

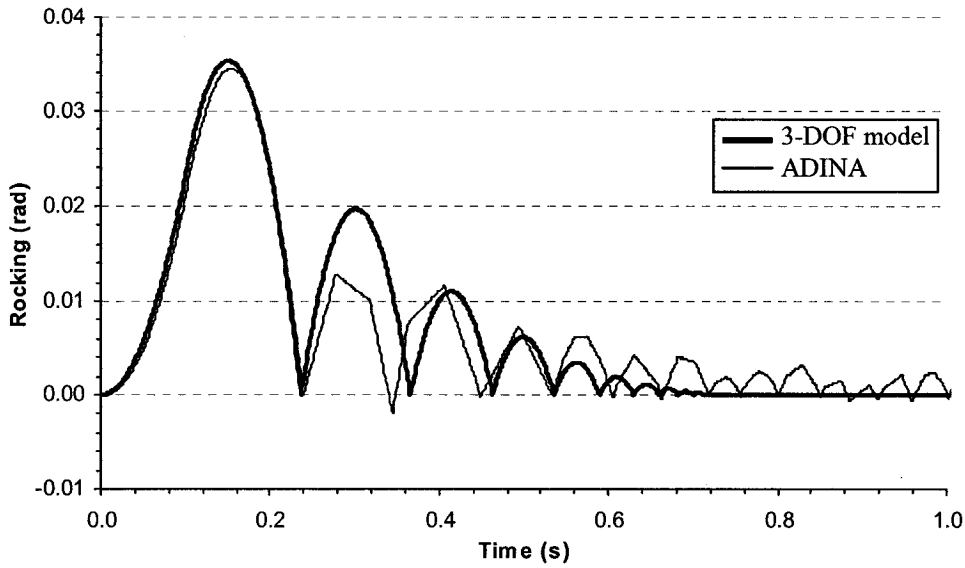

Figure 5.10 Rocking of the low-block due to sudden impulse of 2.0*g* for 0.1 seconds

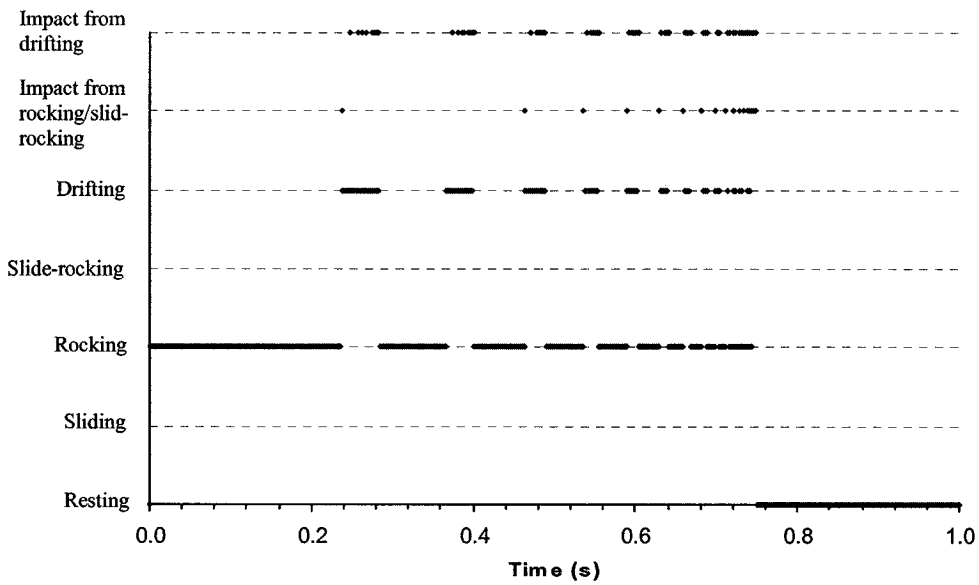

Figure 5.11 Mode of motion of low-block due to sudden impulse of 2.0*g* (*e*=0.75)

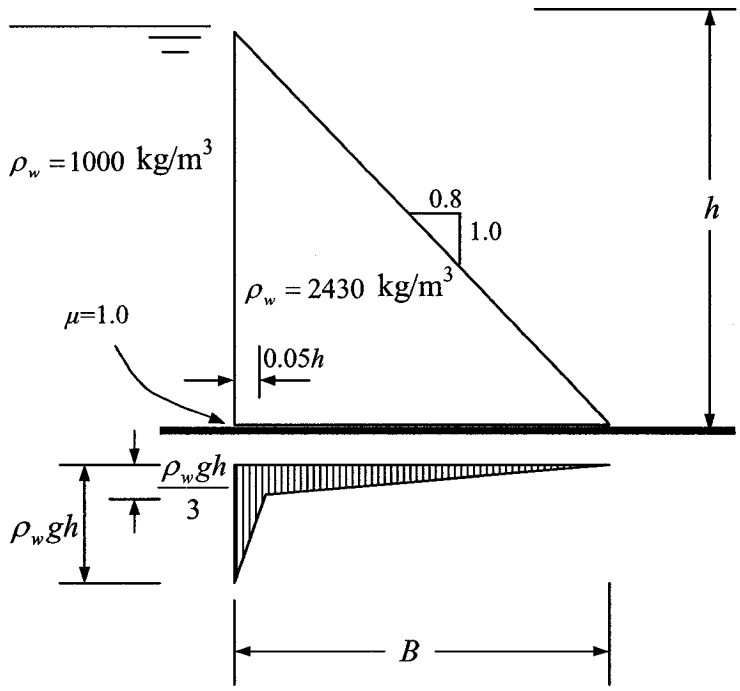

Figure 5.12 Triangular dam cracked at the base

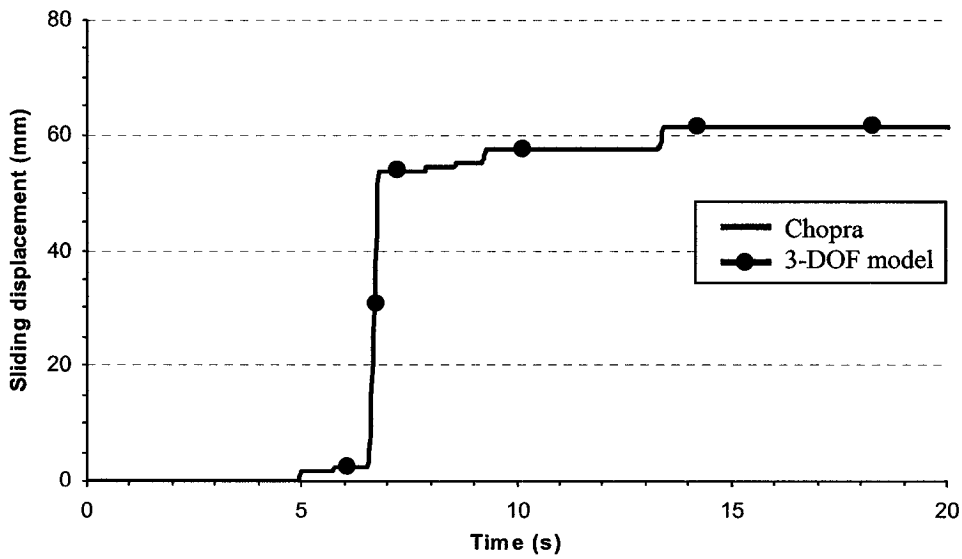

Figure 5.13 Sliding of the triangular dam due to Taft S69E ground motion scaled to 0.5g (μ=1.0)

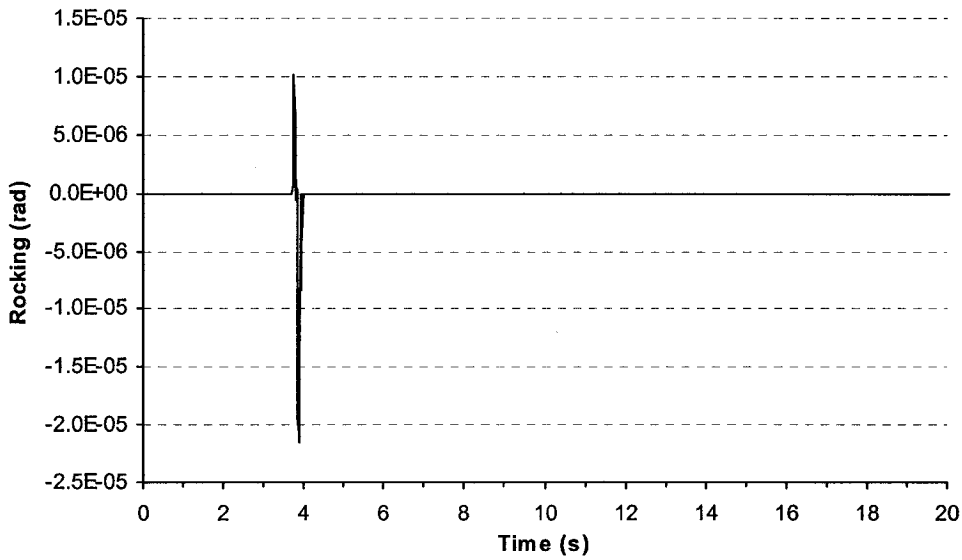

Figure 5.14 Rocking of the triangular dam due to Taft S69E ground motion scaled to 0.8*g* (e=0.75, μ=1.4)

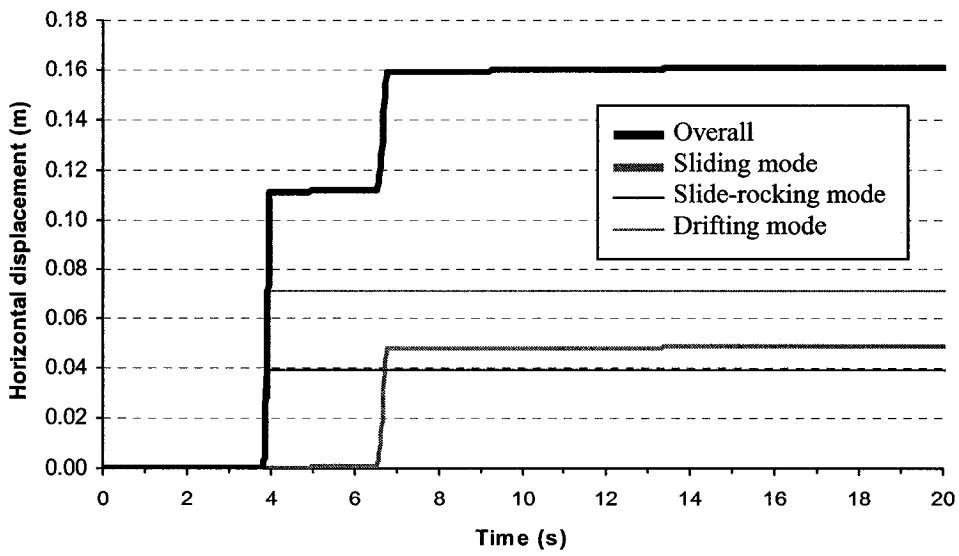

Figure 5.15 Sliding of the triangular dam due to Taft S69E ground motion scaled to 0.8*g* (e=0.75, μ=1.4)

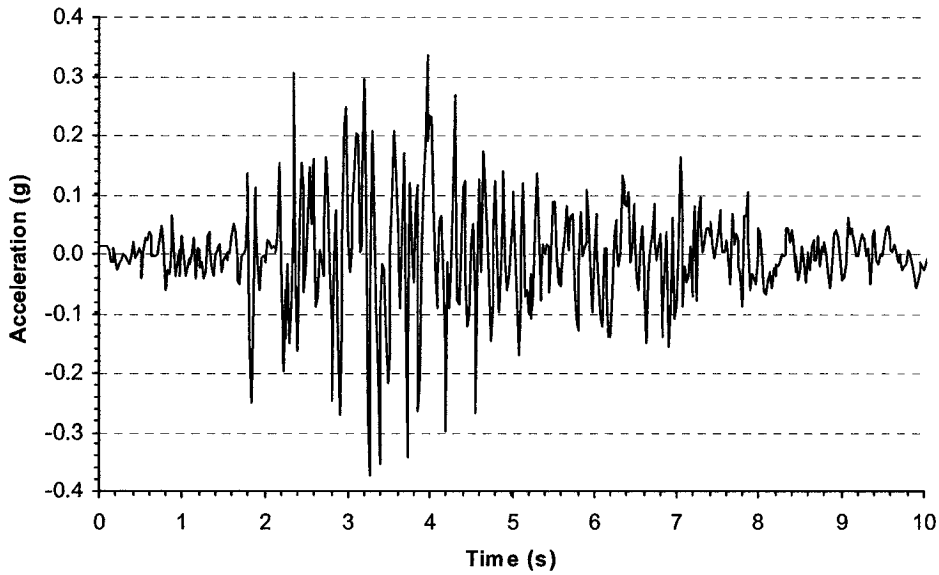

Figure 5.16 Transverse component of Koyna earthquake

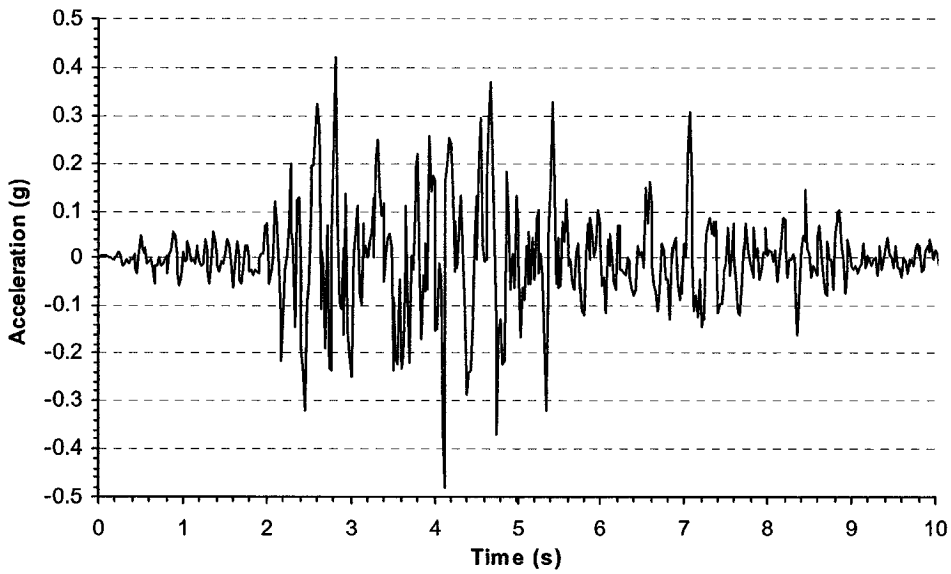

Figure 5.17 Longitudinal component of Koyna earthquake

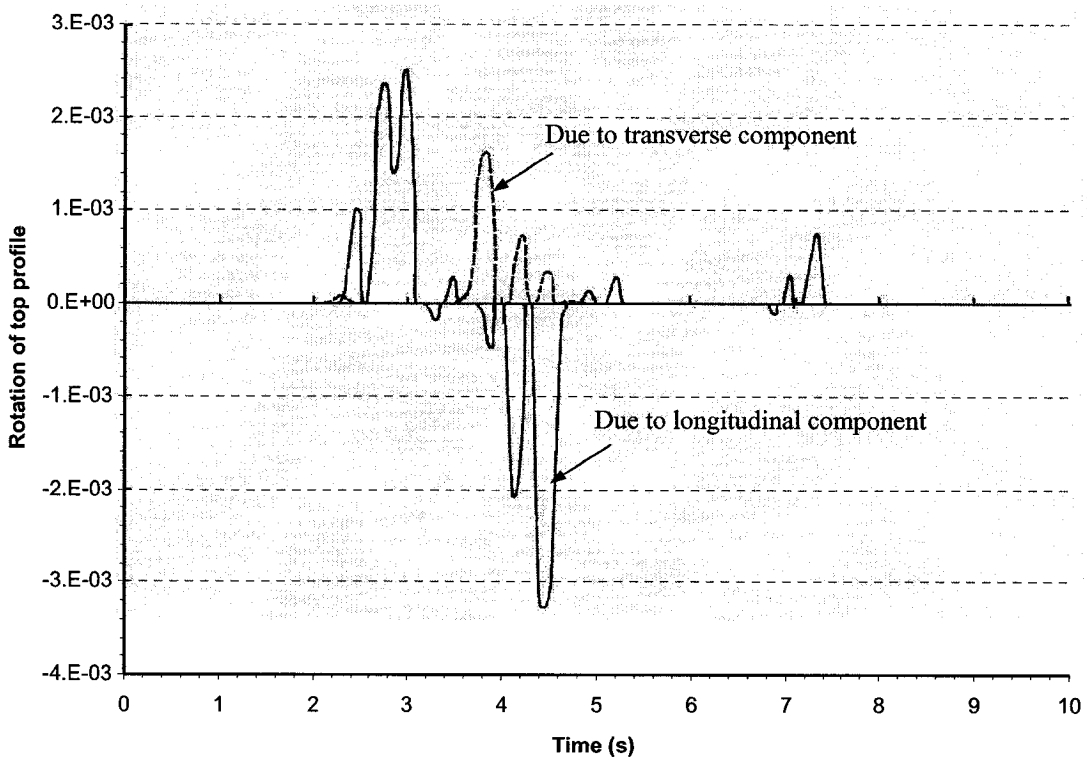

Figure 5.18 Rocking of the upper part of the profile of the cracked monolith of Koyna Dam by Saini and Krishna (1974)

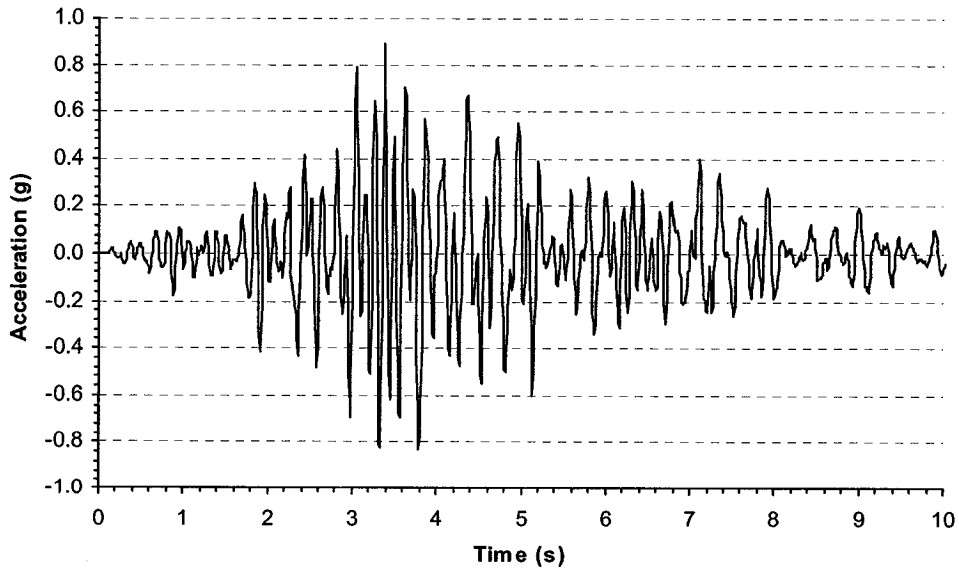

Figure 5.19 Horizontal acceleration at the crack level due to transverse component of Koyna earthquake

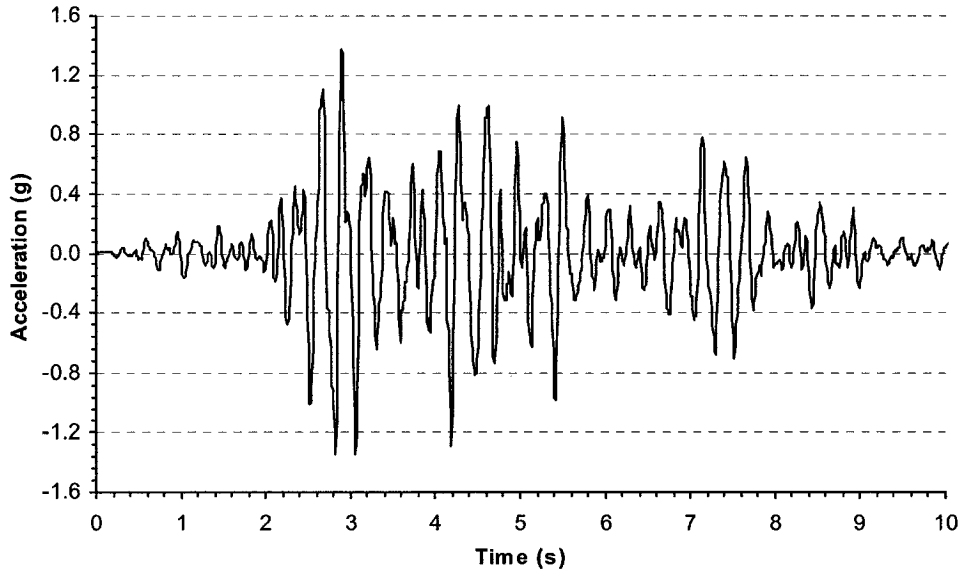

Figure 5.20 Horizontal acceleration at the crack level due to longitudinal component of Koyna earthquake

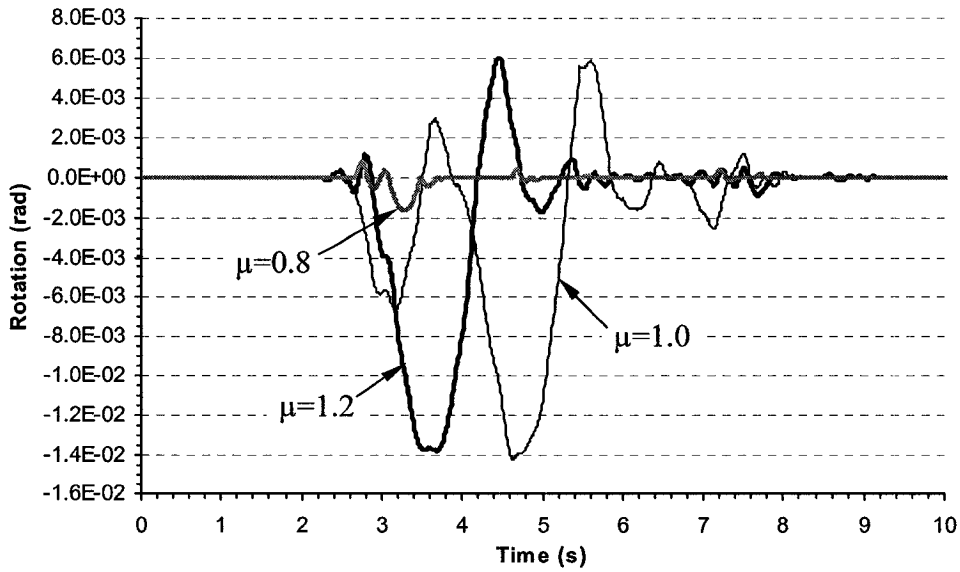

Figure 5. 21 Rocking of upper part of the monolith of Koyna Dam due to longitudinal earthquake (e=0.5, uniform uplift pressure)

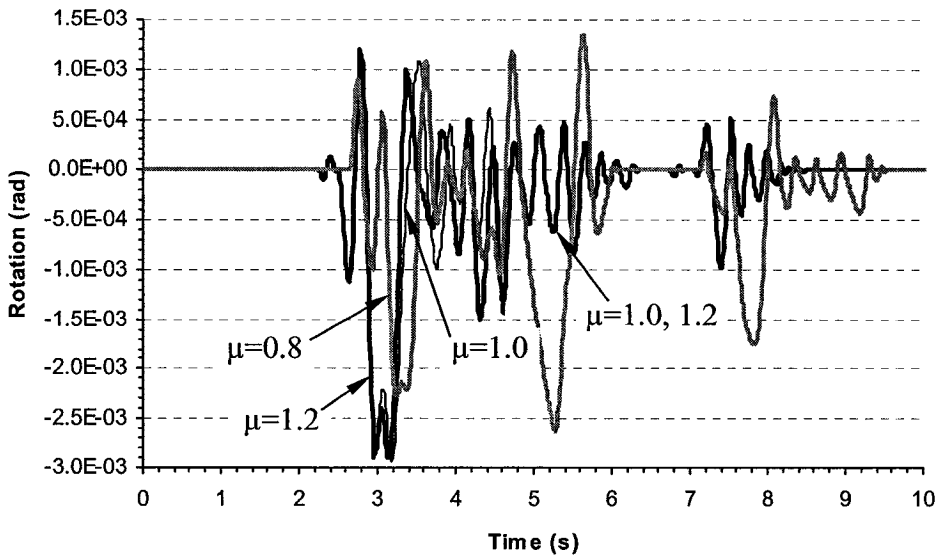

Figure 5. 22 Rocking of upper part of the monolith of Koyna Dam due to longitudinal earthquake (e=0.5, triangle uplift pressure)

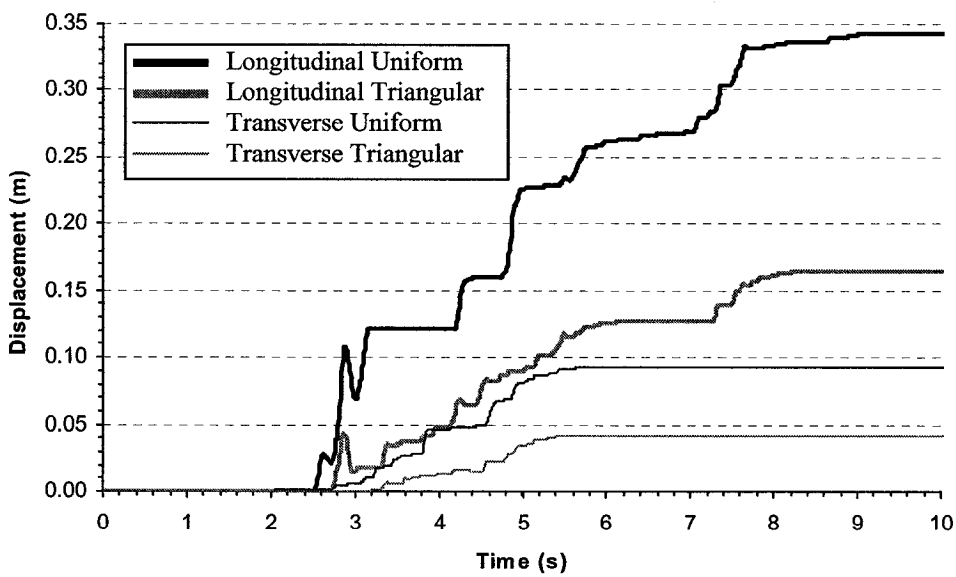

Figure 5.23 Horizontal displacement of the upper part with coefficient of friction 1.2

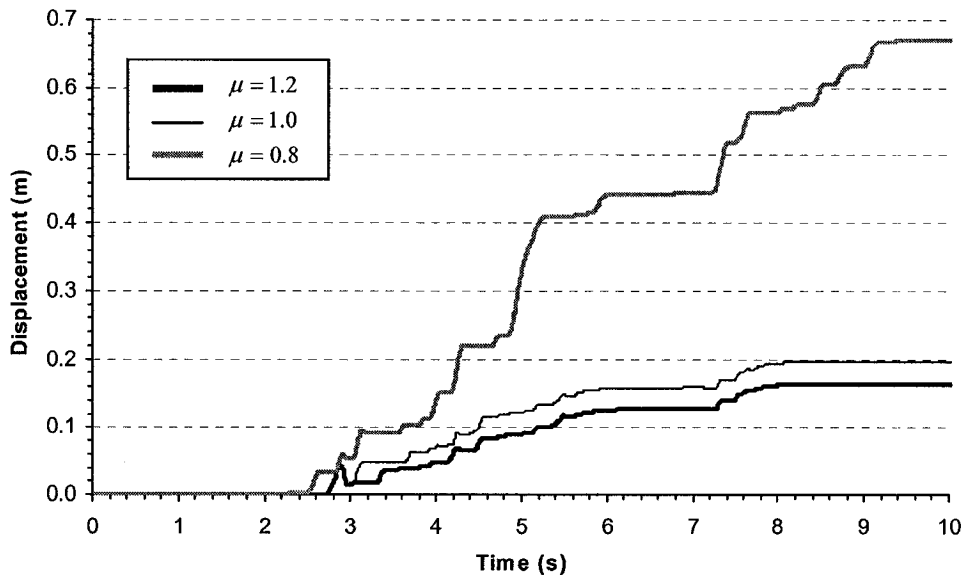

Figure 5. 24 Horizontal displacement of upper part of the monolith of Koyna Dam due to longitudinal component (e=0.5, triangular uplift pressure)

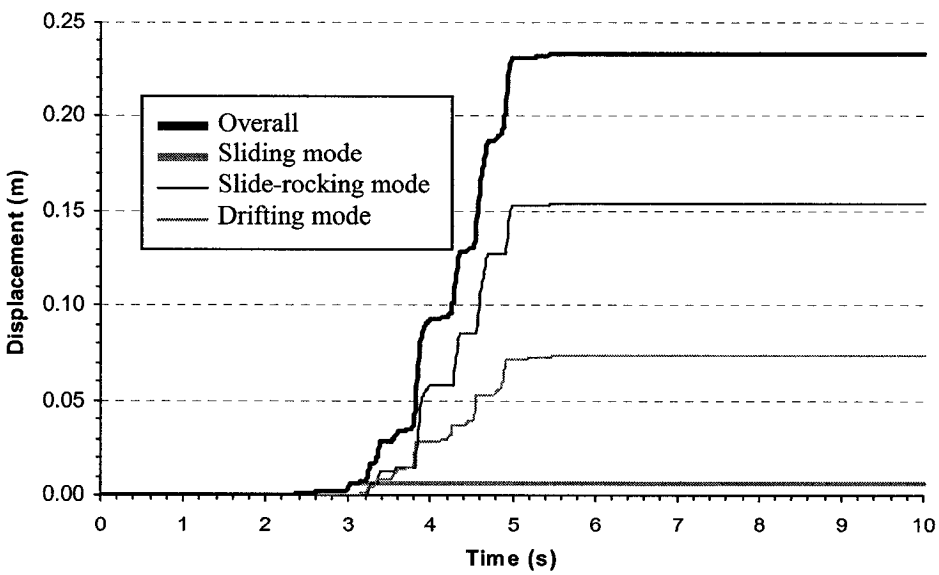

Figure 5. 25 Components of horizontal displacement of upper part of the monolith of Koyna Dam due to transverse earthquake (μ=0.8, e=0.5, triangular uplift pressure)

CHAPTER VI

FEM MODEL: *IDCE* FOR CONTACT SURFACE

6.1 Introduction

Finite element analysis of cracked concrete dams has been carried out to study the seismic responses with the challenge of how to properly treat the crack. As the crack separates the cracked dam into two parts, the whole system becomes anon-linear dynamic system under seismic conditions. The top part is frictionally supported by the lower part fixed at the base where excitation is imposed. If both parts are stuck together the whole structure can be treated as an integrated body. However, for the cracked concrete dam, it is unavoidable that the top part will slip or lose contact locally or even slide and rock as a whole, especially under seismic loading conditions.

Once overall sliding or rocking starts, the upper part behaves like a block on a flexible and vibrating base. This block has the possibility to slide and rock. If relative rocking occurs, impact will follow. At the instant of impact, the local deformation and local vibration will be considerable and their calculation accuracy will determine the dynamic behavior afterwards. If not properly treated, the system will acquire artificial energy and may be out of balance in the process of numerical calculation.

Existing finite element analyses of cracked concrete dams treat the crack as a contact surface with the contact of node-to-node or node-to-surface. The node-to-node model was adopted in static analysis (Okamoto and Nakazawa, 1979; Kikuchi, 1982; Lee, 1994) as well as in dynamic analysis. Danay and Adeghe (1991), Fronteddu (1997) and Fronteddu *et al.* (1998) analyzed the seismic response of cracked concrete dams with *Gap*-friction models to describe the behavior of the crack. El-Aidi and Hall (1989) and

Bhattacharjee and Léger (1993) employed the smeared element technique in the crack propagation analysis as well as to predict sliding of the cracked concrete dam. Both the *Gap*-friction model and the smeared element technique maintain the element connections during the seismic procedure, which are suitable for the case of small displacement. Therefore these kinds of node-to-node models will not introduce noticeable errors if the relative sliding in the cracked concrete dam is insignificant during the seismic procedure. However, considerable sliding in some cases may be expected, where the variable contact conditions at the crack of the cracked concrete dam needs more accurate description.

As for the node-to-surface model as in *ADINA* (1999), Bathe and Chaudhary (1985) and Mir and Taylor (1996) eliminated the disadvantage of the node-to-node contact model; the contact conditions along the contact surface are updated from time to time according to the current configurations of the structure at the moment. Therefore the node-to-surface models are capable of dealing with the dynamic contact conditions in cracked concrete dams for both small and large sliding along the crack.

Nevertheless the phenomenon of penetration into one contact surface by another was noted in the node-to-surface model, as shown in Figure 3.13 and discussed in section 3.2.4. If this model is applied to a concrete dam cracked at a height where the contact surfaces have sharp angles at the ends of the crack, the penetration is unavoidable when the upper part slides and rocks. Of course, this penetration can be lightened with a very fine mesh near both ends of the crack, which would increase tremendously the computation cost.

From the numerical computation point of view, contact models can be classified into two traditional approaches: the penalty approach and the Lagrangian multiplier

method. Penalty approach, considered as a "stiffness" method, has been widely used in finite element analysis for contact problems (Kikuchi, 1982; Hallquist *et al.*, 1985; Bittencourt and Creus, 1998). It fulfills the compatibility equations at the crack by simply introducing a penalty, a large stiffness, without adding any extra unknowns or needing extra treatment in computation. The computation accuracy depends on the magnitude of the penalty. The larger the penalty, the better will be the obtained accuracy of results. Very large stiffness, however, will cause numerical difficulties in many cases due to ill-conditioning of the matrix of the structure.

The potential functional of the whole system consists of the functional $\Pi_e(U)$ in two elastic parts and that of the contact forces. Referring to the frictionless case studied by Bittencourt and Creus (1998), the total potential functional $\Pi(U)$ for the frictional contact problem by the penalty method is

$$\Pi(U) = \Pi_e(U) + \frac{1}{2}\varepsilon g^T g - T^T u \tag{6.1.1}$$

where U is the vector of nodal displacements of the system; ε is a positive penalty number; g is the vector of node gaps of which elements are all zeroes if opened; T is the vector of friction forces which is unknown *a priori* and related to the penalty number; and u is the vector of tangential slip. Equilibrium equations are obtained by minimizing the potential with respect to the unknowns:

$$\frac{\partial \Pi_e}{\partial U} + \varepsilon g^T \frac{\partial g}{\partial U} - F = 0 \tag{6.1.2}$$

where F is the force vector resulting from the friction forces.

The first term of (6.1.2) includes the potential of internal strains and external forces. Therefore

$$\frac{\partial \Pi_e}{\partial U} = M\ddot{U} + C\dot{U} + K_e U - R \tag{6.1.3}$$

where M is the consistent mass matrix; C is the damping matrix; K_e is the elastic stiffness matrix; and R is the vector of external load applied on the system other than the contact forces.

The second term of (6.1.2) leads to the normal contact forces

$$\varepsilon g^T \frac{\partial g}{\partial U} = K_c U \tag{6.1.4}$$

where K_c is the contact stiffness matrix. Therefore, the penalty method will have the equilibrium equations

$$M\ddot{U} + C\dot{U} + (K_e + K_c)U = R + F \tag{6.1.5}$$

Without the difficulty in choosing the big stiffness in penalty approach, the Lagrangian method (Bathe, 1999; Bathe and Miailovich, 1988) is an alternative approach, which can be viewed as "force method". Bathe and Chaudhary (1985) developed a solution algorithm for analysis of the general contact condition with classical Lagrangian multiplier method for static planar and axisymmetric contact problems, in which contact forces were treated as independent unknowns. These extra variables require more computation effort and additional treatment is needed to handle the presence of zero diagonal elements in the global stiffness matrix even if the crack remains closed. This algorithm was extended to dynamic analysis of three-dimensional contact problems (Chaudhar and Bathe, 1986).

Basically the potential functional of the system in the Lagrangian method can be expressed in incremental form (Bathe and Chaudhary, 1985):

$$\pi(U,\lambda) = \pi_e(U) - \sum_k W_k \tag{6.1.6}$$

where π_e is the usual incremental total potential leading to the incremental equilibrium equations without contact conditions, and $\sum_k W_k$ is the incremental potential of the contact forces. Variation of (6.1.6) leads to governing finite element equations

$$\left(\begin{bmatrix} {}^{t+\Delta t}K^{(i-1)} & 0 \\ 0 & 0 \end{bmatrix} + \begin{bmatrix} {}^{t+\Delta t}K_c^{(i-1)} \end{bmatrix} \right) \begin{Bmatrix} \Delta U^{(i)} \\ \Delta\lambda^{(i)} \end{Bmatrix} = \begin{Bmatrix} {}^{t+\Delta t}R - {}^{t+\Delta t}F^{(i-1)} + {}^{t+\Delta t}R_c^{(i-1)} \\ {}^{t+\Delta t}\Delta_c^{(i-1)} \end{Bmatrix} \tag{6.1.7}$$

where ${}^{t+\Delta t}K^{(i-1)}$ is the usual tangent stiffness at time $t+\Delta t$ after iteration $i-1$; ${}^{t+\Delta t}K_c^{(i-1)}$ is the contact stiffness; ${}^{t+\Delta t}R$ is the vector of total applied external forces at time $t+\Delta t$; ${}^{t+\Delta t}R_c^{(i-1)}$ is the vector of updated contact forces after iteration $i-1$; ${}^{t+\Delta t}F^{(i-1)}$ is the vector of nodal point forces equivalent to element stresses after iteration $i-1$; ${}^{t+\Delta t}\Delta_c^{(i-1)}$ is the vector of overlaps; $\Delta U^{(i)}$ is the vector of incremental displacements in iteration i; and $\Delta\lambda^{(i)}$ is the vector of increments in contact forces in iteration i, which are interpreted as Lagrange multipliers.

Perturbed formulation was employed to consider the contact problem. By introducing a penalty in the classical Lagrangian functional of the system, the functional for perturbed Lagrangian approach in the frictionless case is (Simo *et al.*, 1984; Wriggers *et al.*, 1985)

$$\Pi(U,\lambda) = \Pi_e(U) + \lambda^T g - \frac{1}{2\varepsilon}\lambda^2 \tag{6.1.8}$$

where the last term regularizes the classical Lagrangian functional and leads to a stiffness matrix with non-zero diagonal terms. One expects that the solution of (6.1.8) will converge to that of the classical Lagrangian multiplier method when $\varepsilon \to \infty$. From

(6.1.8), the variation of the functional can lead to finite element formulation (Simo *et al.*, 1984; Wriggers *et al.*, 1985).

The augmented Lagrangian method is based on the modified Lagrangian functional augmented by a penalty term associated with the constraint conditions (Simo *et al.*, 1984; Wriggers *et al.*, 1985):

$$\Pi(U,\lambda^k,\varepsilon)=\Pi_e(U)+\begin{cases}\sum_s(-\lambda_s^k g_s+\frac{\varepsilon}{2}g_s^2), & g_s\le\frac{\lambda_s^k}{\varepsilon}\\ \sum_s-\frac{1}{2\varepsilon}(\lambda_s^k)^2, & g_s>\frac{\lambda_s^k}{\varepsilon}\end{cases} \tag{6.1.9}$$

where λ_s^k is the average contact force on the contact segment s and has to be updated, and g_s is the gap in segment s.

It was noted that in both the penalty method and the perturbed Lagrangian method an approximate solution to the original contact problem is obtained, which depends on the arbitrarily chosen penalty parameter, and in practice this parameter can drastically affect the results.

The augmented Lagrangian formulation considers both displacement field and the Lagrangian multipliers in the functional so that its minimum corresponds to the solution of the original contact problem (Eterovic and Bathe, 1991; Zavarise *et al.*, 1995).

It is worthy to note that both the penalty approach and the Lagrangian method enforce point-wise the contact-constraint condition, in the sense that penetration of the bodies is checked on a nodal basis. This leads to problems of convergence when the contact condition changes when the time step is not small enough and the mesh is not very fine.

Eterovic and Bathe (1991) presented a finite element formula for the analysis of contact problems, in which the inequality constraints are enforced directly by means of additional equations to the equilibrium ones.

In the present study, the penalty method is adopted to introduce the constraint conditions between elastic bodies so as to study the seismic behavior of cracked concrete dams. By properly choosing the contactor nodes and corresponding target surfaces, the finite element model *IDCE* (incremental displacement constraint equations) based on the penalty method can avoid the phenomenon of penetration without extra treatment.

6.2 *IDCE* (Incremental Displacement Constraint Equations) model description

6.2.1 Description of contact conditions

In the finite element analysis of contact problem, if relative displacements occur on the contact surface between the adjacent bodies, the configuration of elements besides the contact surface can be illustrated as in Figure 6.1. In general, some nodes on both sides of the surface are in contact and some others are free. Therefore there are two different kinds of status of contact condition for every node on the surface: contact or free.

For free nodes on the contact surface, there is no need of treatment. As for contacting nodes, they are either stuck to the surface or are sliding along the tangent of the surface. Figure 6.2 illustrates the two cases of node I contacting the surface at point I' between nodes J and K of an element. In Figure 6.2, τ is the tangent of the contact surface; n is the outward normal; u and v are the displacements in τ and n

respectively; and V and N are the corresponding friction force and normal force, respectively.

In the case of stuck, node I has the same incremental displacements in both directions as point I', which can be expressed in terms of incremental displacements of nodes J and K via shape functions in the element once the natural coordinate of I' on the element side JK is obtained, i.e.

$$\begin{cases} \Delta u_I = \Delta u_{I'} = f_u(\Delta u_J, \Delta u_K) \\ \Delta v_I = \Delta v_{I'} = f_v(\Delta v_J, \Delta v_K) \end{cases} \tag{6.2.1}$$

where f_u and f_v are functions (Cook, 1989) of the incremental tangential displacements Δu_J, Δu_K and the natural coordinate of I' on side JK.

In the case of sliding, node I has the same incremental displacement in normal direction n as point I', which has the same expression as the second formula in (6.2.1). As for the tangential direction τ, the friction force V depends on the normal contact force N, which is unknown *a priori*. Then we have for the sliding node

$$\begin{cases} V_I = -V_{I'} = sign(\dot{u}_{I'} - \dot{u}_I)\mu_k N \\ \Delta v_I = \Delta v_{I'} = f_v(\Delta v_J, \Delta v_K) \end{cases} \tag{6.2.2}$$

where $\dot{u}_I$ and $\dot{u}_{I'}$ are the tangential velocities of node I and node I' respectively; μ_k is the kinematic coefficient of friction; and N should be compression.

6.2.2 Contact stiffness: Penalty method

Referring to the local coordinates τ and n shown in Figure 6.2, the incremental displacements of point I' can be expressed in terms of those at nodes J and K through the shape function

$$\begin{cases} \Delta u_{I'} = \sum_{i=J}^{K} f_i \Delta u_i \\ \Delta v_{I'} = \sum_{i=J}^{K} f_i \Delta v_i \end{cases} \tag{6.2.3}$$

where the shape functions (Cook 1989) are

$$\begin{cases} f_J = (1-\zeta_{I'})/2 \\ f_J = (1+\zeta_{I'})/2 \end{cases} \tag{6.2.4}$$

In (6.2.4) the natural coordinate $\zeta_{I'} = -1$ when point I' is at node J, while $\zeta_{I'} = 1$ when point I' is at node K. If the element is a higher order one, the shape functions will be changed accordingly.

Denoting the tangential gap g_τ and normal gap g_n for stuck case as below:

$$\begin{cases} g_\tau = \Delta u_{I'} - \Delta u_I \\ g_n = \Delta v_{I'} - \Delta v_I \end{cases} \tag{6.2.5}$$

the expressions for the gaps will be

$$\begin{cases} g_\tau = \begin{bmatrix} -1 & f_J & f_K \end{bmatrix} \begin{bmatrix} \Delta u_I & \Delta u_J & \Delta u_K \end{bmatrix}^T \\ g_n = \begin{bmatrix} -1 & f_J & f_K \end{bmatrix} \begin{bmatrix} \Delta v_I & \Delta v & \Delta v_K \end{bmatrix}^T \end{cases} \tag{6.2.6}$$

For the stuck node, the relationships between the incremental contact forces and the incremental displacements at node I can be obtained as

$$\begin{Bmatrix} \Delta V_I \\ \Delta N_I \end{Bmatrix} = \begin{bmatrix} k_I^\tau & 0 \\ 0 & k_I^n \end{bmatrix} \begin{Bmatrix} \Delta u \\ \Delta v \end{Bmatrix}_I \tag{6.2.7}$$

where the vector of incremental displacements for contacting node I are given by

$$\begin{Bmatrix} \Delta u \\ \Delta v \end{Bmatrix}_I = [\Delta u_I \quad \Delta u_J \quad \Delta u_K \quad \Delta v_I \quad \Delta v_J \quad \Delta v_K]^T \tag{6.2.8}$$

The local contact stiffness matrices k_I^τ and k_I^n in tangent and normal directions, respectively, can be derived by referring to (6.1.4):

$$[k_I^\tau] = \varepsilon_\tau \begin{bmatrix} 1 & -f_J & -f_K \\ -f_J & f_J^2 & f_J f_K \\ -f_K & f_J f_K & f_K^2 \end{bmatrix} \tag{6.2.9}$$

$$[k_I^n] = \varepsilon_n \begin{bmatrix} 1 & -f_J & -f_K \\ -f_J & f_J^2 & f_J f_K \\ -f_K & f_J f_K & f_K^2 \end{bmatrix} \tag{6.2.10}$$

In (6.2.9) and (6.2.10), ε_τ and ε_n are the penalties. Parametric analysis shows that in this study it is proper for both ε_τ and ε_n to be chosen as 1000 times the largest diagonal element in the assembled stiffness matrix of the dam.

For the sliding node, the normal contact condition still holds. However, the tangential connection between node I and the contact surface follows the friction law. Therefore we have for sliding node

$$\begin{cases} V_I = sign(\dot{u}_{I'} - \dot{u}_I)\mu_k N_I \\ \Delta N_I = [k_I^n]\{\Delta v\}_I \end{cases} \tag{6.2.11}$$

(6.2.7) and (6.2.11) show that the contact conditions are fulfilled by the penalty method in the form of *I*ncremental *D*isplacement *C*onstraint *E*quations (*IDCE*).

6.3 Modeling the crack with *IDCE*

On both sides of the crack, all nodes on the surfaces can be modeled with proposed *IDCE* model to simulate the contact conditions. However, only the nodes on one side of the crack, as "contactor surface" in *ADINA* (1999), are necessary to be modeled. This way, the penetration of the other nodes on the opposite surface, which was called "target surface", will not be significant as the adjacent nodes on the contactor surface are in action (Bathe and Chaudhary, 1985).

However, in the case of having sharp corner on the surface as at the end of the crack in the cracked concrete dam, this treatment cannot avoid the penetration, which is remarkable and cannot be neglected. Figure 6.3 and 6.4 show two cases when the upper part of the crack rocks after sliding has happened. In both Figures, the solid dots are the contactor nodes, while the open circles represent the nodes on the target surface.

If the upper part rocks in the direction as in Figure 6.3, no penetration occurs. However, the oscillation movement of the cracked dam might rock in both directions. Therefore the situation in Figure 6.4 is unavoidable. In this case, the pivot position changes a lot and penetration is not detected due to the fact that only the contactor nodes are modeled with *IDCE*. This will obviously result in unreliable responses.

Actually, the penetration at the end of the crack can be avoided by adding only the other two nodes at the ends of target surface to the list of contactor nodes, as shown in Figure 6.5.

In Figure 6.5, the two end nodes on the target surface are also defined as the contactor nodes. They will also be modeled with *IDCE* hence will not penetrate the contactor surface as in Figure 6.4. Since only two more nodes on the target surface are treated as the contactor nodes, little extra computation effort is needed to avoid penetration in any situation.

Therefore, when applying the *IDCE* to the seismic analysis of cracked concrete dams, all nodes on one side of the crack and the two end nodes on the other side of the crack are treated as contactor nodes, and both sides of the crack are considered as target surfaces.

6.4 Solution to the non-linear dynamic equilibrium equations

Having assembled the finite element matrices and the contribution of the *IDCE*, the equilibrium equations at time $t+\Delta t$ for a cracked concrete dam under ground motion can be written as below:

$$M\ddot{U}^{t+\Delta t} + C^{t+\Delta t}\dot{U}^{t+\Delta t} + K_e U^{t+\Delta t} + K_c^{t+\Delta t}\Delta U^{\Delta t} = R - MA^{t+\Delta t} + F_c^t + \Delta F_\tau^{\Delta t} \qquad (6.4.1)$$

where

M = the consistent mass matrix,

$C^{t+\Delta t}$ = the damping matrix at time $t+\Delta t$ depending upon the contact situation between the two parts,

K_e = the constant elastic stiffness matrix of elements,

$K_c^{t+\Delta t}$ = the contact stiffness matrix representing *IDCEs* at time $t+\Delta t$ by,

$U^{t+\Delta t}$ = the displacement vector at time $t+\Delta t$ of the system,

$\dot{U}^{t+\Delta t}$ = the velocity vector at time $t+\Delta t$ of the system,

$\ddot{U}^{t+\Delta t}$ = the acceleration vector at time $t+\Delta t$ of the system,

$\Delta U^{\Delta t}$ = the incremental displacement vector from time t to time $t+\Delta t$,

R = the vector of external constant load applied on the system,

$A^{t+\Delta t}$ = the vector of ground acceleration at time $t+\Delta t$,

F_c^t = the contact force vector at the end of last time step t, which is accumulated from normal contact forces and friction forces on both contactor nodes and target nodes by (6.2.7) and (6.2.11),

$\Delta F_\tau^{\Delta t}$ = the incremental force vector from time t to time $t+\Delta t$ of friction forces V_I at sliding contact nodes and $V_{I'}$ at the related nodes on the target surface, as shown at nodes I, J and K in Figure 6.2.

Substituting the incremental displacement vector

$$\Delta U^{\Delta t} = U^{t+\Delta t} - U^t \tag{6.4.2}$$

into equilibrium equations (6.4.1) yields

$$M\ddot{U}^{t+\Delta t} + C^{t+\Delta t}\dot{U}^{t+\Delta t} + K^{t+\Delta t}U^{t+\Delta t} = R^{t+\Delta t} \tag{6.4.3}$$

where tangential stiffness of the system

$$K^{t+\Delta t} = K_e + K_c^{t+\Delta t} \tag{6.4.4}$$

and the equivalent force vector at time $t+\Delta t$ step

$$R^{t+\Delta t} = R - MA^{t+\Delta t} + F_c^t + K_c^{t+\Delta t}U^t + \Delta F_\tau^{\Delta t} \tag{6.4.5}$$

(6.4.3) shows the governing equations for the dynamic contact problem. The second last term of $R^{t+\Delta t}$ in (6.4.5) depends on the contact status, whereas the last term $\Delta F_{\tau}^{\Delta t}$ depends on the normal contact forces, which is unknown *a priori*. This shows the essence of non-linearity of the problem, and (6.4.3) has to be solved step by step and iteratively.

Many methods can be employed to solve equations in (6.4.3) (Bathe, 1996). In this study, the Newton-Raphson scheme is used to deal with the non-linearity and the Newmark method is adopted to integrate the dynamic equations. In the Newmark method, the unknown velocities and displacements at time $t+\Delta t$ are expressed in terms of unknown accelerations at time $t+\Delta t$:

$$\dot{U}^{t+\Delta t} = \dot{U}^{t} + [(1-\delta)\ddot{U}^{t} + \delta\ddot{U}^{t+\Delta t}]\Delta t \tag{6.4.6}$$

$$U^{t+\Delta t} = U^{t} + \dot{U}^{t}\Delta t + [(\frac{1}{2}-\alpha)\ddot{U}^{t} + \alpha\ddot{U}^{t+\Delta t}]\Delta t^{2} \tag{6.4.7}$$

From (6.4.7) the unknown $\ddot{U}^{t+\Delta t}$ can be expressed in terms of unknown displacements at time $t+\Delta t$:

$$\ddot{U}^{t+\Delta t} = \frac{1}{\alpha\Delta t^{2}}(U^{t+\Delta t} - U^{t}) - \frac{1}{\alpha\Delta t}\dot{U}^{t} - (\frac{1}{2\alpha}-1)\ddot{U}^{t} \tag{6.4.8}$$

Then the unknown velocities can also expressed in terms of unknown displacements at time $t+\Delta t$:

$$\dot{U}^{t+\Delta t} = \frac{\delta}{\alpha\Delta t}(U^{t+\Delta t} - U^{t}) + (1-\frac{\delta}{\alpha})\dot{U}^{t} + (1-\frac{\delta}{2\alpha})\Delta t\ddot{U}^{t} \tag{6.4.9}$$

Substituting (6.4.8) and (6.4.9) into (6.4.3), the non-linear equilibrium equations at time $t+\Delta t$ become

$$\overline{K}^{t+\Delta t}U^{t+\Delta t} = \overline{R}^{t+\Delta t} \tag{6.4.10}$$

where the generalized stiffness matrix $\overline{K}^{t+\Delta t}$ and load vector $\overline{R}^{t+\Delta t}$ are

$$\overline{K}^{t+\Delta t} = K^{t+\Delta t} + a_0 M + a_1 C^{t+\Delta t} \tag{6.4.11}$$

$$\overline{R}^{t+\Delta t} = R^{t+\Delta t} + M(a_0 U^t + a_2 \dot{U}^t + a_3 \ddot{U}^t) + C^{t+\Delta t}(a_1 U^t + a_4 \dot{U}^t + a_5 \ddot{U}^t) \tag{6.4.12}$$

In (6.4.11) and (6.4.12), the constants

$$a_0 = \frac{1}{\alpha \Delta t^2}, \quad a_1 = \frac{\delta}{\alpha \Delta t}, \quad a_2 = \frac{1}{\alpha \Delta t}$$

$$a_3 = \frac{1}{2\alpha} - 1, \quad a_4 = \frac{\delta}{\alpha} - 1, \quad a_5 = \Delta t(\frac{\delta}{2\alpha} - 1)$$

Considering the Rayleigh damping in the system:

$$C^{t+\Delta t} = \beta_K K^{t+\Delta t} + \beta_M M \tag{6.4.13}$$

where β_K and β_M are the damping coefficients of $K^{t+\Delta t}$ and M respectively, the generalized non-linear stiffness matrix $\overline{K}^{t+\Delta t}$ in (6.4.11) and load $\overline{R}^{t+\Delta t}$ in (6.4.12) become

$$\overline{K}^{t+\Delta t} = b_K K^{t+\Delta t} + b_M M \tag{6.4.14}$$

$$\overline{R}^{t+\Delta t} = R^{t+\Delta t} + K^{t+\Delta t} Y_K + M Y_M \tag{6.4.15}$$

where the constants

$$b_K = 1 + a_1 \beta_K, \quad b_M = a_0 + a_1 \beta_M$$

$$Y_K = \beta_K (a_1 U^t + a_4 \dot{U}^t + a_5 \ddot{U}^t)$$

$$Y_M = (a_0 + a_1 \beta_M) U^t + (a_2 + a_4 \beta_M) \dot{U}^t + (a_3 + a_5 \beta_M) \ddot{U}^t$$

Therefore, the generalized equilibrium equations will be

$$\overline{K}^{t+\Delta t} = \overline{K}_0 + b_K K_c^{t+\Delta t} \tag{6.4.16}$$

$$\overline{R}^{t+\Delta t} = \overline{R} + K_c^{t+\Delta t} \overline{Y}_K + \Delta F_\tau^{\Delta t} \tag{6.4.17}$$

where

$$\overline{K}_0 = b_K K_e + b_M M \tag{6.4.18}$$

$$\overline{R} = R - MA^{t+\Delta t} + F_c^t + K_e Y_K + M Y_M \tag{6.4.19}$$

$$\overline{Y}_K = Y_K + U^t \tag{6.4.20}$$

Now the governing equilibrium equations in (6.4.1) become those in (6.4.10). To solve them, the procedure is as follows:

1. Obtain the accumulated contact force vector F_c^t.
2. Check contact conditions for all contactor nodes[a].
3. Compute contact stiffness for every stuck or sliding contactor node.
4. Assemble the generalized stiffness matrix $\overline{K}^{t+\Delta t}$ as in (6.4.16).
5. Assemble the generalized force vector $\overline{R}^{t+\Delta t}$ as in (6.4.17) excluding the friction force increment $\Delta F_\tau^{t+\Delta t}$.
6. Assume $\Delta F_\tau^{t+\Delta t} = 0$.
7. Add $\Delta F_\tau^{t+\Delta t}$ to $\overline{R}^{t+\Delta t}$.
8. Solve (6.4.10).

---

[a] For a free contactor node, if the distance between a contactor node to a target surface is equal to or smaller than a given small value, 10^{-4} mm, and the node is moving toward the surface, the contact condition changes to stuck. For a sliding node, if the value of its velocity is below a certain value, 10^{-4} mm/s, the contact condition changes to stuck. For a stuck contact node, if the normal contact force becomes negative (tension), the contact condition changes to free, while it will start to slide if the tangential contact force exceeds the frictional limit determined by the friction law.

9. Transform the displacements on the contact surfaces into their local coordinate systems to calculate incremental contact force as in (6.2.7) for stuck contactor node or in (6.2.11) for sliding contactor node. As for friction forces, they are obtained from (6.2.11).

10. Calculate $\Delta F_{\tau}^{t+\Delta t}$ and go to step 7 if no case from below occurs:

- A stuck contactor node becomes free or starts to slide;
- A sliding contactor node becomes stuck or free;
- A free contactor node contacts the target surface;

Otherwise, modify the contact conditions and go to step 3.

11. If $\Delta F_{\tau}^{t+\Delta t}$ is converged[b], go to step 1 for next time step until all time steps are gone through.

6.5 Verifications of *IDCE* model

The validity of the proposed *IDCE* model for seismic analysis of cracked dams was verified with 3 examples for sliding, rocking-impact and penetration.

6.5.1 A block on a flexible foundation to verify *IDCE* for sliding

An artificial rectangular block 8 m×16 m resting on a foundation subjected to a triangle impulse was used to verify the *IDCE* model for sliding. To compare with the theoretical solution based on the rigid assumption both the block and the foundation are

[b] Relative difference between the frictional force applied and that determined by the friction law should not be larger than a given value, normally 10^{-3} in this study.

intentionally assigned a very large modulus $E = 200$ GPa and Poisson's ratio $\nu = 0$. The coefficient of friction between the block and the foundation is 0.2. The finite element model and the impulse are illustrated in Figure 6.6, in which all elements are 4-node plane strain elements. Damping effect is neglected.

The proposed sliding and theoretical solution derived with rigid assumption are shown in Figure 6.7. It is shown that the proposed *IDCE* model can almost precisely predict the sliding of the block on the foundation. The relative difference of the residual sliding is 0.104%.

6.5.2 A block on a flexible foundation to verify *IDCE* for rocking and impact

Consider the same block on the foundation as in Figure 6.6, subject to the ground acceleration in Figure 6.8. Assume the coefficient of friction is 1.2 to avoid pure sliding. In this case the block will rock and impact. Figure 6.9 illustrates the rotation of the block during the whole process, which includes rocking, impact and drifting. Also shown is the response predicted by the proposed rigid 3-*DOF* model with coefficient of restitution of 0.9. Both responses are consistent in terms of peak rotation and trend of variation, indicating the proposed *IDCE* model for dealing with rocking and impact problems is satisfactory.

6.5.3 A block with a crack to verify *IDCE* for dealing with penetration

Figure 6.10 is the mesh of 8-node plane stress elements (Zienkiewicz 1971) for a 10m×20m block with a crack at its mid-height. Assume the coefficient of friction at the crack is 1.0. The ground acceleration is shown in Figure 6.11. As the peak acceleration

exceeds the limit of 1.0*g* to initiate sliding and rocking, the upper part of the cracked block is expected to slide and rock as well as impact. Therefore, the penetration phenomenon would occur if it were not properly dealt with as explained in section 6.3.

To verify the validity of proposed *IDCE* model, 5 types of treatment are considered as below:

Type 1: Only nodes on the surface A are treated as contactor nodes (Figure 6.12.a).

Type 2: Only nodes on the surface B are treated as contactor nodes (Figure 6.12.b).

Type 3: Nodes on the surface A and two end nodes on surface B are treated as contactor nodes (Figure 6.12.c).

Type 4: Nodes on the surface B and two end nodes on surface A are treated as contactor nodes (Figure 6.12.d).

Type 5: All nodes on the surface A and B are treated as contactor nodes (Figure 6.12.e).

Under the ground excitation, the upper part will slide to the left and rock counter clock-wise with respect to the lower part. Relative rotation and sliding of the upper part of the cracked block are illustrated in Figures 6.13 and 6.14. For type 1, penetration is expected at the left end node of surface B. This makes the upper part much easier to rock than other types as shown in Figure 6.14. For type 2, there will not be penetration at the left end node of surface B for it is a contactor node. However, the right end node of surface A in type 2 may penetrate surface B. Therefore both type 1 and type 2 can not predict correctly the response of the upper part of the crack block.

Figures 6.13 and 6.14 show clearly that types 3, 4 and 5 give the same results for both sliding and rotation of the upper part, indicating the *IDCE* model is effective to avoid penetration by adding only two more contactor nodes as type 3 or type 4. This means, in addition to contactor nodes on one surface, only two more nodes at the ends of the other surface are needed to be treated as contactor nodes to avoid penetration.

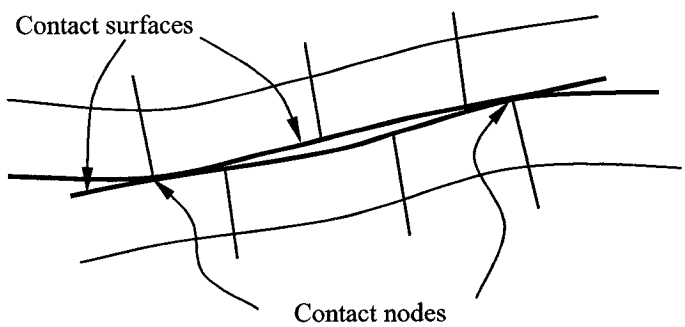

Figure 6.1 General configuration of elements on the contact surface

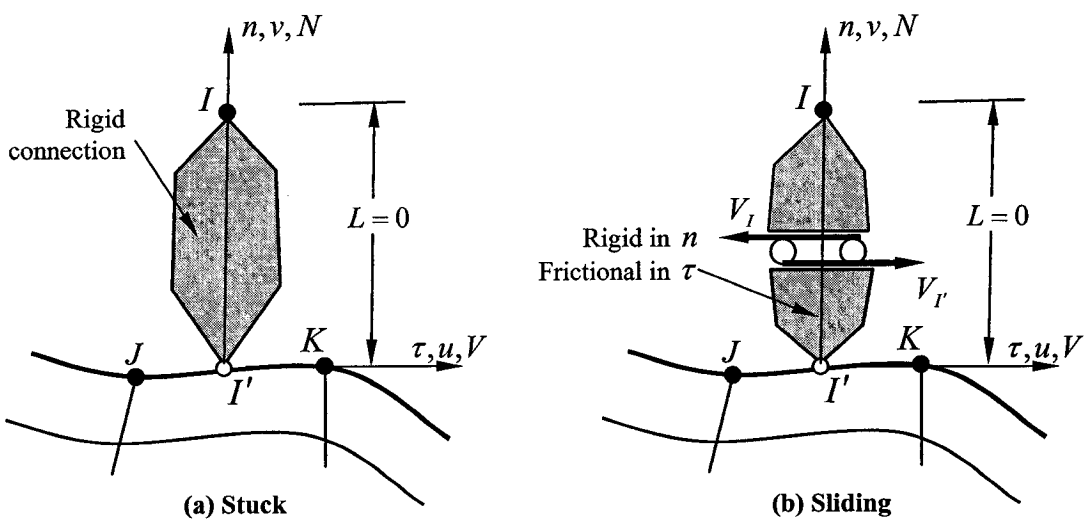

Figure 6.2 Contacting node

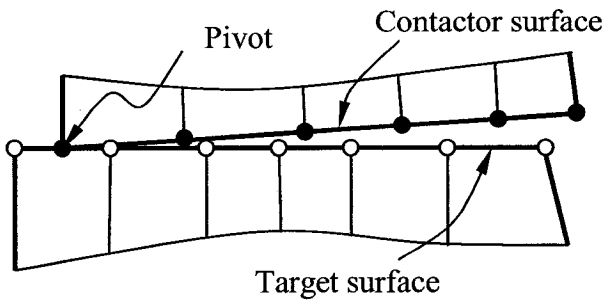

Figure 6.3 Upper part rocks while pivot is a contactor node contacting the target surface

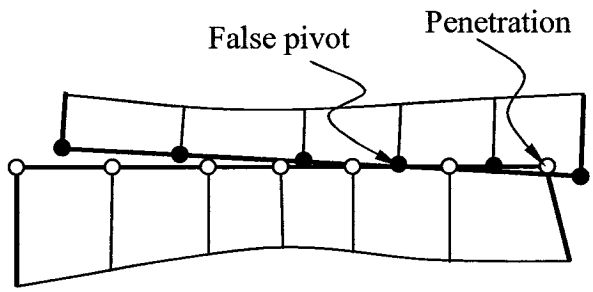

Figure 6.4 Upper part rocks while pivot is a target node

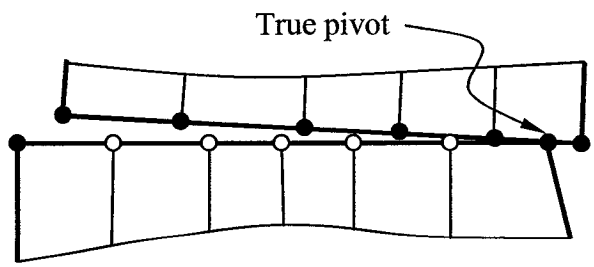

Figure 6.5 Upper part rocks without penetration by adding two contactor nodes on target surface

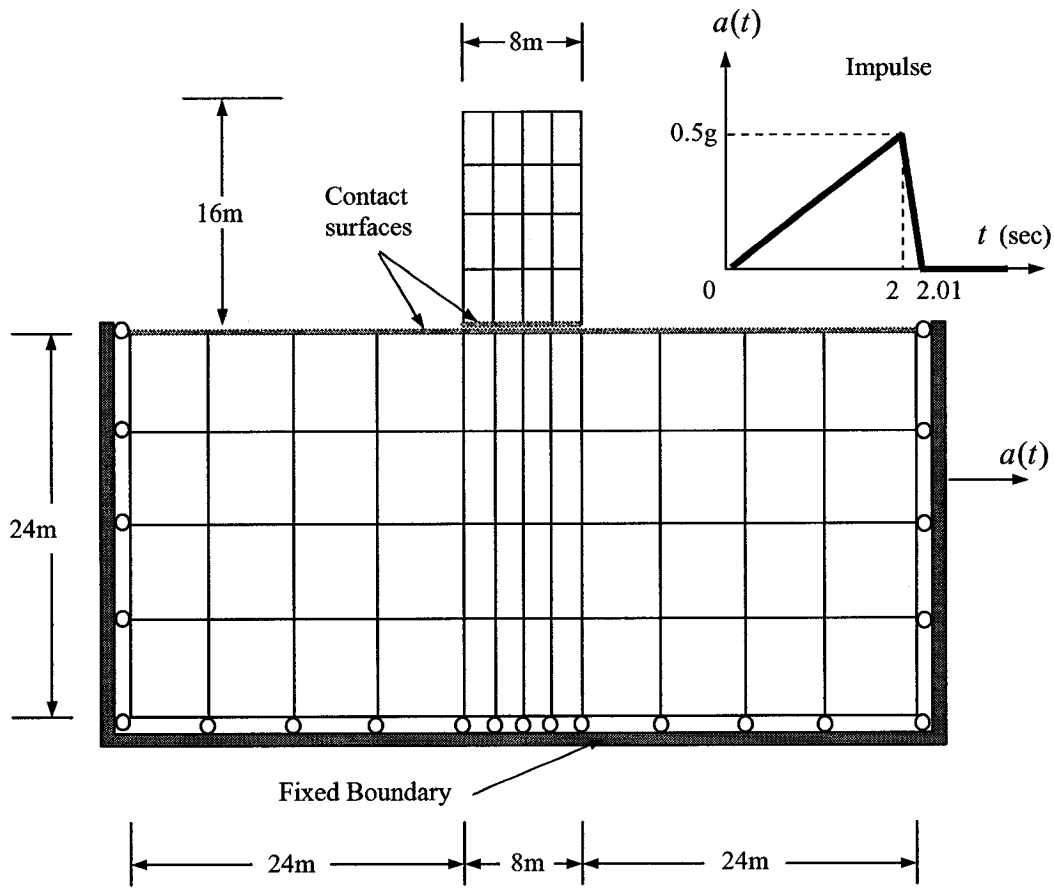

Figure 6.6 A rectangular block on a flexible foundation

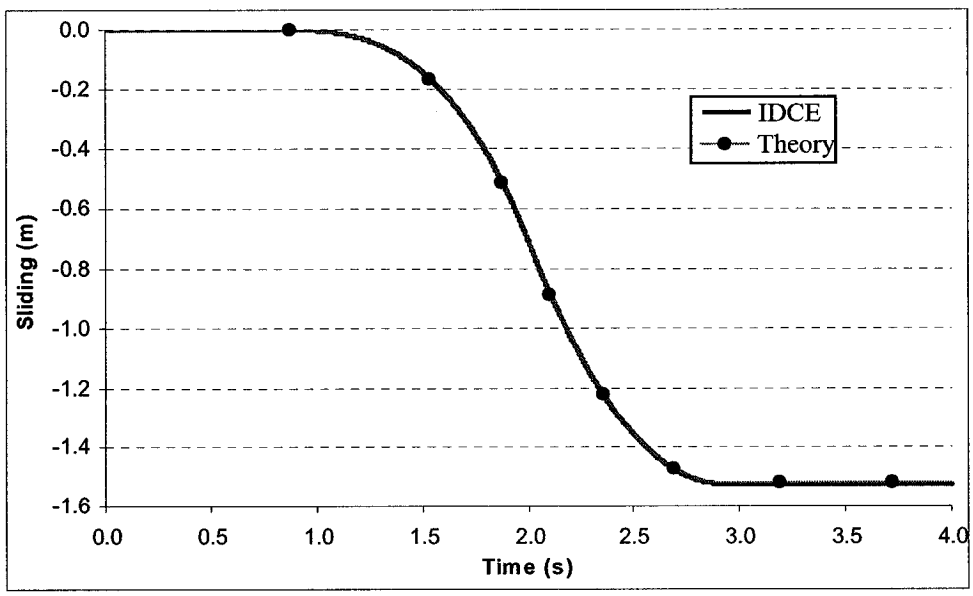

Figure 6.7 Sliding of the block on the flexible foundation

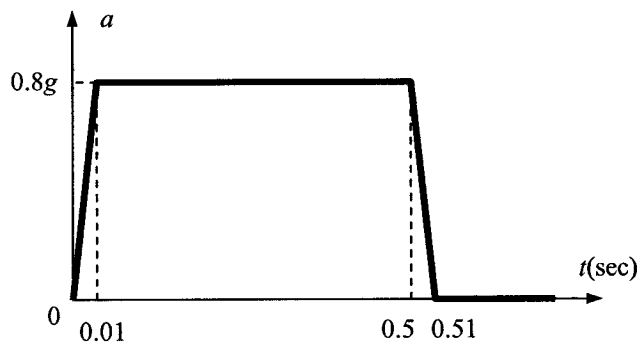

Figure 6.8 Ground acceleration to initiate rocking of the block on the flexible foundation

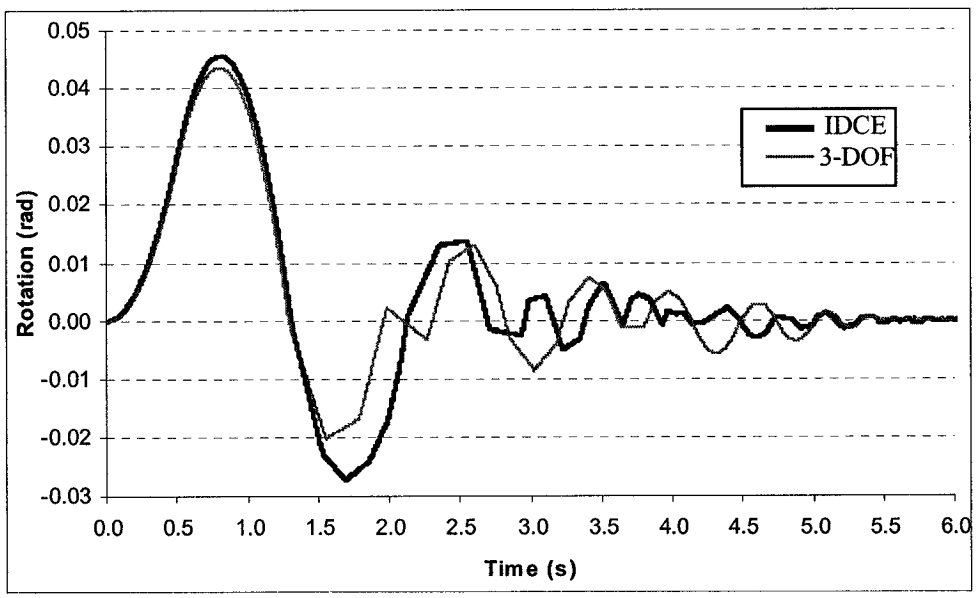

Figure 6.9 Rock-impact of the block on the flexible foundation

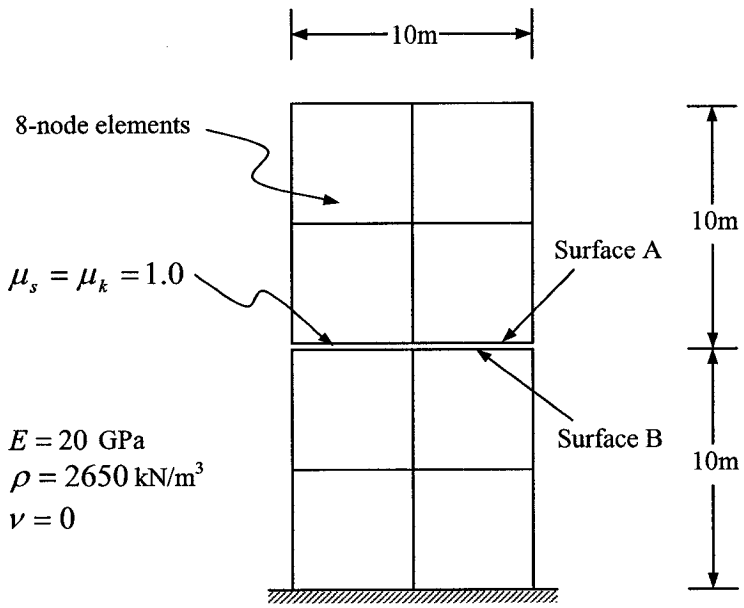

Figure 6.10 A 10 m × 20 m block with a crack at its mid-height

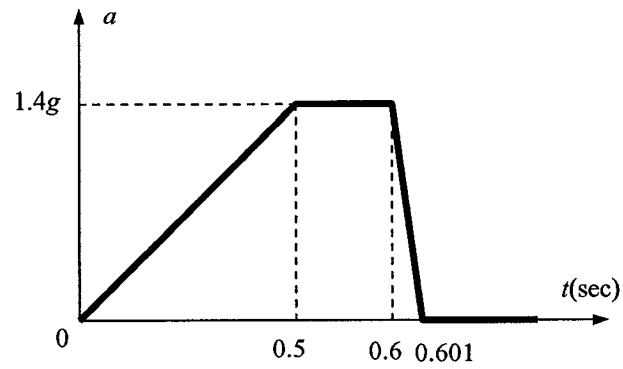

Figure 6.11 Ground acceleration to verify *IDCE* for dealing with penetration

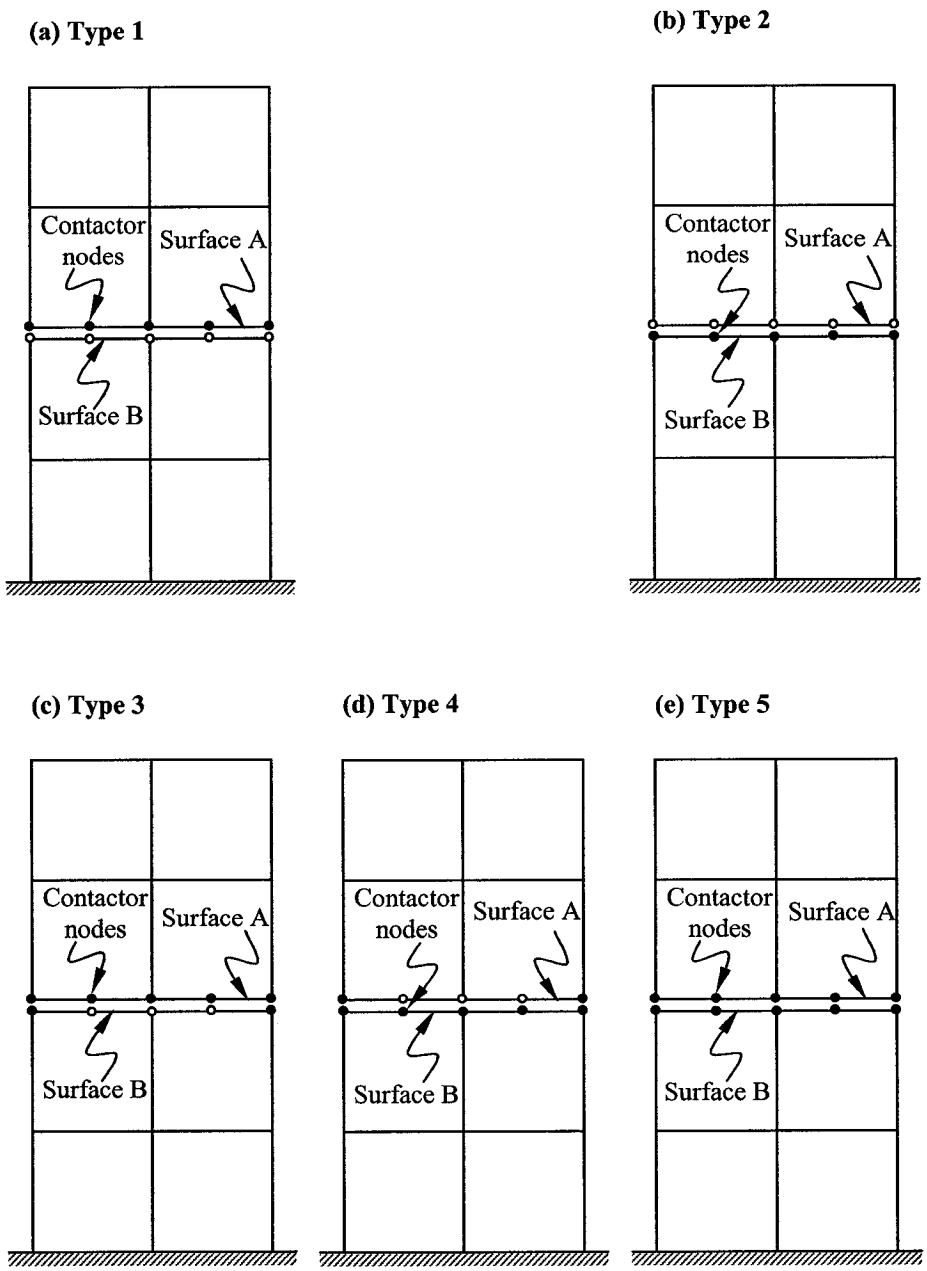

Figure 6.12 Types of treatment of crack with *IDCE*

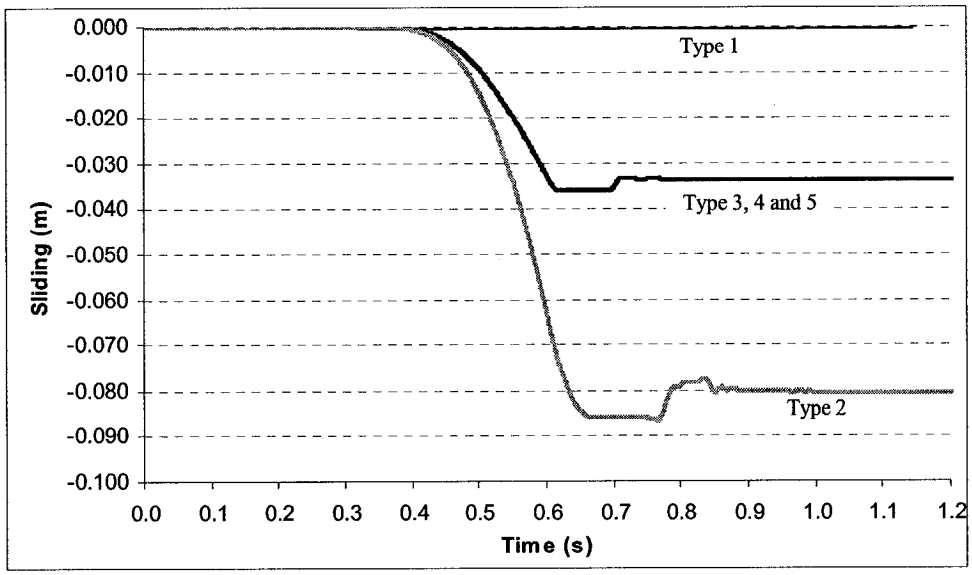

Figure 6.13 Relative sliding of the upper part of the cracked block

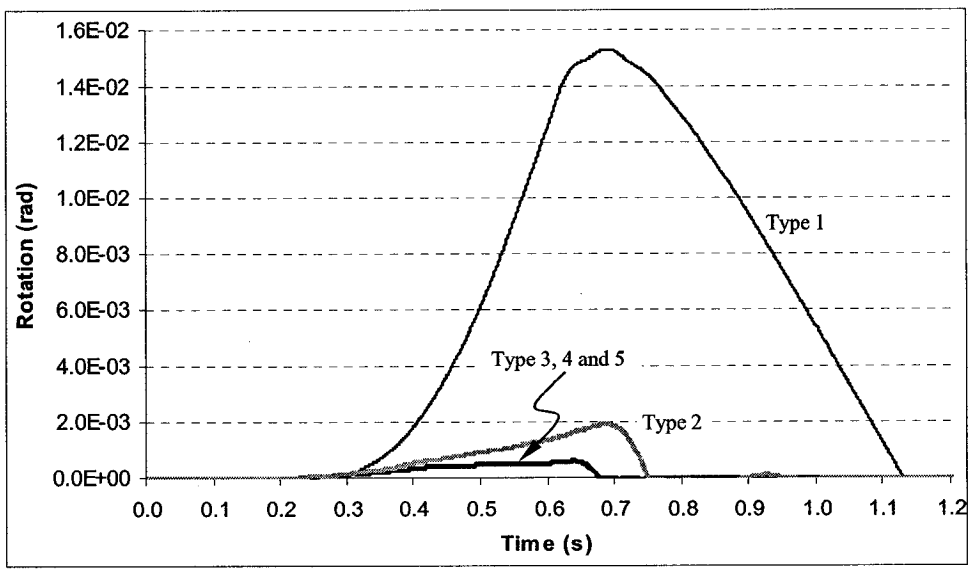

Figure 6.14 Relative rotation of the upper part of the cracked block

CHAPATER Ⅶ

SEISMIC ANALYSIS OF CRACKED DAMS

7.1 Introduction

In this chapter, the triangular dam in Figure 5.12 is first studied with the proposed *IDCE* finite element model to investigate the base sliding behavior. Through this application, the proposed *IDCE* model demonstrates its consistency and superiority compared with the 3-*DOF* model. Then the safety of the cracked Koyna Dam is studied with the *IDCE* mode by analyzing the cracked monolith with the assumption that the crack penetrates horizontally the crest. To further reveal the seismic behavior of cracked concrete gravity dams, a cracked typical dam is further studied in two cracked cases. For the case of the crack at a height, the *IDCE* finite element model is applied, whereas both the 3-*DOF* rigid and the *IDCE* models are used for the case of the crack at the base. For both cases the effects of coefficient of friction and water level are studied with the El Centro 1940 NS and Taft 1952 S69E earthquakes, respectively.

7.2 The triangular dam

7.2.1 Introduction to the triangular dam

The triangular dam in Figure 5.12 (h=121.92 m) was also studied by Chopra and Zhang (1991) with one-degree-of-freedom flexible model including the dynamic effect of the fundamental mode of vibration. According to the geometry, uplift pattern, water level and earthquake acceleration imposed for this artificial dam, only sliding motion occurs if considering it as a one-degree-of-freedom system. Therefore, the overall rocking that

may be initiated in the proposed *IDCE* model because of the flexibility of the dam should be quite limited. The application of the proposed *IDCE* model to this dam is expected to confirm existing research, as well as to reveal more reasonable seismic behavior of the dam. The finite element mesh with variable-node isoparametric plane elements is shown in Figure 7.1. The dynamic effect of the full reservoir water is represented by a distributed virtual mass (Westergaard, 1931). The main responses of this dam to the S69E component of Taft 1952 earthquake are summarized and compared with the results by Chopra and Zhang (1991) in Table 7.1 and Figures 7.2 to 7.4. The seismic response to larger coefficient of friction and more violent earthquake is also presented as in Table 7.3, Figure 7.5 and 7.6.

7.2.2 Sliding behavior of the triangular dam

Figure 7.2 shows that the present study is quite consistent with the result by the one-degree-of-freedom flexible model (Chopra and Zhang, 1991) for the modulus of the dam of 27.61 GPa (4×10^6 psi), where the relative error for the residual sliding at the base is about 5%. This confirms that the one-degree-of-freedom flexible model (Chopra and Zhang, 1991) is applicable for estimating the base sliding of concrete gravity dams when the rocking mode is not initiated.

It is worthy to note that the modulus of the dam affects the base sliding as indicated in Table 7.1, in which the values of sliding displacements by the one-degree-of-freedom flexible model are the approximate estimations according to Figure 6 of Chopra and Zhang (1991). From Table 7.1 and Figure 7.3, it is clear that although the predicted sliding displacements by the proposed *IDCE* model and the one-degree-of-freedom

flexible model are quite close for modulus 27.61GPa (4×10^6 psi), they are quite different for other values of modulus, indicating that the modulus of the dam affects significantly the response. In the one-degree-of-freedom flexible model, the sliding displacement increases while the modulus of the dam increases from 3.45 GPa (0.5×10^6 psi) to 27.61 GPa (4×10^6 psi), whereas the sliding displacement reduces while the modulus of the dam increases from 27.61GPa (4×10^6 psi) to infinite large. In the proposed *IDCE* model, however, the residual sliding displacement increases as the modulus either increases or decreases from 27.61GPa. When the modulus becomes very small or very large, the sliding displacement is also very small or converges to that of rigid model.

The difference of the responses between the two models is mainly due to the fact that the one-degree-of-freedom flexible model neglects the effect of high order mode vibration of the dam, which may be initiated and participate in the response. Table 7.2 illustrates the first three periods of vibration, from which it is found that bending and vertical tension/compression periods are 43.0% and 38.5%, respectively, of the fundamental one. It is natural that these modes of vibration will be initiated when impact occurs, and their effect on the sliding displacement will become more and more evident as the earthquake proceeds.

It is also noted that the response relates to the periods of the earthquake and the dam. The average period of the component S69E of Taft 1952 earthquake is about 0.258 seconds in the first 20-second period. Referring to Table 7.2, the dam with modulus 27.61 GPa has the fundamental period 0.262 seconds, which is the closest to 0.258 second. The corresponding residual sliding by the one-degree-of-freedom flexible model (Chopra and Zhang 1991) is correspondingly the closest to that by the proposed *IDCE* model. As the

modulus decreases, all periods of the dam increase so that the periods of higher order vibration may become close to or larger than the average period of the earthquake. For instance, if the modulus is 13.81GPa, the average period of the earthquake of 0.258 seconds is nearer to the second period 0.1593 seconds than to the fundamental one of 0.3705 seconds. Furthermore, it is shorter than the third period for modulus 3.45 GPa. This means the second, the third, or even the higher modes of vibration of the dam, which can be initiated by impact, will participate markedly in the seismic response of the dam.

However, the fundamental period of the dam becomes lower than the average period of the earthquake, if the modulus of the dam is 41.42 GPa or higher. If the modulus is relatively high, the fundamental period of the dam is relatively short compared to the average period of the earthquake, causing the dam to behave like a rigid body as indicated in Table 7.1 and Figure 7.3.

Contrary to the proposed *IDCE* model that is able to include high order modes of vibration of the dam, the one-degree-of-freedom flexible model (Chopra and Zhang, 1991) considers only the fundamental mode, meaning that other modes that may participate in the response are excluded. This may be the reason why the residual sliding displacements by the one-degree-of-freedom flexible model are generally less than those by *IDCE* finite element model, whereas the absolute error of residual sliding between these two models becomes quite small for very rigid dam as indicated in Table 7.1.

7.2.3 Rocking behavior of the triangular dam

Although the triangular dam with coefficient of friction and full reservoir water will not rock for the given earthquake of peak acceleration 0.5g according to the criterion

established for rigid model, it does rock in the *IDCE* finite element model. Figure 7.4 shows the rocking for modulus 27.61 GPa (4×10^6 psi) with maximum rotation of 5.04×10^{-4} radians in the downstream direction. The corresponding opening at the upstream face is 49.2 mm. The rocking is mainly in downstream direction due to the hydraulic pressure. However, the triangular dam rocks in upstream direction a few times during the most violent period of the earthquake between 3.8 and 8.5 seconds. It is natural to reckon that the rocking and accompanying impact initiate bending, tension/compression, and other higher modes of vibration besides the fundamental one, which enhances the downstream sliding with the help of hydraulic pressure.

Because of rocking and impact, vertical modes of vibration are obviously initiated such that the triangular dam experiences drifting movement as shown in Figure 7.5 with accumulated upstream drifting of 7.8 mm.

7.2.4 The triangular dam with larger coefficient of friction and more violent earthquake

With more violent ground motion and larger coefficient of friction as might be expected in cracked concrete gravity dams, the triangular dam in Figure 7.1 will not only slide, but also rock based on the criterion for rigid assumption. In this case, one-degree-of-freedom model, either rigid or flexible, is inapplicable. Therefore, the proposed 3-*DOF* and *IDCE* finite element models are adopted to study the seismic response. Table 7.3 summarizes the seismic response of the triangular dam with the full reservoir water,

the coefficient of friction of 1.4 and the Taft 1952 S69E earthquake with peak acceleration scaled to 0.9g.

Table 7.3 and Figure 7.6 show that the proposed *IDCE* model predicts 565.5 mm downstream sliding, while 3-*DOF* rigid model with coefficient of restitution e=0.5 estimates the sliding displacement of 155.4 mm. Both models indicate that the triangular dam will drift, and the accumulated amount may be 23.7 mm (3-*DOF* rigid model) or 27.2 mm (*IDCE* model). According to Figure 7.6, the time-histories of sliding estimated by the two models are completely different, indicating that the flexibility of the dam affects markedly its seismic response. Figure 7.7 demonstrates that the triangular dam will rock in both directions as predicted by both models. In the 3-*DOF* rigid model, the rocking angle is so small that the openings on both the upstream and downstream faces are less than 4 mm. However, the *IDCE* model estimates that the openings may be 128.3 mm and 86.2 mm on the upstream and downstream faces, respectively, which indicates the flexibility of the dam also affects markedly its rocking.

7.2.5 Summary of the seismic behavior of the triangular dam

With horizontal hydraulic pressure of full reservoir water and uplift pressure, the triangular dam with the coefficient of friction at the base of 1.0 will slide if imposing the component S69E of Taft 1952 earthquake scaled to 0.5g of peak acceleration. The induced downstream base sliding is about 0.359 m for the modulus of the dam 27.62 GPa. This amount of sliding is consistent with the one-degree-of-freedom flexible model that represents the effect of the fundamental mode of vibration. With other values of modulus for the dam, between 13.81 GPa and 41.42 GPa, the downstream sliding

displacement will be around 0.4 m. Although the dam would not rock in the rigid model, it experiences sliding, rocking, impact and drifting movements in the *IDCE* model.

With coefficient of friction 1.4 and peak acceleration 0.9g for the same earthquake component, the triangular dam will experience sliding, rocking, impact and drifting modes of motion as predicted by the proposed 3-*DOF* and *IDCE* finite element models. Under the effect of the full reservoir water, this dam will slide 565.5 mm in downstream direction for modulus 27.61 GPa, of which 4.8% is from drifting, whereas the 3-*DOF* rigid model predicts 155.4 mm downstream sliding.

In all cases studied, rocking angle is quite limited due to hydraulic pressure and low position of the mass center of the dam. However, the limited rocking and accompanying impact initiate other modes of vibration than the fundamental one such that the residual downstream sliding displacement is enhanced.

7.3 Application of *IDCE* model to cracked Koyna Dam

The *IDCE* model was used to analyze the stability of cracked Koyna Dam shown in Figure 3.1. Both longitudinal and transverse components of Koyna earthquake shown in Figure 5.16 and Figure 5.17, respectively, were imposed on the cracked dam. The same coefficients of 0.8, 1.0 and 1.2 as in Chapter 5 were used. As for the uplift pattern, both uniform and triangular pressures were considered. Some responses of the upper part of Koyna Dam for all these cases are summarized in Table 7.4.

7.3.1 Rocking behavior and overturning stability

Computations with the *IDCE* model show that in all the cases the upper part of the cracked Koyna Dam rocks limitedly. The largest angle of rocking is just 4.49×10^{-3}

radians (0.257°), occurring in downstream direction caused by longitudinal earthquake component for coefficient of friction of 1.2 with triangular uplift pressure assumption. This indicates that the cracked Koyna Dam is quite safe in overturning if the 1967 earthquake is imposed again.

The upper part will rock towards the downstream, except when the longitudinal earthquake component is imposed and the triangular uplift pressure is assumed. This is due to the hydraulic pressure of high level of water in the reservoir. Only when the longitudinal earthquake component with higher peak acceleration is applied, could the upper part rock a few times towards the water.

The rocking magnitude is consistent for triangular uplift pressure, showing that larger coefficient of friction yields larger rotation. This means larger coefficient of friction makes the upper part harder to slide and more energy is put into rocking mode. However, in the case of uniform uplift pressure, which was assumed by Saini and Krishna (1974) for conservative reason, this consistency is not upheld. If the uniform uplift pressure is assumed, the longitudinal component will cause rocking of 3.40×10^{-3} radians for coefficient of friction 1.0. However, the corresponding rocking is 2.93×10^{-3} radians for coefficient of friction 1.2.

Results in Table 7.4 also show that uniform uplift pressure assumption could not help ensure conservative rotation. In the case of longitudinal earthquake component and coefficient of friction 1.2, for instance, the peak rotation is 2.93×10^{-3} radians for uniform uplift pressure. Nevertheless, the corresponding value is 4.49×10^{-3} radians for triangle uplift pressure, as shown in Figure 7.8. This phenomenon occurs also in the case of transverse earthquake component. Figure 7.9 illustrates rotations of the upper part for

both types of uplift pressure with coefficient of friction 1.2 and transverse component of the earthquake.

Acknowledging that uniform uplift pressure in cracked Koyna Dam provides a moment helping the upper part to rock towards the water, it is realized that triangular uplift pressure may in general yield larger rocking in downstream direction. It is just the case when the transverse component is applied as shown in Table 7.4.

7.3.2 Sliding behavior and stability

The upper part of cracked Koyna Dam will slide along the crack in all cases. However, sliding becomes stable when the earthquake diminishes after 9 seconds. The residual sliding displacement is quite small; therefore the stability in sliding of the cracked Koyna Dam under the same strength of earthquake as 1967 will be maintained.

The residual sliding displacement is consistent with coefficient of friction as illustrated in Figure 7.10. However in the case of longitudinal component and uniform uplift pressure as shown in Table 7.4, the coefficient of friction 1.0 yields residual sliding 340.0 mm which is larger than 175.6 mm for coefficient of friction 1.2.

In the case of triangular uplift pressure, the maximum sliding is 162.9 mm caused by transverse component of earthquake with coefficient of friction 0.8. The minimum residual sliding is 59.6 mm caused by longitudinal component with coefficient of friction 1.2. In the assumption of uniform uplift pressure, the maximum and minimum residual sliding are 340.0 mm and 175.6 mm, respectively, caused by the longitudinal earthquake component.

It is noted form Table 7.4 that longitudinal component with larger peak acceleration does not necessarily yield larger residual sliding displacement. It is even inversely proportional for all coefficients of friction when triangular uplift pressure is adopted: the residual sliding displacements caused by the transverse earthquake component are 162.9 mm, 125.7 mm and 82.8 mm, respectively, for coefficient of friction 0.8, 1.0 and 1.2, whereas the longitudinal earthquake component with larger peak acceleration yields less sliding and the corresponding sliding displacements are 135.3 mm, 101.1 mm and 59.6 mm, respectively.

For the largest coefficient of friction 1.2, Figure 7.11 indicates the longitudinal earthquake component with larger peak acceleration inversely yields less sliding, indicating that the seismic behavior of cracked concrete dams depends on not only the strength of the earthquakes but also their details.

Figure 7.11 also shows that the uniform uplift pressure yields larger sliding displacement than triangular uplift pressure for both components of earthquake and all of coefficient of friction. This indicates that uplift affects the sliding markedly.

Drifting is noted when the longitudinal component of earthquake is imposed with triangular uplift pressure for all coefficients of friction. This drifting is consistent with the coefficient of friction. The accumulated drifting displacements are 26.7 mm and 1.5 mm for the coefficient of friction 0.8 and 1.2, respectively. Figure 7.12 shows the drifting component and overall sliding displacement caused by the longitudinal component with triangular uplift and coefficient of friction 1.0.

7.3.3 Conclusions for the stability of cracked Koyna Dam

Based on the above discussion, the cracked Koyna Dam is safe in both overturning and sliding, when the ground excitation similar to the 1967 Koyna earthquake is imposed with the assumption that the coefficient of friction at the crack is no less than 0.8.

The maximum rocking would be less than 4.49×10^{-3} radians in downstream direction. The residual sliding displacement along the crack will be less than 162.9 mm if triangular uplift pressure is assumed. Even if the unrealistic uniform uplift pressure is adopted, the residual sliding displacement would not beyond 340 mm.

Drifting motion is noted in some cases. This means rocking and impact will cause the upper part to drift under the hydraulic pressure. Therefore large coefficient of friction cannot prevent the relative sliding. However, the jump movement at the instance of impact, which is less then 10 mm in general, is quite small compared with the height of asperities on the crack. This implies that the true sliding displacement would be less than predicted.

7.4 The cracked typical dam

7.4.1 Introduction

The original typical concrete dam has the geometry in Figure 7.13. The modulus of the concrete $E = 20\,\text{GPa}$. Poisson's ratio $\nu = 0.143$. The density of the concrete $\rho_d = 2650\,\text{kg/m}^3$. The reservoir water depth is h_w. The density of the water $\rho_w = 1000\,\text{kg/m}^3$.

It is assumed that the typical dam is cracked either at the base as in Figure 7.14 or at a height as in Figure 7.15, respectively. Three values of coefficient of friction 0.8, 1.0 and 1.2 are used to study the effect of this parameter on the seismic behavior. Triangular uplift pattern is adopted for the cracks at both the base and the height.

Both the 3-*DOF* model and the *IDCE* model are applied for the analysis of the case of a crack at the base. Regarding the crack at a height, only the *IDCE* model is employed. Figure 7.16 and Figure 7.17 are the finite element meshes for the crack at the base and at a height, respectively.

The two inputs are the El Centro 1940 NS and Taft 1952 S69E earthquakes as shown in Figure 7.18 and Figure 7.19. Both are scaled to 0.4g of peak acceleration. In all cases, the damping ratio is 5%.

It is known that the water level obviously affects the seismic behavior. For the case of crack at the base with peak acceleration 0.4g, the lowest water levels to overcome the static friction force and to initiate sliding in the downstream direction for the coefficient of friction 0.8, 1.0 and 1.2 are 52.0 m, 71.1 m and 87.1 m, respectively, according to equation (4.3.12). To initiate sliding and for comparison, therefore, water levels 100 m, 95 m and 90 m are considered with 3-*DOF* rigid model for all values of coefficient of friction. In the *IDCE* finite element model, water level 100 m is considered to compare with the 3-*DOF* rigid model; whereas 50 m and 0 m water levels are adopted to study the influence of the flexibility of the dam on the seismic response when the water level is lower than the critical level determined in the rigid model or the reservoir is empty.

For the case of crack at the height, only the *IDCE* model is applied with water levels 100 m, 95 m and 90 m.

Due to the fact that the stiffness of the system keeps changing during the seismic process because of the change of the contact condition at the crack, the mass proportional and stiffness proportional damping coefficients in equation (6.4.13) also keep changing for given damping ratio of 5%. To simplify the calculation, damping coefficients in equation (6.4.13) are assumed to be of the original dam without crack, if both parts of the cracked dam are stuck to each other. If the upper part is rocking, sliding as a whole or drifting, damping coefficients are derived only from the lower part for the same damping ratio of 5%, neglecting the damping in the upper part. The coefficients, derived from the first and third natural frequencies, of Raleigh damping for all cases are illustrated in Table 7.5.

7.4.2 Crack at the base

Sliding behavior by 3-DOF rigid model. The responses from the 3-*DOF* rigid model are summarized in Table 7.6. It shows that the sliding of the typical dam cracked at the base is stable for all water levels and all considered coefficients of friction under both El Centro 1940 NS and Taft 1952 S69E earthquakes with peak acceleration of 0.4g. The largest residual sliding displacement is 1.487 m with water level 100 m and coefficient of friction 0.8 caused by Taft 1952 S69E earthquake component.

Table 7.6 shows that the residual sliding displacement is proportional to the water level and inversely proportional to the coefficient of friction. Figure 7.20 illustrates the sliding process for different water level of the typical dam with coefficient of friction 0.8

subject to Taft 1952 S69E earthquake component. Figure 7.21 shows the influence of coefficient of friction on the residual sliding displacement caused by the El Centro 1940 NS record.

It is worthy to note the case of coefficient of friction 0.8, with water level of 100 m, as shown in Figure 7.20. The critical acceleration to initiate sliding by equation (4.3.12) is just 0.031g in this case, indicating the dam will slide with very small excitation. Figure 7.20 shows that the typical dam slides almost all the time during the process of earthquake, resulting in a quite large amount of residual sliding displacement 1487 mm. This indicates that coefficient of friction of 0.8 is relatively low when the reservoir water is full. However, the residual sliding displacement will be 161mm if the coefficient of friction is 1.0.

Sliding behavior by IDCE model. The typical dam cracked at the base is also studied with the *IDCE* finite element model. The responses are summarized in Table 7.7. Water levels 50 m and 0 m are considered to study the response when the water is under the level that initiates static sliding for 3-*DOF* rigid model. Water level 100 m is to compare the largest residual sliding displacements with those from the 3-*DOF* rigid model.

From Table 7.7 and Figure 7.22, it is noted that the typical dam cracked at the base will have negligible horizontal displacement when the reservoir is empty. The negligible sliding is obviously due to the local deformation caused by the ground excitation. However, the typical dam slides for the water level 50 m, which is below the critical level that will overcome the static friction and initiate sliding as indicated in the 3-*DOF* rigid model. Under Taft S69E earthquake with water level 50 m, the typical dam

will slide 9.8 mm, 7.1 mm and 6.3 mm corresponding to coefficients of friction 0.8, 1.0 and 1.2, respectively. These displacements are still very small, but indicate that the sliding can be initiated with water below the critical level determined by the 3-*DOF* rigid model. This phenomenon also suggests that *IDCE* finite element model may predict more sliding displacement than 3-*DOF* rigid model when the water is above the critical level. It is noted in Figure 7.22 that the accumulated sliding is reduced around 2.5 seconds. This is due to a few peaks of downstream ground acceleration.

For water level of 100 m, the typical dam would fail if the coefficient of friction were 0.8 since the cracked dam would keep sliding in downstream direction with increased velocity and the displacement would be dozens of meters for both El Centro 1940 NS and Taft 1952 S69E records. If the coefficient of friction is increased, the residual sliding displacement can be reduced very much and become stable. With El Centro 1940 NS record, the residual displacements are 491.0 mm and 244.0 mm for coefficients of friction 1.0 and 1.2, respectively. With Taft record, these two values become 657.4 mm and 209.8 mm, respectively.

Comparison of IDCE finite element model with 3-DOF rigid model for sliding. It is noted form Tables 7.6 and 7.7 that the *IDCE* finite element model predicts very different residual displacements from the 3-*DOF* rigid model. However, it is reasonably expected that the flexible *IDCE* finite element model converge to the rigid 3-*DOF* model when increasing the modulus E to infinity. Therefore the typical dam cracked at the base is taken as an example in this regard under the condition of coefficient of friction 1.2, full reservoir water and Taft 1952 S69E earthquake component.

Table 7.8 shows that the residual sliding displacements by the *IDCE* finite element model converges to that of the 3-*DOF* rigid model as the modulus E of the material is increased. The process of sliding shown in Figure 7.23 demonstrates clearly that the stiffer the system is, the closer the results are by the two models. This verifies again that the flexibility of the system affects the seismic behavior, and that the proposed two models have their own advantages when applied to cracked concrete dams.

Rocking behavior. For all cases, the typical dam cracked at the base will not rock according to the 3-*DOF* rigid model. In the *IDCE* finite element model, however, the toe and heel of the dam base will open and close due to vibration of the dam. Neglecting the local deformation at the base, the average rotation of the base can be approximately determined according to the openness of the toe and the heel as shown in Table 7.9.

From Table 7.9, it is obvious that the typical dam cracked at the base is safe in rocking except for the failure cases when coefficient of friction is 0.8 and water level is 100 m. The maximum rotation of the base among all other cases is 5.63×10^{-4} radians. The corresponding openness at the toe of the crack is just 45.04 mm.

Discussions and conclusions. Based on the seismic behavior of the typical dam cracked at the base as revealed with both 3-*DOF* rigid and *IDCE* finite element models, the following is concluded:

The typical dam cracked at the base is unsafe if the coefficient of friction is 0.8 when the reservoir water is full under the earthquakes in Figure 7.18 and 7.19. In this case the 3-*DOF* rigid model predicts that the cracked dam will slide more than 1 m before becoming stable, whereas the *IDCE* finite element model estimates that the cracked dam will fail. Larger residual sliding displacement by the finite element model is due to the

fact that vibration of the cracked dam reduces the normal contact force and makes it easier to slide with lateral hydro pressure.

If the coefficient of friction is 1.0, the typical dam cracked at the base with full reservoir water will slide 491 mm and 657 mm and then become stable under the excitation of El Centro 1940 NS and Taft 1952 S69E earthquakes, respectively. These values are higher than the corresponding residual sliding displacements 191 mm and 161 mm obtained from the 3-*DOF* rigid model, also showing the considerable effect of vibration of the cracked dam on the residual sliding displacement.

If the coefficient of friction is 1.2, the residual sliding displacement will be less than 244 mm (El Centro) or 209.8 mm (Taft) according to the *IDCE* finite element model. These values will be just 51.2 mm (El Centro) and 35.7 mm (Taft) according to the 3-DOF rigid model. This means the typical dam cracked at the base is quite safe against given earthquake records, if the crack has effective aggregate interlock that is the equivalent of coefficient of friction of 1.2.

The rotation of the typical dam cracked at the base is so small in the *IDCE* finite element model that the safety against overturning is certainly no problem. However, the small rocking of the cracked dam helps increase sliding markedly. If impact in the *IDCE* finite element model is neglected, which accompanies the opening and closing of the toe and heel of the crack at the base, the residual sliding displacement will be underestimated as shown in the rigid model that ignores the opening and closing of the crack due to local deformation and vibration.

7.4.3 Crack at a height

As the 3-*DOF* rigid model does not consider the contact condition that the upper part of the cracked dam is supported at a point between the two lower corners, this model may induce unexpected errors if the upper part slides significantly. Therefore only the *IDCE* finite element model is employed to study the typical dam cracked at the height of 90 m. Responses caused by El Centro 1940 NS and Taft 1952 S69E earthquakes in Figure 7.18 and Figure 7.19 for different coefficients of friction and different water levels are summarized in Table 7.10 and Table 7.11.

Sliding behavior. The upper part of the typical dam cracked at the height of 90 m will slide along the crack in all cases, mainly in the downstream direction. The sliding is stable after the earthquake excitation stops. The maximum residual sliding displacement of 649.2 mm is induced by Taft 1952 S69E earthquake with coefficient of friction 0.8 when the reservoir is full. Figure 7.24 shows the sliding of the upper part caused by Taft 1952 S69E earthquake component with coefficient of friction 0.8.

Table 7.10 shows clearly that the residual sliding displacement is consistently proportional to the coefficient of friction for both types of earthquake and two water levels 95 m and 100 m as shown in Figure 7.25 for the sliding of the upper part with water level 95 m induced by El Centro 1940 NS earthquake component. With large coefficient of friction of 1.2 the upper part will slide less, but coefficient of friction cannot prevent the upper part from sliding. The residual sliding displacements induced by El Centro 1940 NS and Taft 1952 S69E earthquakes with coefficient of friction 1.2 and water level 100 m are 209.7 mm and 316.4 mm, respectively.

The upper part still slides even if the water level is 90 m for which there is no hydro pressure on the upper part. This is due to drifting of the upper part after impacts. The maximum residual sliding displacements for water level 90 m is 90.8 mm induced by El Centro 1940 NS earthquake while the coefficient of friction is1.0. If induced by Taft 1952 S69E earthquake, this maximum value is 85.2 mm.

Rocking behavior. The upper part of the typical dam cracked at the height of 90 m will rock with respect to the crack in all cases. But the largest rotation with respect to the lower part is just 0.0149 radians ($\mu = 1.2$, $h_w = 100$ m) in downstream direction. The corresponding opening of the crack at the upstream face is 119.2mm.

Compared with the case of water level 95m, rotations in both directions for full water are considerably higher for each type of earthquake and every coefficient of friction. Take the coefficient of friction of 1.2 with El Centro 1940 NS as an example. The maximum rotations of the upper part for water level 95 m are 0.008441 radians and 0.004387 radians in downstream and upstream directions, respectively, whereas these two values will be 0.0128 and 0.0135, respectively, if the reservoir is full.

Even if the water level is so low that there is no hydro pressure on the upper part, it still has residual sliding displacement for each type of earthquake and every coefficient of friction. Figure 7.26 demonstrates the overall sliding and its drifting component for the case of El Centro NS earthquake component and coefficient of friction 1.0. From this Figure, it is very interesting to note that the majority of the residual sliding of the upper part is due to its drifting after impacts. This suggests that rocking and impact are necessarily to be considered in estimating the sliding displacement of cracked concrete dam.

Discussions and conclusions. According to the behavior revealed by the above finite element analysis, we have conclusions as below for the typical dam cracked at the height of 90 m:

The upper part is safe in sliding if the coefficient of friction is 1.0 or greater. The largest sliding displacement of 649.2mm is induced in the downstream direction by the Taft 1952 S69E earthquake component for coefficient of friction 0.8 with full reservoir water.

The residual sliding displacement is always in the downstream direction and consistently proportional to water level due to the hydro pressure. However, even if the water level is below the crack, the upper part still slides owning to its drift after impact.

The residual sliding displacement is nearly always inversely proportional to the coefficient of friction. However, large coefficient of friction, such as 1.2, cannot prevent the upper part from sliding along the crack. This is also due to the drifting motion of the upper block after impact.

The upper part is safe also in overturning, as the rocking is very small in all cases. The largest rotation with respect to the lower part is 0.0149 radians induced by Taft 1952 S59E earthquake component in downstream direction for coefficient of friction 1.2 with full reservoir water. This amounts to a crack mouth opening of 119 mm at the upstream face.

However, rocking affects sliding in all cases. While the crack is closing the normal contact force is decreased, and hence this may lead to shear overcoming the static friction. After impact, the upper part receives impulse and vibrates in vertical direction, which may also decrease the normal contact forces and even result in drifting. Therefore,

rocking, although it might be small, has to be considered for estimating the safety against sliding of cracked concrete dams.

7.4.4 Summary of the seismic behavior of the cracked typical dam

According to the analysis of the typical dam cracked at both the base and at the height of 90 m, respectively, under the excitation of El Centro 1940 NS and Taft 1952 S69E earthquake components, we can summarize as below:

If cracked at the base, the typical dam is stable in both sliding and overturning when the coefficient of friction is 1.0 or higher even if the reservoir is full, as predicted by both the 3-*DOF* rigid model and the *IDCE* finite element model. If the coefficient of friction is 0.8, the 3-*DOF* rigid model shows the residual sliding displacements are as large as 1120mm and 1487mm for El Centro 1940 NS and Taft 1952 S69E earthquakes, respectively, whereas the typical dam in this case will fail according to the *IDCE* finite element model.

For the case of the crack at the base of the dam, the 3-*DOF* rigid model underestimates the residual sliding displacement compared to the *IDCE* finite element model. This is due to the fact that the flexible model can reflect the vibration of the cracked dam, which increases its instability.

If cracked at a height, the typical dam is stable in both sliding and overturning in all considered cases, as shown by both models.

In both cases of cracks, the residual sliding displacements are in the downstream direction for all cases. The amount of sliding is proportional to the water level, showing

that the lateral hydro pressure is an important factor in the estimation of the safety in sliding.

In both cracked cases, the residual sliding displacement will consistently decrease as the coefficient of friction increases. However, the residual sliding displacement is still 244.0 mm (cracked at the base, El Centro 1940 NS earthquake) and 316.4 mm (cracked at the height) for full reservoir water when coefficient of friction is as high as 1.2. This indicates that large coefficient of friction cannot prevent completely the upper part of the cracked typical dam from sliding along its crack.

In both cracked cases, rotation of the dam above the crack is quite limited. So there is no safety problem against overturning. However, rocking is related to sliding, as the rocking and accompanying impact of the cracked dam can reduce the normal contact force, even causing drifting of the upper part in some cases.

Table 7.1 Summary of seismic responses of the triangular dam caused by Taft 1952 S69E earthquake ($\mu = 1.0$)

Modulus of the dam (GPa)	Residual sliding (m) by Chopra and Zhang (1991)	Proposed *IDCE* model				
		Residual sliding (mm)	Downstream rocking		Upstream rocking	
			Maximum rotation (10^{-4} rad)	Opening at the upstream face (mm)	Maximum rotation (10^{-4} rad)	Opening at the downstream face (mm)
∞*	0.063+	0.095	0.10	1.0	0.06	0.8
41.42	0.271	0.432	2.03	19.8	0.82	8.0
27.61	0.378	0.359	5.04	49.2	1.06	10.3
13.81	0.232	0.424	6.15	60.0	1.40	13.6
6.90	0.171	0.495	7.30	71.2	1.57	15.3
3.45	0.030	0.311	4.32	42.1	0.03	0.3

Table 7.2 First three periods of the triangular dam with empty reservoir

Method	Mode	Period (s)					Mode shape
		$E = 41.42$ GPa	$E = 27.61$ GPa	$E = 13.81$ GPa	$E = 6.90$ GPa	$E = 3.45$ GPa	
Chopra and Zhang (1991)	1	0.2286	0.2800	0.3960	0.5600	0.7920	Horizontal swaying
SAP2000	1	0.2139	0.2620	0.3705	0.5240	0.7410	Horizontal swaying
	2	0.0920	0.1126	0.1593	0.2252	0.3186	Bending
	3	0.0823	0.1008	0.1425	0.2016	0.2850	Vertical tension/compression

* In the *IDCE* model, using modulus E=2000 GPa.

+ Estimated from Figure 3 of Chopra and Zhang (1991).

Table 7.3 Summary of the seismic response of the triangular dam subject to Taft 1952 S69E of 0.9g peak acceleration ($\mu = 1.4$, e=0.5 in the 3-*DOF* model)

Model		Residual down-stream sliding (mm)	Accumulated drifting (mm)	Downstream rocking		Upstream rocking	
				Max (10^{-4} rad)	Opening at up-stream face (mm)	Max (10^{-4} rad)	Opening at down-stream face (mm)
3-*DOF*		155.4	23.7	0.13	1.3	0.39	3.8
IDCE	E=27.61 GPs	565.5	27.2	13.11	128.3	8.84	86.2
	E=2000 GPa	166.5	83.3	0.08	8.3	0.07	6.4

Table7.4 Summary of the response of the upper part of the monolith of cracked Koyna Dam by *IDCE* finite element model

Earthquake component		Transverse						Longitudinal					
Uplift pattern		Uniform			Triangular			Uniform			Triangular		
Coefficient of friction		0.8	1.0	1.2	0.8	1.0	1.2	0.8	1.0	1.2	0.8	1.0	1.2
Peak rocking ($^{10-4}$ rad)	Downstream	1.93	2.7	21.4	20.9	24.9	33.6	27.2	34.0	29.3	23.1	24.0	44.9
	Upstream	0.0	0.0	0.0	0.0	0.0	0.0	0.0	0.0	0.8	15.3	15.7	3.2
Open (mm)	Upstream face	37.7	51.0	40.0	42.1	47.4	62.9	50.9	64.5	54.8	45.7	45.4	83.8
	Downstream face	0.0	0.0	0.0	0.0	0.0	0.0	0.0	0.0	0.0	28.4	29.0	6.5
Residual sliding (mm)		257.9	222.8	186.9	162.9	125.7	82.8	250.0	340.0	175.6	135.3	101.1	59.6
Residual drifting distance Percentage of residual sliding		0.0 0.0%	0.0 0.0%	0.0 0.0%	0.0 0.0%	0.0 0.0%	0.0 0.0%	0.0 0.0%	0.0 0.0%	0.0 0.0%	26.7 19.7%	25.3 25.0%	1.5 2.5%

Table 7.5 Damping coefficients of cracked typical dam

	Cracked at the base			Cracked at the height					
				Two parts stuck			Rocking and/or sliding		
Water Level (m)	100	50	0	100	95	90	100	95	90
1st Frequency (rad)	16.98	22.50	22.69	16.98	17.92	19.13	19.15	19.65	20.59
3rd Frequency (rad)	60.18	61.45	61.49	60.18	60.81	61.21	63.61	63.68	63.92
Stiffness proportional damping coefficient	0.001296	0.001191	0.001188	0.001296	0.001270	0.001245	0.001208	0.001200	0.001183
Mass proportion al damping coefficient	1.324162	1.647130	1.657221	1.324162	1.383863	1.457345	1.472099	1.501518	1.557523

Table 7.6 Residual downstream sliding (mm) of the typical dam cracked at the base (3-*DOF* rigid model)

Earthquake		El Centro 1940 NS			Taft 1952 S69E		
Water Level (m)		90	95	100	90	95	100
Coefficient of friction	0.8	181.7	384.6	1120.2	148.8	439.2	1487.0
	1.0	40.8	86.9	191.4	28.6	60.6	161.0
	1.2	8.4	21.9	51.2	3.6	15.0	35.7

Table 7.7 Residual downstream sliding (mm) of the typical dam cracked at the base (*IDCE* model)

Earthquake		El Centro 1940 NS			Taft 1952 S69E		
Water Level (m)		0	50	100	0	50	100
Coefficient of friction	0.8	-0.4	3.2	Failure	-0.6	9.8	Failure
	1.0	-0.1	-1.0	491.0	-0.2	7.1	657.4
	1.2	-0.1	-1.1	244.0	-0.1	6.3	209.8

Table 7.8 *IDCE* finite element model converges to 3-*DOF* rigid model when increasing the modulus of the material by studying the residual downstream sliding of the typical dam cracked at the base (μ=1.2, h_w=100m, Taft 1952 S69E)

Model	*IDCE*				3-*DOF*
Modulus (GPa)	E=20	E=200	E=2000	E=20000	E=∞
Residual sliding (mm)	217.84	94.03	51.79	36.62	35.71
Relative error	83.61%	62.02%	31.05%	2.48%	----

Table 7.9 Base rotation (10^{-4} radians) of the typical dam cracked at the base (*IDCE* model)

Earthquake			El Centro 1940 NS			Taft 1952 S69E		
Water Level (m)			0	50	100	0	50	100
Coefficient of friction	0.8	downstream	0.03	0.30	Failure	0.04	0.26	Failure
		upstream	0.85	1.49	Failure	0.97	1.11	Failure
	1.0	downstream	0.03	0.36	2.49	0.00	0.31	4.07
		upstream	0.91	1.63	1.75	1.00	1.17	1.35
	1.2	downstream	0.00	0.37	5.51	0.04	0.34	5.63
		upstream	0.09	1.71	1.70	0.99	1.19	0.73

Table 7.10 Residual downstream sliding (mm) of the typical dam cracked at a height (*IDCE* model)

Earthquake		El Centro 1940 NS			Taft 1952 S69E		
Water Level (m)		90	95	100	90	95	100
Coefficient of friction	0.8	66.1	200.1	414.8	117.9	328.6	649.2
	1.0	90.8	159.7	285.2	85.2	209.1	381.9
	1.2	66.1	101.7	209.7	81.0	157.3	316.4

Table 7.11 Relative rotation (10^{-4} radians) of upper part of the typical dam cracked at a height (*IDCE* model)

Earthquake			El Centro 1940 NS			Taft 1952 S69E		
Water Level (m)			90	95	100	90	95	100
Coefficient of friction	0.8	downstream	54.40	54.02	85.96	41.15	49.73	82.47
		upstream	50.47	52.41	64.65	28.75	19.98	43.83
	1.0	downstream	37.91	59.77	137.64	45.90	62.27	130.88
		upstream	51.81	45.03	127.28	31.22	41.73	59.10
	1.2	downstream	44.72	84.41	128.41	46.49	84.19	149.02
		upstream	51.15	43.87	135.19	31.60	55.53	67.70

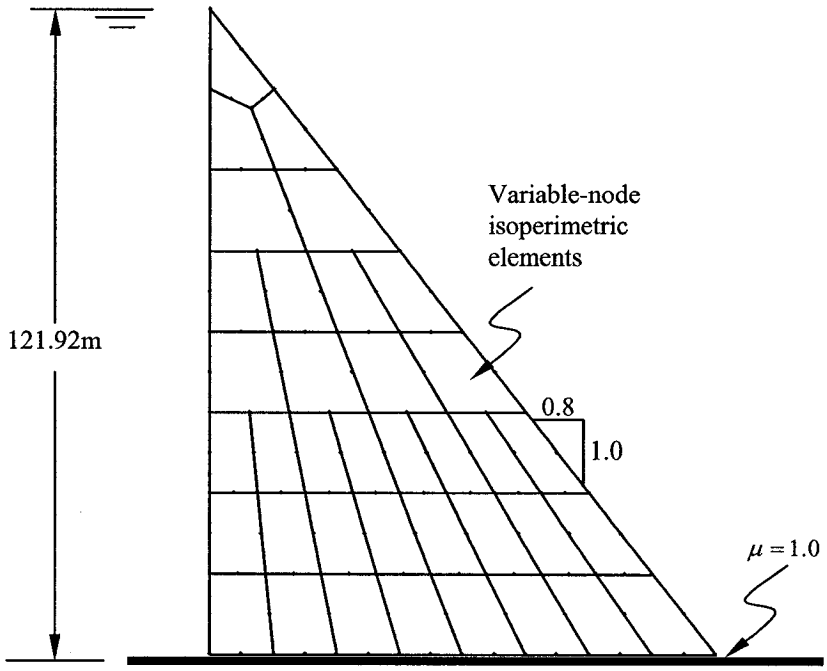

Figure 7.1 Finite element mesh of the triangular dam with coefficient of friction 1.0 at the base

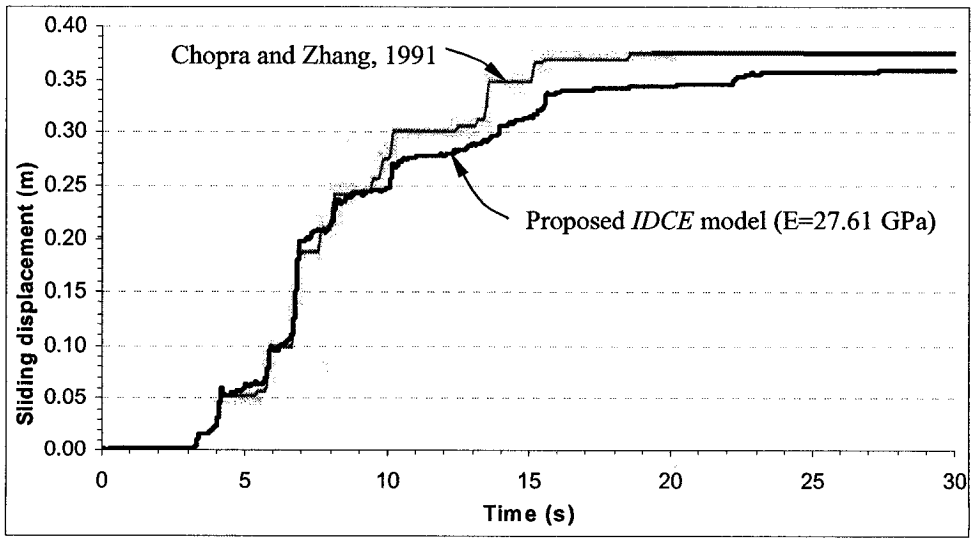

Figure 7.2 Base sliding of the triangular dam induced by Taft 1952 S69E earthquake with peak acceleration of 0.5g ($\mu = 1.0$)

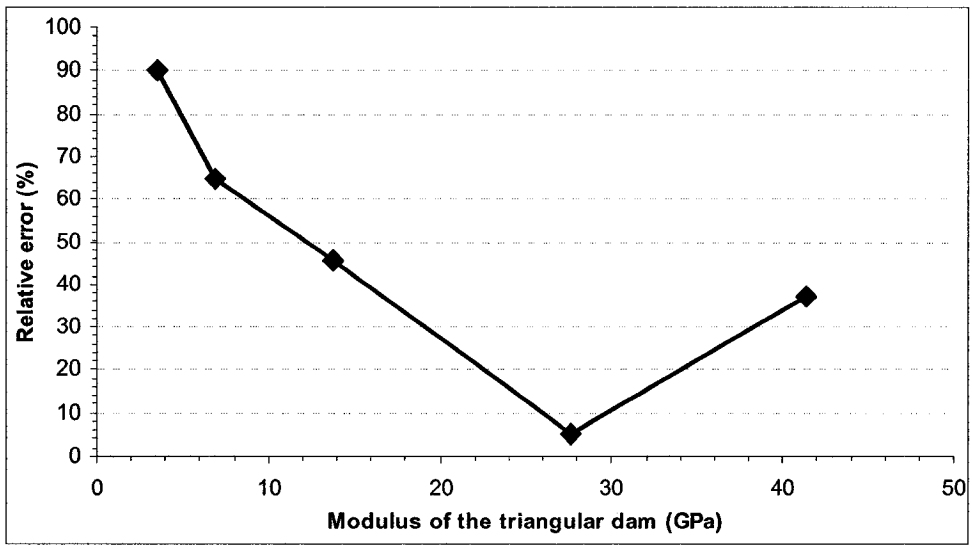

Figure 7.3 Comparison of sliding of one-degree-of-freedom flexible model to that of *IDCE* model for the triangular dam ($\mu = 1.0$)

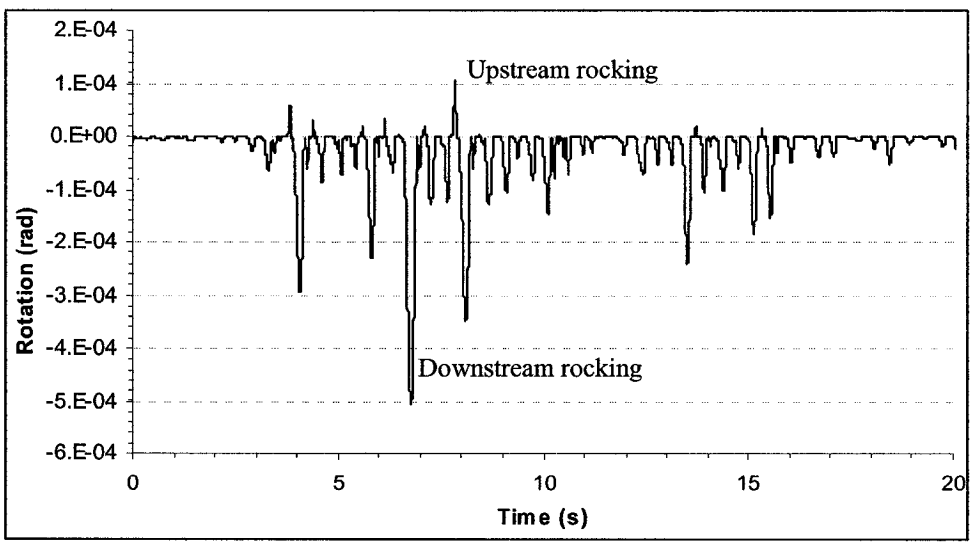

Figure 7.4 Rocking of the triangular dam caused by Taft 1952 S69E earthquake

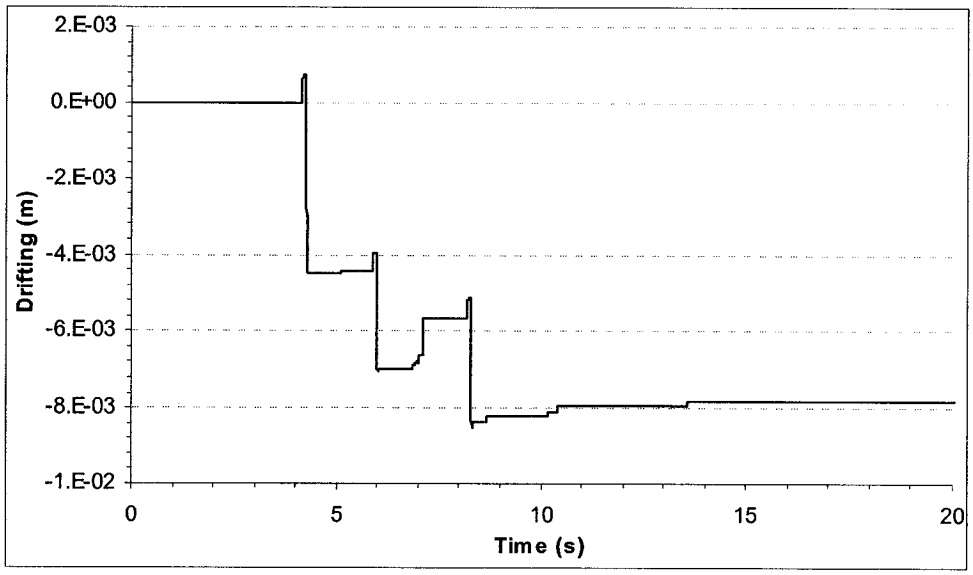

Figure 7.5 Drifting of the triangular dam caused by Taft 1952 S69E earthquake (*IDCE* model, $\mu = 1.0$)

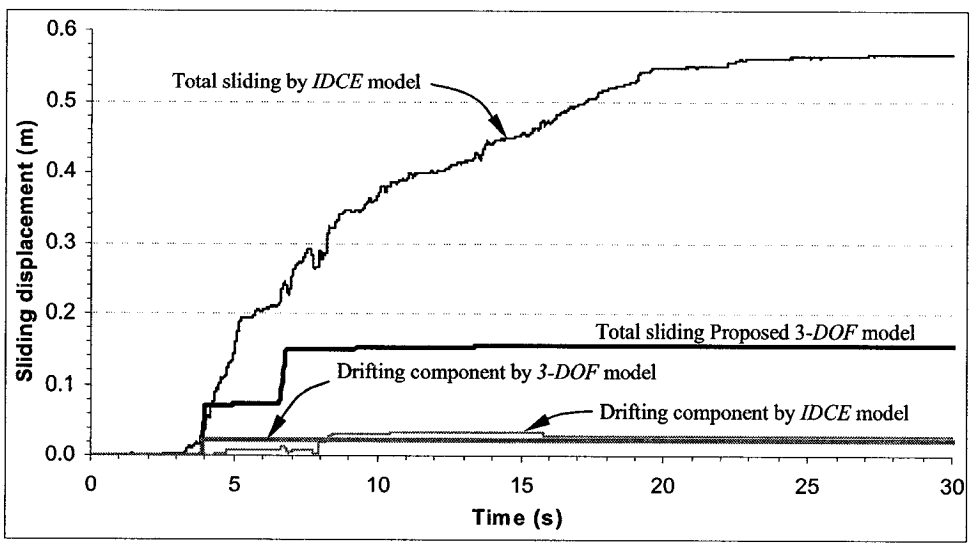

Figure 7.6 Base sliding of the triangular dam (E=27.61 GPa) induced by the S69E component with peak acceleration scaled to 0.9g of the Taft 1952 earthquake ($\mu = 1.4$)

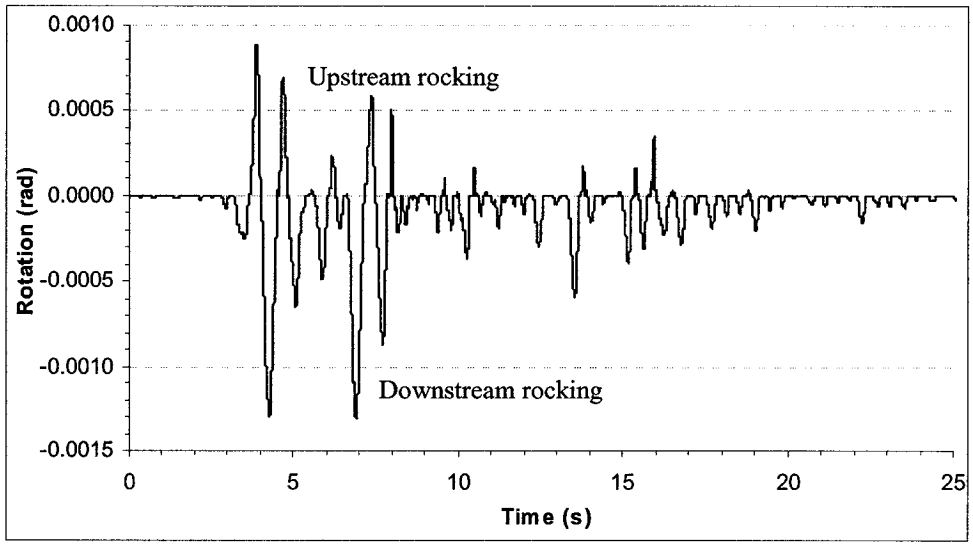

Figure 7.7 Base sliding of the triangular dam induced by the S69E component with peak acceleration scaled to 0.9g of the Taft 1952 earthquake ($\mu = 1.4$)

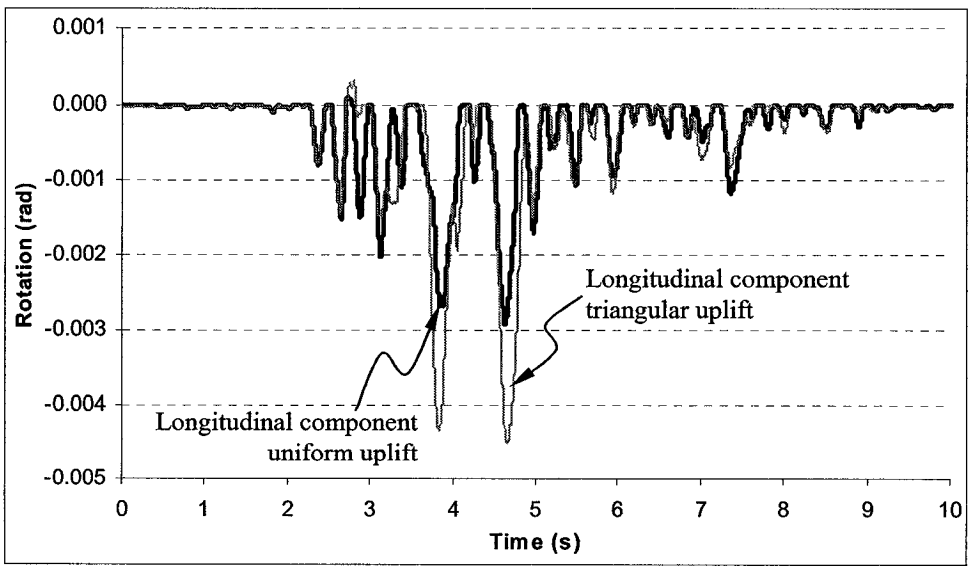

Figure 7.8 Rocking of the upper part of cracked Koyna Dam caused by longitudinal component of Koyna earthquake ($\mu = 1.2$)

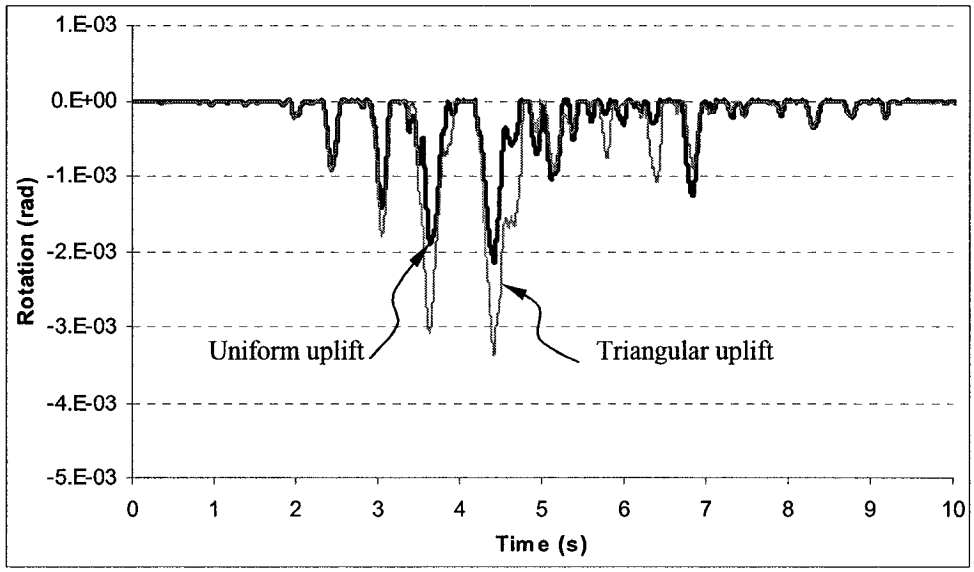

Figure 7.9 Rocking of the upper part of cracked Koyna Dam caused by transverse component of Koyna earthquake ($\mu = 1.2$)

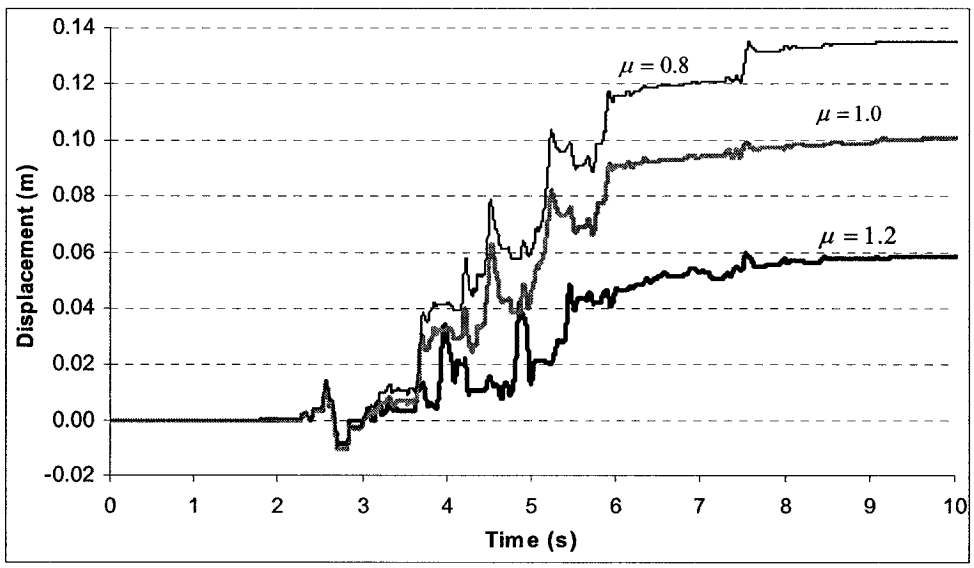

Figure 7.10 Sliding of the upper part of cracked Koyna Dam with triangular uplift caused by longitudinal component of Koyna earthquake

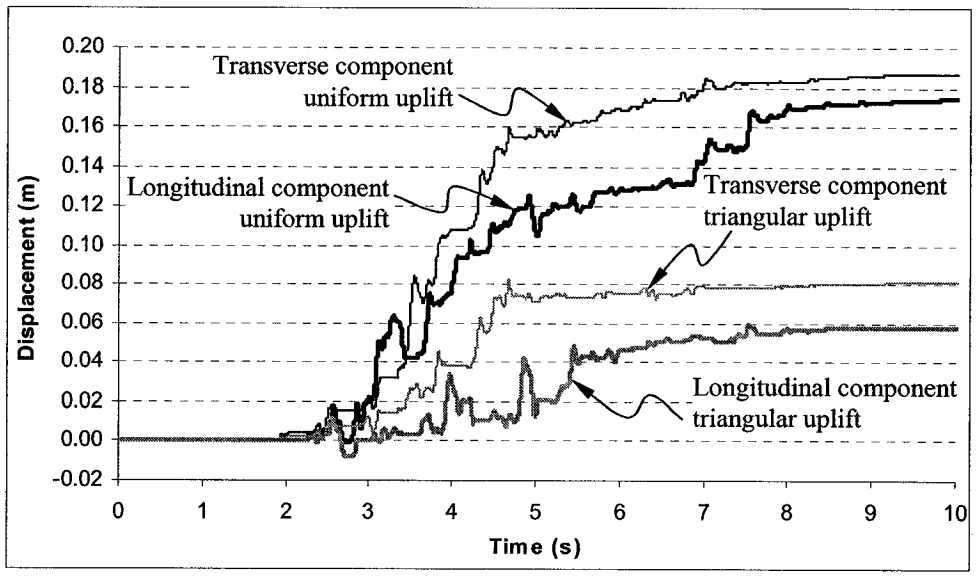

Figure 7.11 Sliding of the upper part of Koyna Dam ($\mu = 1.2$)

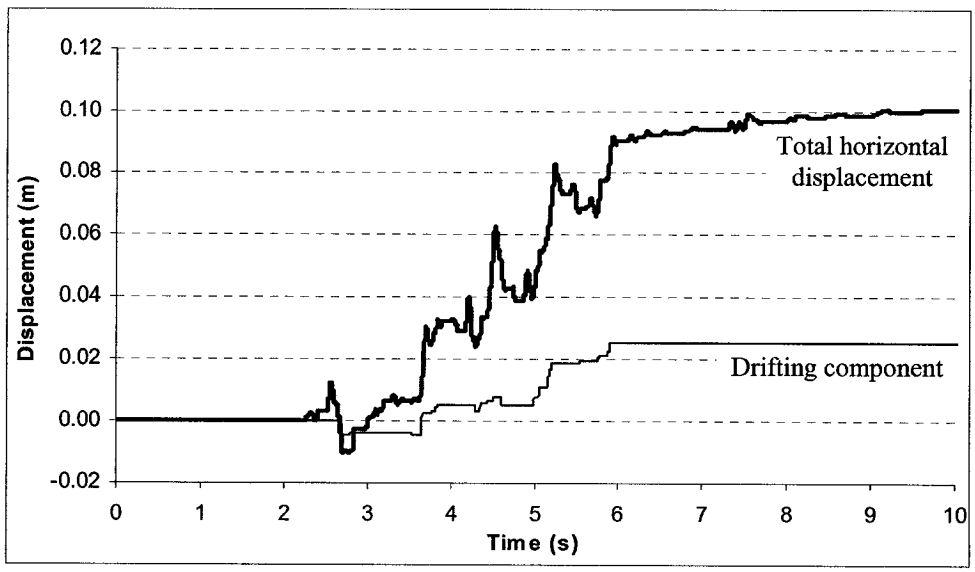

Figure 7.12 Drifting component in horizontal displacement of upper part of cracked Koyna Dam in the case of $\mu = 1.0$, triangular uplift and longitudinal component of Koyna earthquake

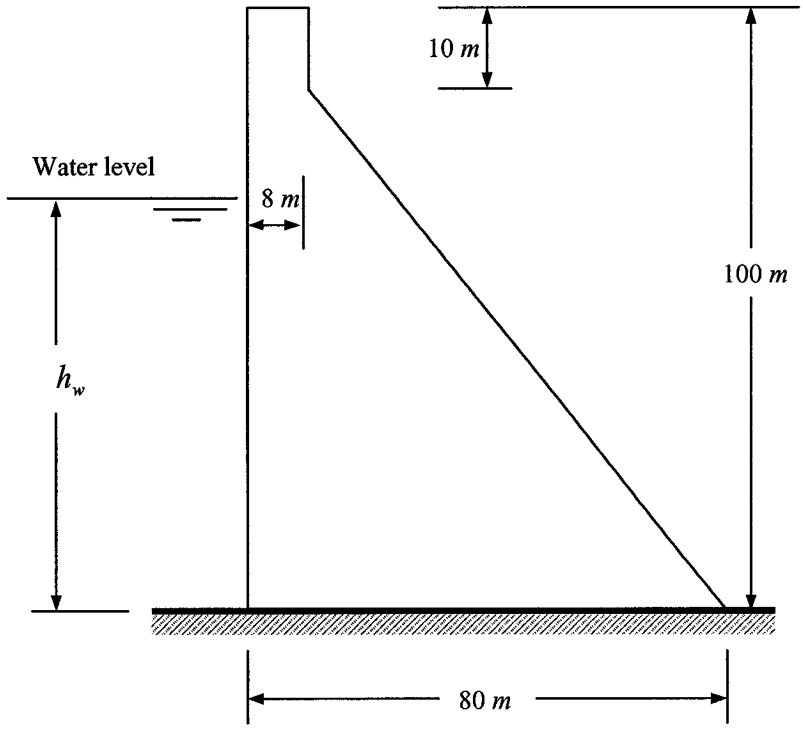

Figure 7.13 Typical concrete dam

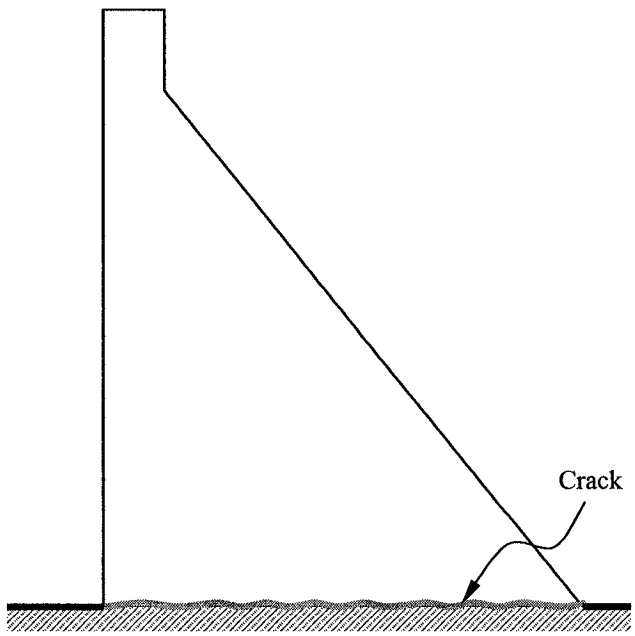

Figure 7.14 Typical concrete dam with crack at the base

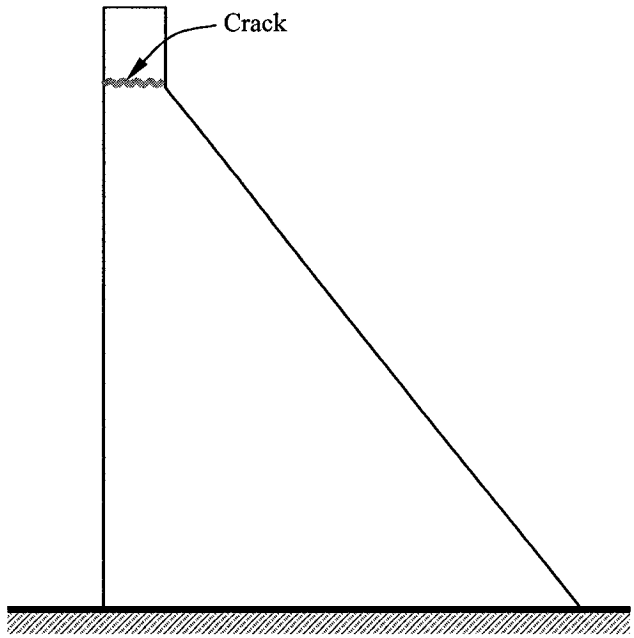

Figure 7.15 Typical concrete dam with crack at a height

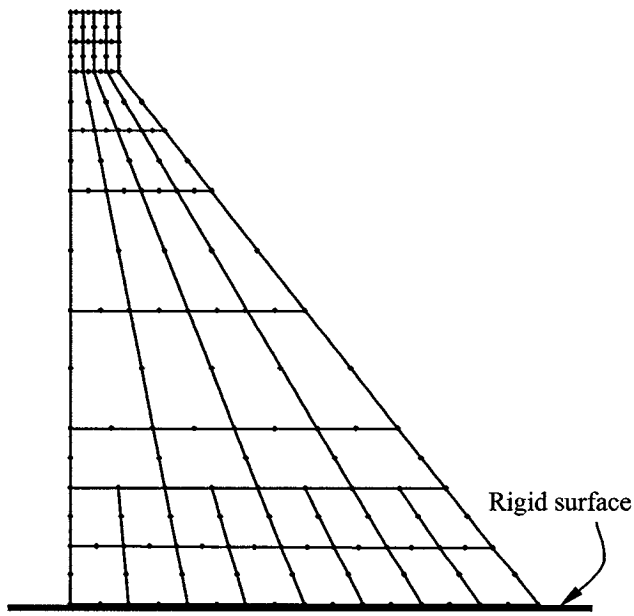

Figure 7.16 Finite element mesh of the typical dam cracked at the base

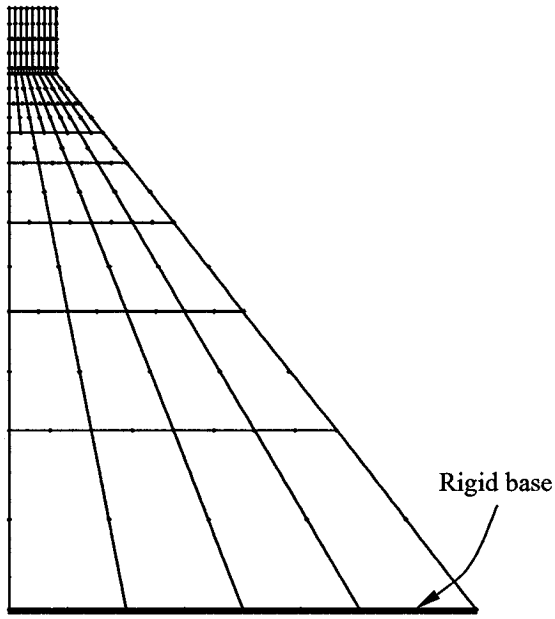

Figure 7.17 Finite element mesh of the typical dam cracked at a height

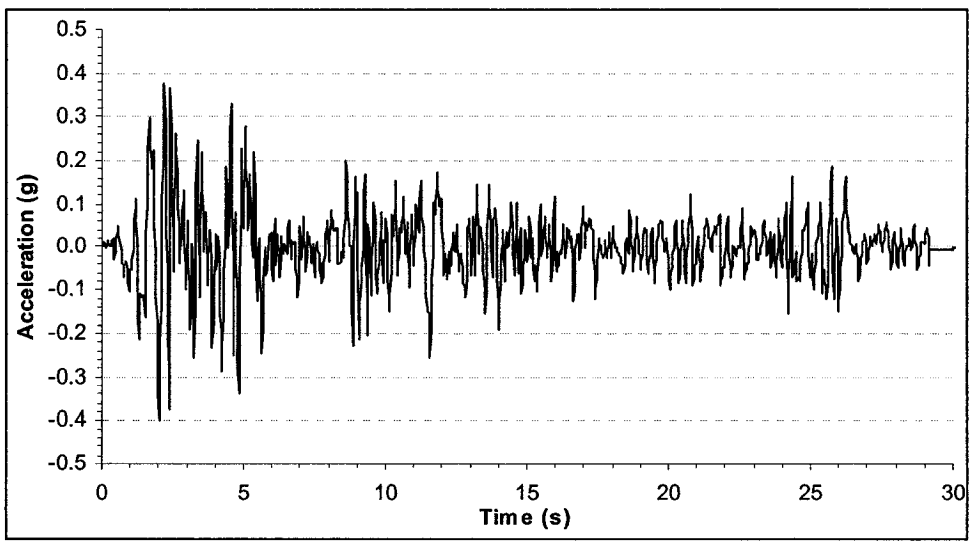

Figure 7.18 Scaled El Centro 1940 NS earthquake acceleration record

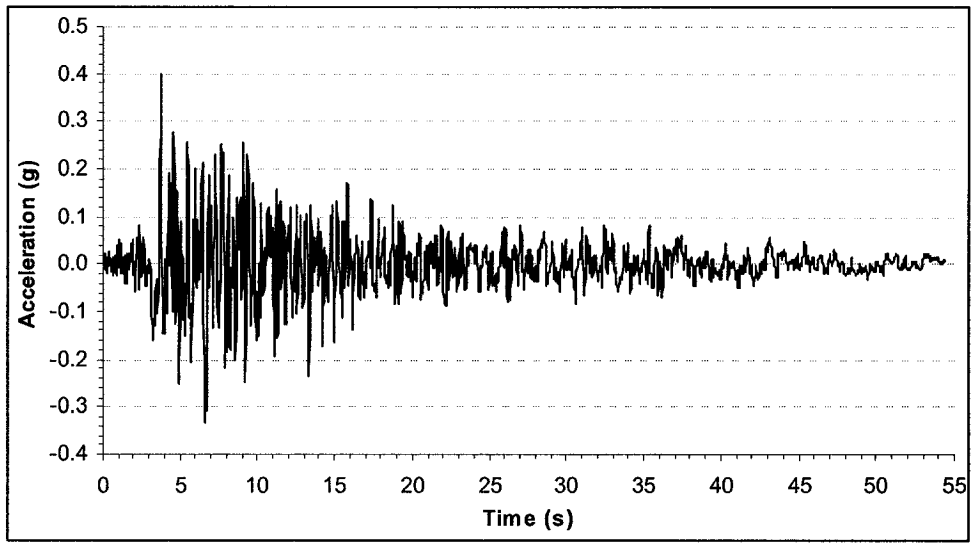

Figure 7.19 Scaled Taft 1952 S69E earthquake acceleration record

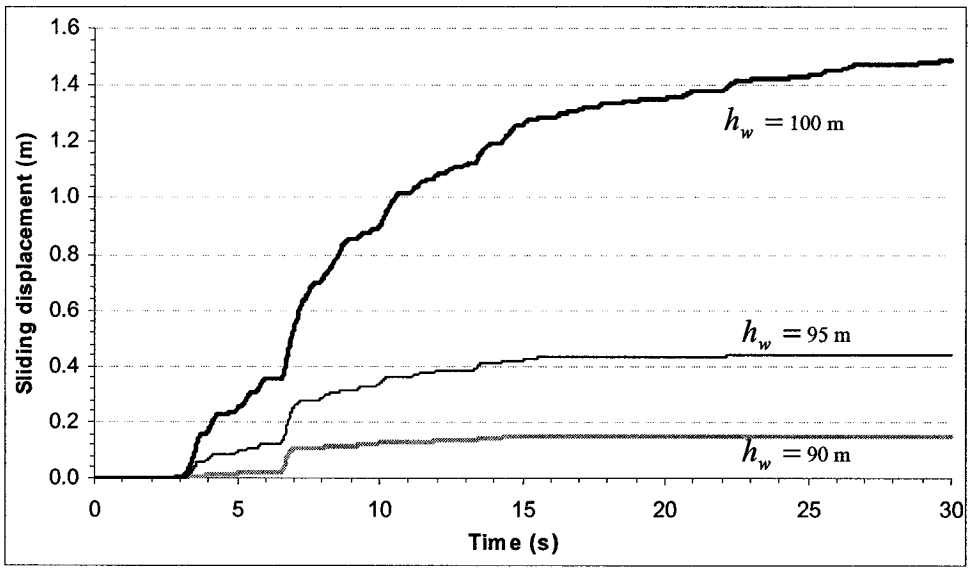

Figure 7.20 Sliding of the typical dam cracked at the base with coefficient of friction 0.8 caused by Taft 1952 S69E component (3-*DOF* rigid model)

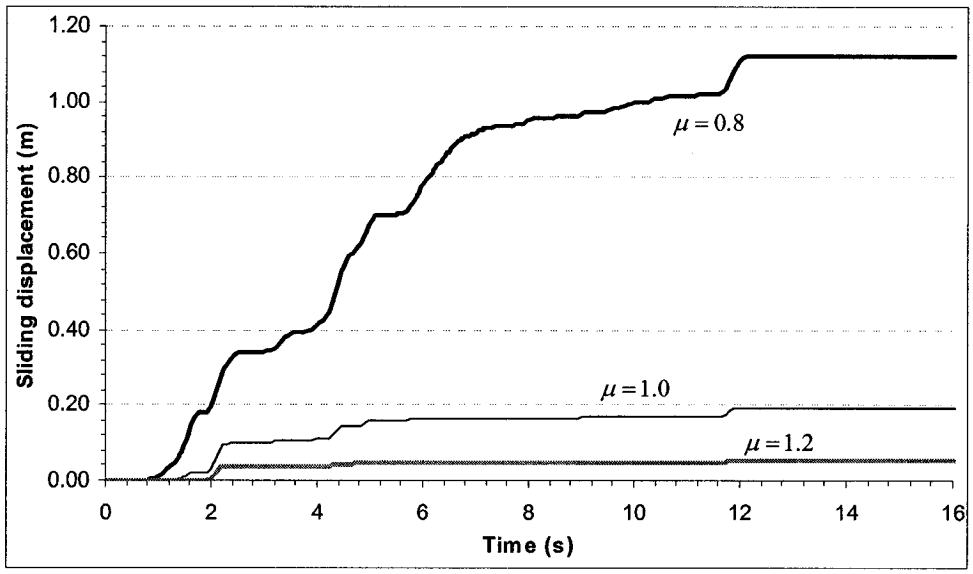

Figure 7.21 Sliding of the typical dam cracked at the base with water level 100 m caused by El Centro 1940 NS (3-*DOF* rigid model)

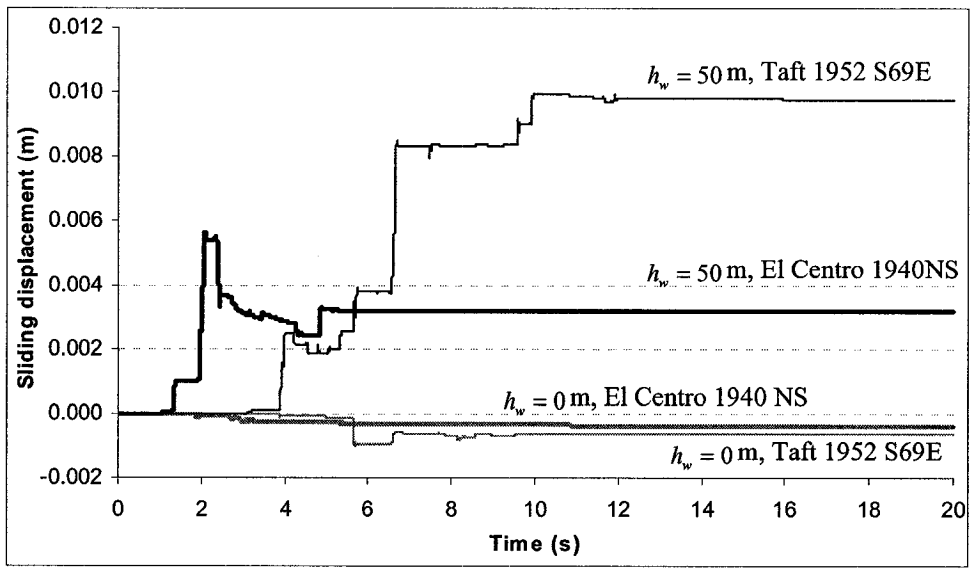

Figure 7.22 Sliding of the typical dam cracked at base with coefficient of friction 0.8 and lower water level (*IDCE* model)

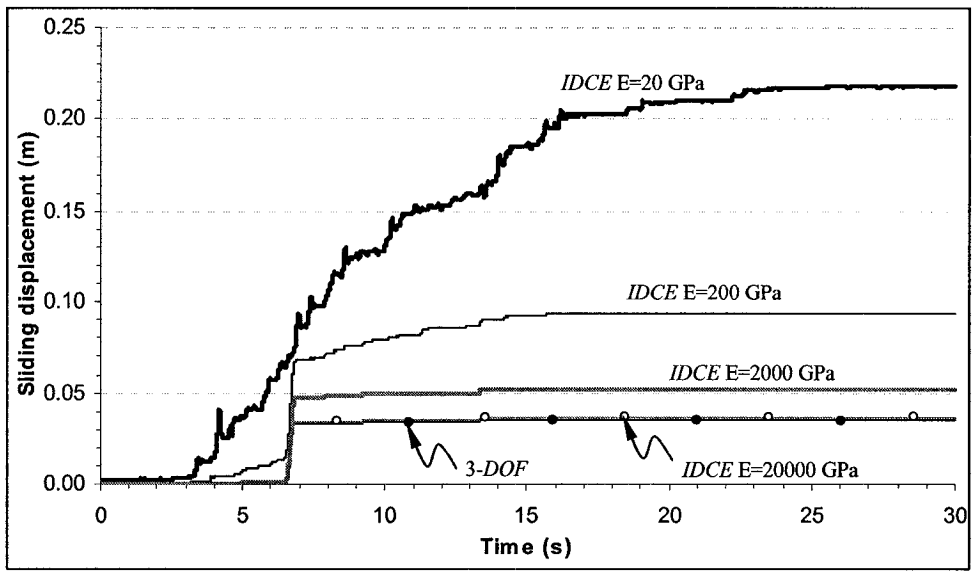

Figure 7.23 Comparison of models for sliding caused by Taft 1952 S69E of the typical dam cracked at the base with coefficient 1.2 and full water

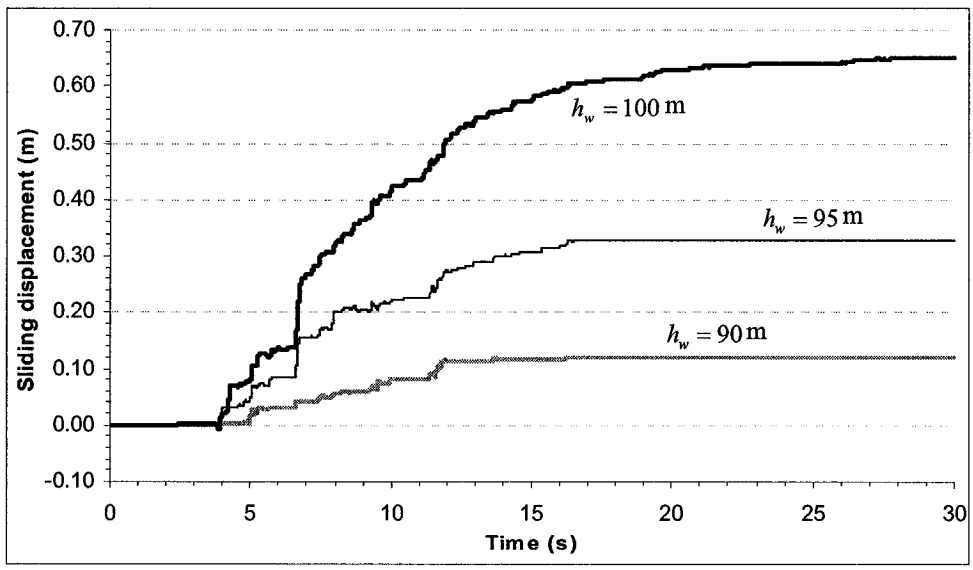

Figure 7.24 Sliding of the upper part of the typical dam cracked at 90 m with coefficient of friction 0.8 caused by Taft 1952 S69E (*IDCE* model)

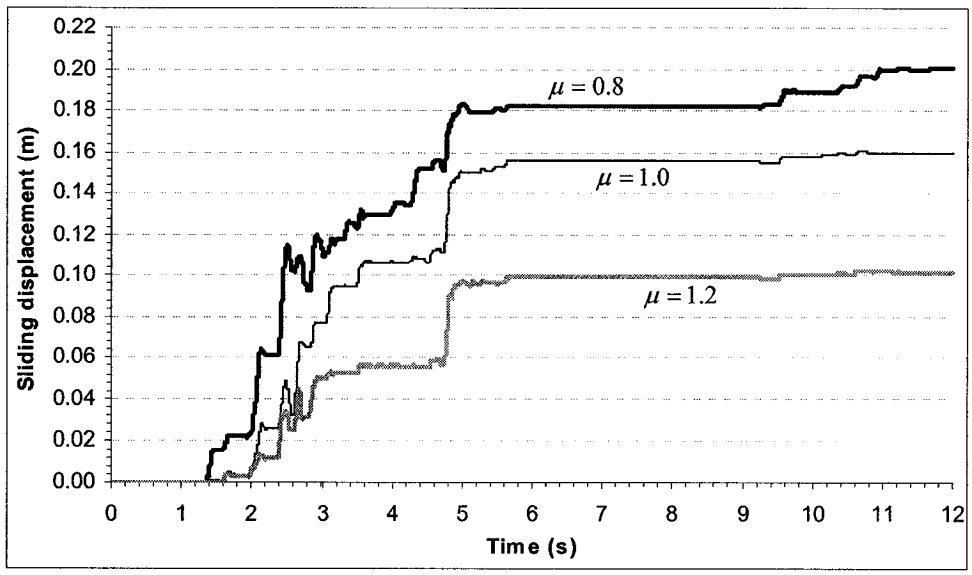

Figure 7.25 Sliding of the upper part of the typical dam cracked at 90 m with water 95m caused by El Centro 1940 NS (*IDCE* model)

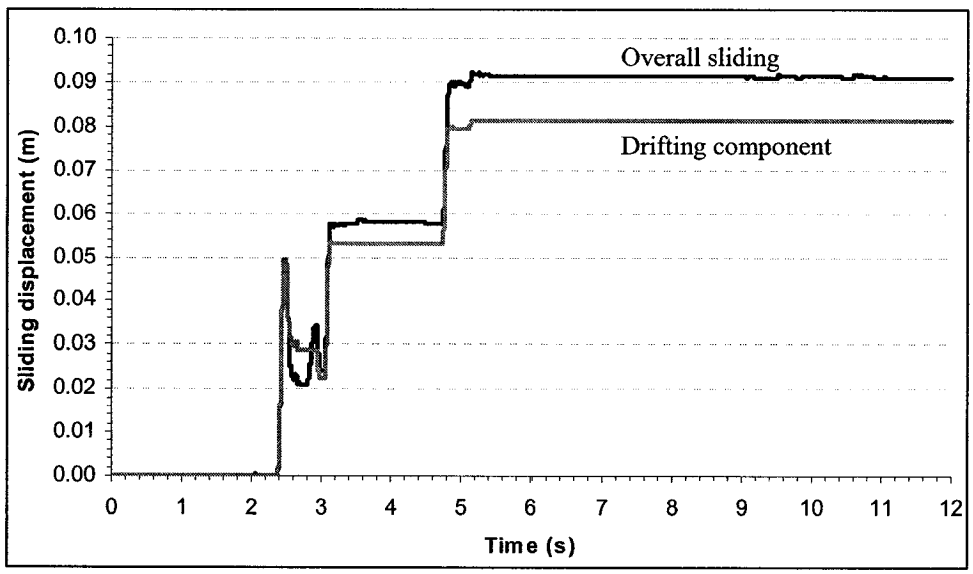

Figure 7.26 Overall sliding and drifting component of the upper part of the typical dam cracked at the height of 90 m with coefficient of friction 1.0, water level 90 m and El Centro 1940 NS (*IDCE* model)

CHAPTER VIII

CONCLUSIONS AND RECOMMENDED FUTURE WORK

8.1 Conclusions

3-*DOF* rigid and *IDCE* finite element models are proposed and applied to study the seismic behaviour of cracked concrete gravity dams. From the analyses and results presented in this thesis, the following principal conclusions have been derived:

1. The proposed 3-*DOF* rigid model is the first rigid model considering the general geometry and all possible modes of motion in the seismic analysis of cracked concrete dams. In this model, the block above the crack in a concrete dam is considered as a rigid with 3 degrees-of-freedom. The motions of the block are classified into sliding, rocking, slide-rocking and drifting.
2. The proposed *IDCE* finite element model describes the contact conditions at the crack by use of incremental displacement constraint equations accompanied by the friction law in the seismic procedure. The constraint equations are introduced into the finite element model via a penalty method.
3. Owing to assumptions in the 3-*DOF* rigid model, it is very effective in the case that the crack locates at the base of the dam and the dam is relatively rigid. Because of its simplicity, the 3-*DOF* rigid model does not include the change of contact condition after sliding in the case of crack at a height. However, this simple model is able to give a fast and rough estimation of the seismic behaviour for cracked concrete dams. The stiffer the dam is, the more accurate the estimation will be.
4. As there is no assumption introduced in the *IDCE* finite element model except the elasticity of the material, it is more adaptable than the 3-*DOF* rigid model and can be

applied to cases of cracks both at the dam base and at a height. If cracked at a height, a very simple treatment can avoid the phenomenon of penetration that may induce remarkable error in the responses.

5. Computation results by the two proposed models are consistent and satisfactory compared with each other as well as with available theoretical or numerical solutions.
6. Seismic analysis of the triangular dam for base sliding with the proposed *IDCE* model demonstrates its good agreement with one-degree-of-freedom flexible model if rocking conditions are not satisfied and the fundamental period of the dam is close to the average period of the earthquake. With full reservoir water and coefficient of friction 1.0 at the base, the triangular dam will be safe if imposing S69E component (peak acceleration scaled to 0.5g) of Taft 1952 earthquake, with residual downstream sliding 565.5 mm or less.
7. If the equivalent coefficient of friction at the crack is as high as 1.4 and the peak acceleration is 0.9g, the triangular dam will experience sliding, rocking, impact and drifting motion, where one-degree-of-freedom model is inapplicable. In this case, the triangular dam is still safe in both sliding and rocking. The *IDCE* model estimates that the dam will rock with maximum rotation of 13.11×10^{-4} radians and 128.3 mm of opening at the upstream face, which are much larger than those values predicted in 3-*DOF* rigid model. Regarding the sliding displacements, the two proposed models yield completely different sliding processes, and the residual values are quite difference, indicating that the flexibility of the dam affects the seismic behavior considerably.

8. Application of both models to the cracked Koyna Dam shows the upper part of the cracked monolith will be stable when either the transverse or longitudinal component of the Koyna earthquake is imposed, even if the coefficient of friction at the crack is as low as 0.8. The residual sliding displacement of the upper part of the cracked monolith is proportional to the coefficient of friction. If the coefficient of friction is 1.0 or larger, the corresponding residual displacement can be reduced to 195.7 mm or even less.
9. Computations for the cracked Koyna Dam also show that the rocking of the upper part is relatively small. Therefore the safety of the cracked Koyna Dam against overturning is guaranteed if a similar earthquake is applied. However, the rocking mode has to be included for properly predicting the stability of the cracked dam against sliding, due to these facts: rocking reduces the normal contact force and impact may cause drifting.
10. To reveal the seismic behaviour of cracked concrete gravity dams in general, a typical concrete gravity dam with cracks at the base and at a height, respectively, are studied by use of the two proposed models with two types of earthquakes, three water levels and three coefficients of friction.
11. Both models reveal consistently the seismic behaviour of the cracked typical dam. The cracked typical dam will always slide in downstream direction. Its residual sliding displacement is proportional to the water level and inversely proportional to the coefficient of friction under the given earthquake. With peak acceleration of 0.4g, both El Centro 1940 NS and Taft 1952 S69E earthquakes will cause the typical dam cracked at the base to slide significantly, or even fail, if the coefficient of friction at

the crack is 0.8 and the reservoir is full. The estimated maximum residual sliding displacement, however, will still be 209.8 mm even if the coefficient of friction is 1.2.

12. The *IDCE* finite element model reveals that the typical dam cracked at the base exhibits residual sliding displacement in the downstream direction even if the water is below the critical level that statically initiates sliding of the cracked dam. The typical dam cracked at a height will drift even if the water level is below the crack, revealing that in the absence of hydro pressure the rocking and impact may cause the upper part of the cracked dam to slide along the crack. The typical dam in each of the cracked situations acquires quite different residual sliding displacement for different earthquakes with the same magnitude of peak acceleration. This indicates that the stability of the cracked dam relies severely on not only the peak acceleration of the ground motion but also the details of the acceleration record.
13. This study suggests that the 3-*DOF* rigid model can be employed to first estimate the safety of cracked concrete dams against sliding and overturning. If the concrete dam is cracked at quite low position, such as at the base, the *IDCE* finite element model, which considers the flexibility of the dam, should be used to reveal more accurately its seismic behaviour.

8.2 Recommended future work

Although the two proposed models are quite satisfactory for predicting the seismic behaviour of cracked concrete gravity dams as demonstrated in the previous chapters, the prediction can be more practical if efforts are made in following aspects:

1. In the current study of this research, only horizontal excitation of the ground is considered. Actually, the vertical component of ground motion affects the seismic response. To fully review the seismic behaviour of cracked concrete gravity dams, modifications to include vertical excitation in the proposed models are necessary.
2. Presently both programs for the proposed models are mainly for the purpose of the research, and the data preparation and response analysis rely on the users. With user-friendly pre- and post-programs, the efficiency of the analysis can be much enhanced. Therefore it is needed to develop pre- and post-processing subroutines with easy-to-use interfaces to help prepare the original data of the models and explain the seismic behaviour of the cracked dams.
3. The proposed 3-*DOF* rigid model needs very limited data preparation and is so effective that the computation just costs a few seconds. However, it is suitable for relatively rigid dams. By contrast, the *IDCE* finite element model is applicable to either flexible or quite rigid dams with large amount of data preparation and computation costs (for example, 2 hours of computation on a computer of 1000 MHz for 1 second history of earthquake with time step of 2×10^{-6} seconds). Therefore, it is in great need to classify the cracked concrete gravity dams cracked at the base into two groups according to proper criteria such as fundamental frequency, height or slenderness of the dam so that one can reasonably choose either the 3-*DOF* rigid model or the *IDCE* flexible model to predict the seismic behaviour.
4. In both models, the Mohr-Coulomb friction law is adopted and the aggregate effect is represented by a high value of coefficient of friction. In fact, the mechanism of shear

transfer is very complex which depends upon the history of contact. So more realistic friction law needs to be introduced into this study.

5. The present study shows that there exists a possibility that the cracked concrete gravity dam may drift in some cases. This is achieved based on the implied assumption that the crack is flat and the aggregate effect can be represented by a large equivalent coefficient of friction. However, the crack in the dam is normally not straight. If considering the reality of the crack, the coefficient of friction will not be impractically as large as 1.0 or 1.2, and the asperities on the crack will prevent the cracked dam from drifting if the opening is not large enough. Therefore, a practical approach is needed to realistically consider the geometry of the crack in the proposed *IDCE* finite element model.
6. Asperities on the crack are very easy to be damaged in the seismic process. This damage will change the profile of the crack and its mechanical properties. Therefore the non-linear property of concrete is unavoidably encountered in future study, making the seismic behaviour analysis of cracked concrete gravity dams to be a dynamic contact problem with geometrically changeable contact surface and non-linear material properties.
7. In reality, cracks are likely to develop at the base and at a height where the section changes abruptly. The proposed *IDCE* model needs to be applied to the cases of two or more cracks in order to study the seismic behaviour of cracked concrete gravity dams with both the base crack and the crack at a height.

REFERENCE

1. ADINA R&D, Inc. (1999). "Automatic Dynamic Incremental Nonlinear Analysis: Theory and Modeling Guide." Printed in USA.
2. Aslam, M., Godden, W. G., and Scalise, D. T. (1980). "Earthquake rocking response of rigid bodies." *ASCE, J. Struct. Div.*, 106(ST2), 377-392.
3. Bathe, K. J. (1996). "Finite element procedures." *Prentice Hall, Inc., New Jersey.*
4. Bathe, K. J., and Chaudhary, A. (1985). "A solution method for planar and axisymmetric contact problems." *Int. J. Num. Method Eng.* 21, 65-88.
5. Bathe, K. J., and Mijailovich, S. (1988). "Finite element analysis of frictional contact problems." *J. Theoretical and App. Mech., Special issue, supplement*, 31-45.
6. Bhattacharjee, S. S., and Léger, P. (1994). "Application of NLFM models to predict cracking in concrete gravity dams." *ASCE, J. Struct. Eng.*, 120(4), 1225-1271.
7. Bhattacharjee, S. S., and Léger, P. (1993). "Seismic cracking and energy dissipation in concrete cravity dams." *Earthquake Eng. Struct. Dyn.*, 22, 991-1007.
8. Bittencourt, E., and Creus, G. J. (1998). "Finite element analysis of three-dimensional contact and impact in large deformation problems." *Computers and Structures*, 69, 219-234
9. Chaudhary, A. B., and Bathe, K. J. (1986). "A solution method for static and dynamic analysis of three-dimensional contact problems with friction." *Computers and Structures*, 24(6), 855-873.
10. Chávez, J. W., and Fenves, G. L. (1995). "Earthquake response of concrete gravity dams including base sliding." *ASCE, J. Struct. Eng.*, 121(5), 865-875.

11. Chopra, A. K., and Zhang, L. (1991). "Earthquake-induced base sliding of concrete gravity dams." *ASCE, J. Struct. Eng.*, 117(12), 3698-3719.

12. Computers and Structures, Inc. (1999). "SAP2000: Integrated Finite Element Analysis and Design of Structures." Berkeley, California, USA.

13. Cook, R. D. (1989). "Concepts and applications of finite element analysis." *John Wiley & Sons, Inc., New York.*

14. Danay, A., and Adeghe, N. (1993). "Seismic-induced slip of concrete gravity dams." *ASCE, J. Struct. Eng.*, 119(1), 108-129.

15. El-Aidi, B., and Hall, J. (1989). "Non-linear earthquake response of concrete gravity dams part 1: modeling." *Earthquake Eng. Struct. Dyn.*, 18, 837-851.

16. El-Aidi, B., and Hall, J. (1989). "Non-linear earthquake response of concrete gravity dams part 2: behavior." *Earthquake Eng. Struct. Dyn.*, 18, 853-865.

17. Eterovic, A. L., and Bathe, K. J. (1991). "On the treatment of inequality constraints arising from contact conditions in finite element analysis." *Computers & Structures*, 40(2), 203-209.

18. Fronteddu, L. (1997). "Experimental and numerical evaluation of the effect of concrete lift joints on static and seismic response of gravity dams." *PhD thesis, Dept. of Civil Eng., École Polytechnique de Montréal, Université de Montréal, Montreal, PQ, Canada.*

19. Fronteddu, L., Léger, P., and Tinawi, R. (1998). "Static and Dynamic behavior of concrete lift joints interfaces." *ASCE, J. Struct. Eng.*, 124(12), 1418-1430.

20. Hallquist, J. O. and Goudreau, G. L., and Benson, D. J. (1985). "Sliding interfaces with contact-impact in large-scale Lagrangian computations." *Computer method appl. Mech. Eng.*, 51, 107-137

21. Horyna, T., Black C. J., and Rudolf J. (1999). "Experimental and numerical analyses of a base-excited model of a concrete gravity dam monolith." *8th Canadian Conference on Earthquake Engineering, Vancouver*, 733-738.

22. Ishiyama, Y. (1982). "Motions of rigid bodies and criteria for overturning by earthquake excitations." *Earthquake Eng. Struct. Dyn.*, 10, 635-650.

23. Jefferson, A. D. (1998). "Plastic-damage model for interfaces in cementitious materials." *ASCE, J. Eng. Mech.*, 124(7), 775-782.

24. Kane, T. R., and Levinson, D. A. (1985). "Dynamics: Theory and Applications." *McGraw-Hill Book Company, New York.*

25. Kikuchi, N. (1982). "A smoothing technique for reduced integration penalty methods in contact problems." *Int. J. num. method. Eng.*, 18, 343-350.

26. Kodikara, J. K., and Johnston, I. W. (1994). "Shear behavior of irregular triangular rock-concrete joints." *Int. J. Rock Mech. Min. Sci. & Geomech.*, 31(4), 313-322.

27. Leahy, J. G. (1999). "The numerical treatment of local variables in three-dimensional frictional contact problems using the boundary element method." *Computers and Structures*, 71, 383-395.

28. Lee, S. S. (1994). "A computational method for frictional contact problem using finite element method." *Int. J. Num. Method. Eng.*, 37, 217-228.

29. Léger, P., and Katsouli, M. (1989). "Seismic stability of concrete gravity dams." *Earthquake Eng. Struct. Dyn.*, 18, 889-902.

30. Lorenzana, A., and Garrido, A. A. (1998). "A boundary element approach for contact problems involving large displacement." *Computers and Structures*, 68, 315-324.

31. MacLaughlin, M., Sitar, N., Doolin, D., and Abbot, T. (2001). "Investigation of slope-stability kinematics using discontinuous deformation analysis." *Int. J. Rock Mech. & Mining Sciences*, 38, 753-762.

32. Mir, R. A., and Taylor, C. A. (1996). "An investigation into the base sliding response of rigid concrete gravity dams to dynamic loading." *Earthquake Eng. Struct. Dyn.*, 25, 79-98.

33. Mohamed, A. A., and Richard, N. W. (1999). "Enhanced contact model for shear friction of normal and high-strength concrete." *ACI Structural Journal,* 96(3), 348-360.

34. Okamoto, N., and Nakazawa, M. (1979). "Finite element incremental contact analysis with various frictional conditions." *Int. J. Num. Method. Eng.*, 14, 337-357.

35. Parisch, H. (1989). "A consistent tangent stiffness matrix for three-dimensional no-linear contact analysis." *Int. J. Num. Method. Eng.*, 28, 1803-1812.

36. Pompei, A., Scalia, A., and Sumbatyan, M. A. (1998). "Dynamics of rigid block due to horizontal ground motion." *ASCE, J. Eng. Mech.*, 124(7), 713-717.

37. Saini, S. S., and Krishna, J. (1974). "Overturning of top profile of the Koyna Dam during severe ground motion." *Earthquake Eng. Struct. Dyn.*, 2, 207-217.

38. Shenton III, H. W. (1996). "Criteria for initiation of slide, rock and slide-rock rigid-body modes." *ASCE, J. Eng. Mech.*, 122(7), 690-693.

39. Shenton III, H. W., and Jones, N. P. (1991). "Base excitation of rigid bodies. I : Formulation." *ASCE, J. Eng. Mech.*, 117(10), 2286-2306.

40. Shenton III, H. W., and Jones, N. P. (1991). "Base excitation of rigid bodies. II: periodic slide-rock response." *ASCE, J. Eng. Mech.*, 117(10), 2307-2328.

41. Simo, J. C., Wriggers, P., and Taylor, R. L. (1985). "A perturbed Lagrangian fomulation for the finite element solution of contact problems." *Computer Meth. Applied Mech. & Eng.*, 50, 163-180.

42. Tassios, T. P., and Vintzeleou, E. N. (1987). "Concrete-to-concrete friction." *ASCE, J. Struct. Eng.*, 113(4), 832-849.

43. Tiniawi, R., Léger, P., Leclerc, M., and Cipolla, G. (2000). "Seismic safety of gravity dams: from shake table experiments to numerical analysis." *ASCE, J. Struct. Eng.*, 126(4), 518-529.

44. Tiniawi, R., Léger, P., Leclerc, M., and Cipolla, G. (1999). "Shake table experiments for cracking and sliding response of concrete dams." *8th Canadian Conference on Earthquake Engineering, Vancouver*, 739-744.

45. Tomas, H., Cameron, B., and Jachym, R. (1999). "Experiments and numerical analysis of a base-excited model of a concrete gravity dam monolith." *8th Canadian Conference on Earthquake Engineering, Vancouver*, 733-738.

46. Walraven, J. (1993). "Rough cracks subjected to earthquake loading." *ASCE, J. Struct. Eng.*, 120(5), 1510-1524.

47. Walraven, J. C. (1981). "Fundamental analysis of aggregate interlock." *ASCE, J. Struct. Div.*, 107(11), 2245-2270.

48. Walraven, J., Frénay, J., and Pruijssers, A. (1987). "Influence of concrete strength and load history on the shear friction capacity of concrete members." *PCI Journal*, 32(1). 67-84.

49. Westergaard, H. M. (1931). "Water pressures on dams during earthquakes." *ASCE* Proceedings, 418-433.

50. Wriggers, P, Simo, J. C., and Taylor, R. L. (1985). "Penalty and augmented Lagrangian formulations for contact problems." *Proceedings of the NUMETA '85 Conference/Swansea/7-11*, 97-106.

51. Yim, C. S., Chopra, A. K., and Penzien J. (1980). "Rocking responses of rigid blocks to earthquakes." *Earthquake Eng. Struct. Dyn.*, 8, 565-578.

52. Zavarise, G., Wriggers, P., and Schefler, B. A. (1995). "On augmented Lagrangian algorithms for thermomechanical contact problems with friction." *Int. J. Num. Methods Eng.*, 38, 2929-2949.

53. Zhang Chuhan, Pekau, O. A., Jin Feng, and Wang Guanglun. (1997). "Application of distinct element method in dynamic analysis of high rock slope and blocky structures." *Soil Dynamics and Earthquake Engineering*, 16, 385-394.

54. Zienkiewicz, O. C. (1971). "The finite element method in engineering science." *McGraw-Hill Publishing Company Limited, London.*

APPENDIX

NATURAL PERIODS OF THE DAMS AND ACCELERATION SPECTRA OF THE EARTHQUAKES

The first 5 natural periods of vibration of intact Koyna Dam ($E = 3.1\times10^4$ MPa, $\nu = 0.2$) and the typical dam ($E = 2.0\times10^4$ MPa, $\nu = 0.143$) with empty reservoir are as follows:

Table A.1 Natural periods of the dams

Mode	1	2	3	4	5
Period (s) of Koyna dam	0.3254	0.1218	0.0925	0.0627	0.0413
Period (s) of the typical dam	0.2842	0.1292	0.1052	0.0768	0.0521

Acceleration spectra (5% damping ratio) of the 4 earthquake records employed in this study are as follows:

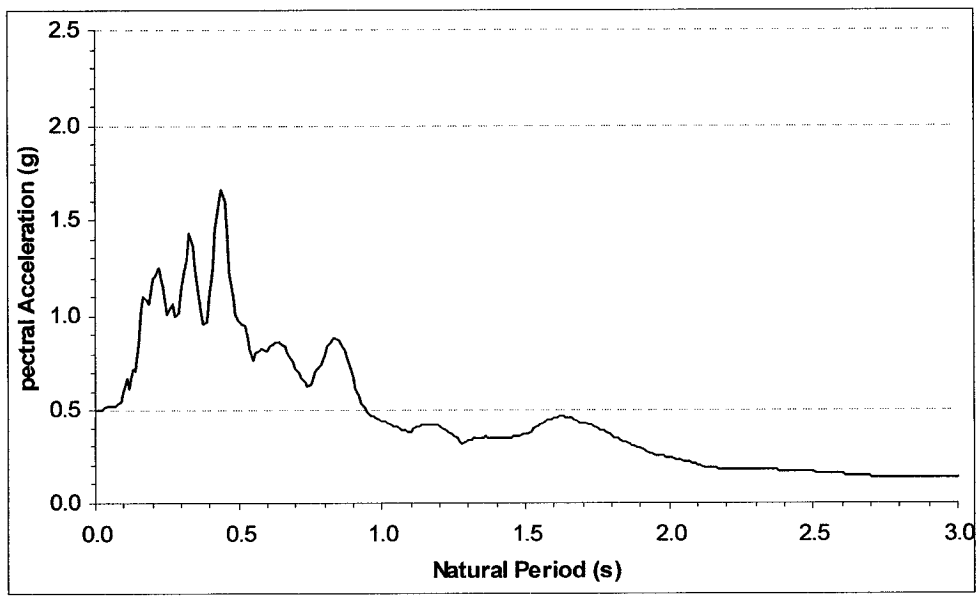

Figure A.1 Acceleration spectrum of Taft 1952 earthquake S69E component with peak acceleration scaled to 0.5g and damping ratio of 5%

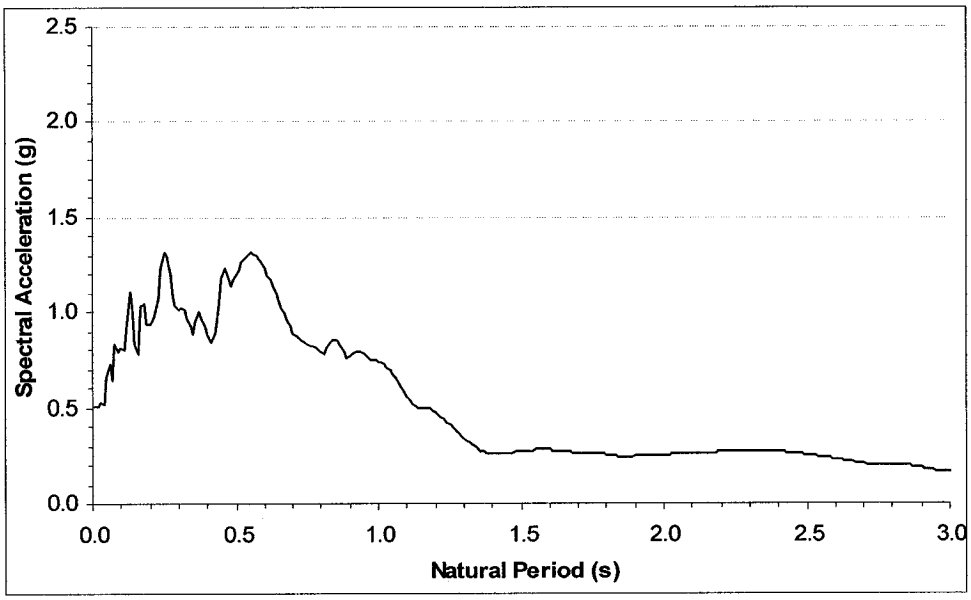

Figure A.2 Acceleration spectrum of El Centro 1940 earthquake NS component with peak acceleration scaled to 0.5g and damping ratio of 5%

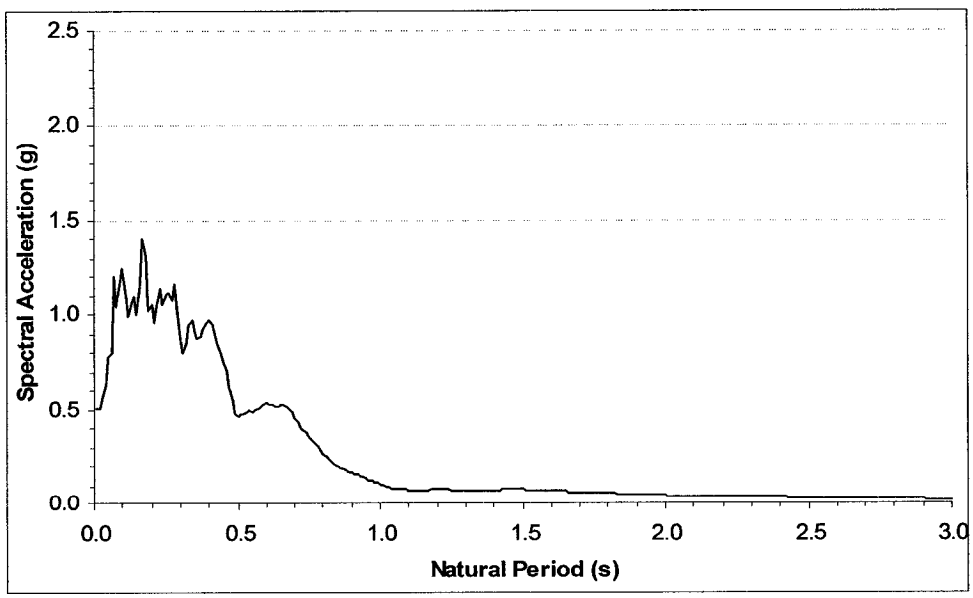

Figure A.3 Acceleration spectrum of Koyna 1967 earthquake longitudinal component with peak acceleration scaled to 0.5g and damping ratio of 5%

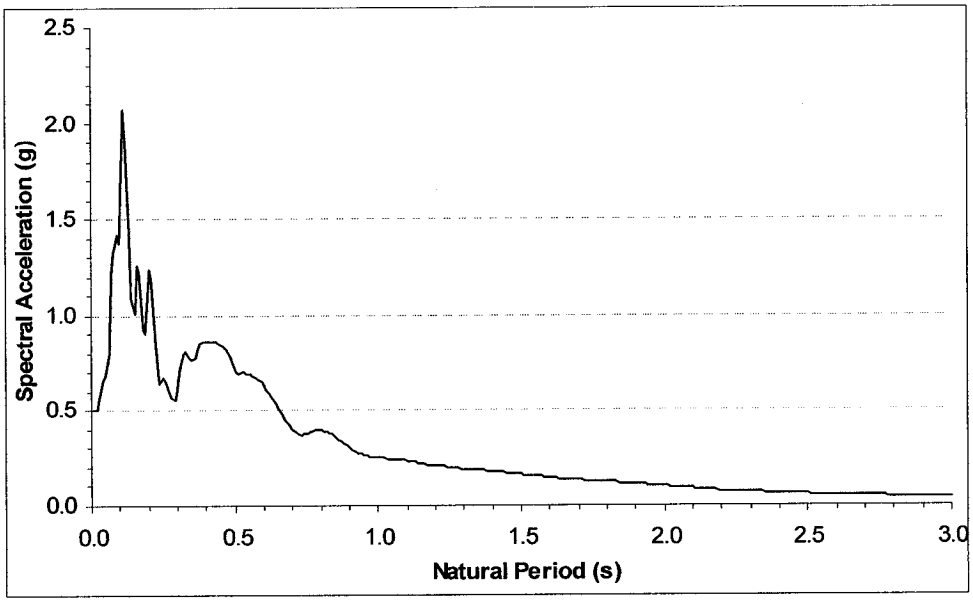

Figure A.4 Acceleration spectrum of Koyna 1967 earthquake transverse component with peak acceleration scaled to 0.5g and damping ratio of 5%